



UNIVERSITAT POLITÈCNICA  
DE CATALUNYA  
BARCELONATECH

EUM/CO/18/4600002153/BV

# ISS-LIS data analysis based on LMA networks in Europe

Report version:	Rev. 2
Date:	20190625
Prepared by:	J. Montanyà, O. van der Velde, N. Pineda and J. López
Distribution:	EUMETSAT, UPC

**UPC Lightning Research Group**

## PAGE ISSUE RECORD

This Document consists of the following pages at the issues shown

Document	Pages	Issue	File Name and Format
	1 - X	1	
	1 - X	2	
	1-X	3	

## DOCUMENT CHANGE LOG

Issue	Change References	Issue Date	Pages Affected	Remarks	Init.
1					
2					
3					

(This page is intentionally left blank)

## Acronyms

ASPKE: Absolute Sample Position Knowledge Error

CCD: Charged-Coupled Device.

CG: Cloud-to-ground.

DE: Detection efficiency.

FFA: Flash false alarm.

FFAR: Flash false alarm rate.

FDE: Flash detection efficiency.

FOV: Field-of-view.

IC: Intra-cloud.

IFOV: Instantaneous field-of-view.

ISS: International Space Station.

LI: Lightning imager.

LIS: Lightning Imaging Sensor.

LLS: Lightning Location System or network.

LMA: Lightning Mapping Array.

MTG: Meteosat Third Generation.

PDE: Pulse detection efficiency.

PFA: Pulse false alarm.

TA: Time accuracy.

UPC: Technical University of Catalonia.

VHF: Very High Frequency.

(This page is intentionally left blank)

## Table of contents

1	Technical specifications/comparison ISS-LIS and LMA	8
1.1	ISS-LIS Lightning Imaging Sensor on the ISS	8
1.2	Ebro Lightning Mapping Array	10
2	Data selection	14
2.1	Methodology of data selection	14
2.2	Dataset	15
2.3	Sensitivity analysis	117
2.3.1	Theoretical location accuracy	18
2.3.2	Experimental evaluation of the E-LMA performance	20
2.3.3	Sensitivity analysis	31
2.4	Conclusions	38
2.5	Description of the key properties of the dataset	40
3.	Definition of the evaluation of the ISS-LIS using the LMA	43
4.	Evaluation of ISS-LIS	45
4.1	Flash detection efficiency and false alarm	45
4.2	Flash duration	61
4.3	Distribution of ISS-LIS events with height and power	71
4.4.	ISS-LIS radiance	79
4.5	Location accuracy	83
5.	Model of lightning for test cases	90
6.	Validation of LI and routine monitoring	95
6.1	Introduction	95
6.2	Definition of the performance evaluation	95
6.2.1	Flash Detection Efficiency	95
6.2.2	Flash False Alarm (FFAR)	102
6.2.3	Absolute Sample Position Knowledge Error (ASPKE)	106
6.2.4	Time Accuracy (TA)	109
6.2.5	LI L1b L2 Pulse detection efficiency (PDE)	111
6.2.6	LI L1b L2 Pulse false alarm (PFAR)	115
6.3	Strategy	119
6.3.1	Locations of LMAs and experience in campaigns	119
6.3.2	Annual number of thunderstorms	119
6.3.3	Recommendations for validation and operation	120
7.	Conclusions	121
	References	126
	Annex A Weather radar	128
	Annex B Regional VHF interferometer total lightning location system	130

(This page is intentionally left blank)

## 1 Technical specifications/comparison ISS-LIS and LMA

### 1.1 ISS-LIS Lightning Imaging Sensor on the ISS

#### 1.1.1 Overview

LIS (Lightning Imaging Sensor) is an optical sensor on board of the ISS. LIS is composed by:

Imaging system and focal plane CCD: A telescope with a field-of-view (FOV) of  $80^{\circ} \times 80^{\circ}$  that converges its entering light to a  $5^{\circ}$  wide beam to an interference filter at  $777.4 \pm 1$  nm. At the focal plane, a CCD array of  $128 \times 128$  converts light to electric signals.

Real-time signal processor and background remover: Lightning is discriminated from images by subtracting individual images from averaged background images. After subtraction, signals over a threshold are considered lightning. Thresholds can be modified, for instance, during daytime these are higher than during night time observations.

Event processor and formatter: signals accepted as lightning are processed. These lightning pulses are called EVENTS. In a lightning flash events will form groups, so a lightning flash will be composed by a number of groups of events:

- Event: corresponds to an excited pixel on the CCD.
- Group: One or more events that take place in adjacent CCD pixels occurring at the same integration time.
- Flash: It is formed by one or more groups that occur within 330 ms and 16.5 km of separation.

Data is also grouped in Area which is defined as contiguous region on the surface of the Earth that has produced lightning during a single orbit of the LIS instrument.

#### 1.1.2 Summary of key properties

Summary of technical specifications:

Field-of-View (FOV):	$80^{\circ} \times 80^{\circ}$
CCD Array Size:	$128 \times 128$ pixels
Dynamic Range:	$>100$
Pixel IFOV:	4 km (nadir) to 8 km
Interference Filter wavelength:	777.4 nm
Filter bandwidth:	1 nm
Detection threshold:	$4.7 \mu\text{J m}^{-2} \text{sr}^{-1}$

Signal to noise ratio:	6
Detection Efficiency (DE)	~90 %
False Event Rate (FER)	<5 %
Measurement accuracy	
Location:	1 pixel
Intensity:	10 %
Time:	tag at frame rate
Frame rate (integration time):	2 ms
Telemetry data rate:	8 kb/s

### 1.1.3 Data used in this work

There are currently 4 types of data within the dataset:

- Non-Quality Controlled Lightning Imaging Sensor (LIS) on International Space Station (ISS) Provisional Science Data
- Non-Quality Controlled Lightning Imaging Sensor (LIS) on International Space Station (ISS) Provisional Backgrounds
- NRT Lightning Imaging Sensor (LIS) on International Space Station (ISS) Provisional Science Data
- NRT Lightning Imaging Sensor (LIS) on International Space Station (ISS) Provisional Backgrounds.

LIS data is contained within HDF-4/netCDF-4 format files. These files include information related to:

- Orbit Summary
- One Second
- Point Summary
- View time
- Bg Summary
- Area
- Event
- Flash
- Group
- Raster Images

In this work we use the following data extracted from the HDF files.

- Event: date, time, location and radiance.
- Group: ID of the group that an event belongs, time, location of the radiance-weighted centroid, radiance
- Flash: date, time, location of the radiance-weighted centroid, radiance.
- Location: View time of  $0.5^\circ \times 0.5^\circ$  grid cells. That will be used to verify that an LMA flash not reported by the ISS-LIS actually was in the FOV.

## 1.2 Ebro Lightning Mapping Array

In July 2011 a 6-station Lightning Mapping Array (LMA, *Rison et al.* 1999; *Thomas et al.* 2004) was deployed in the Ebro Delta (eastern Spain, Figure 1). Over the course of 2012 the system was gradually expanded to 11 stations. The region was chosen for its proximity to both warm season and cold season thunderstorms which often produce sprites and elves in the coastal region or over the Mediterranean Sea (e.g. *Soula et al.* 2010, *Montanyà et al.* 2010). In 2015 the Ebro-LMA was reduced to 7 stations (see figure 1.2.1) when 6 stations were uninstalled and moved to Colombia to create the Colombia LMA.

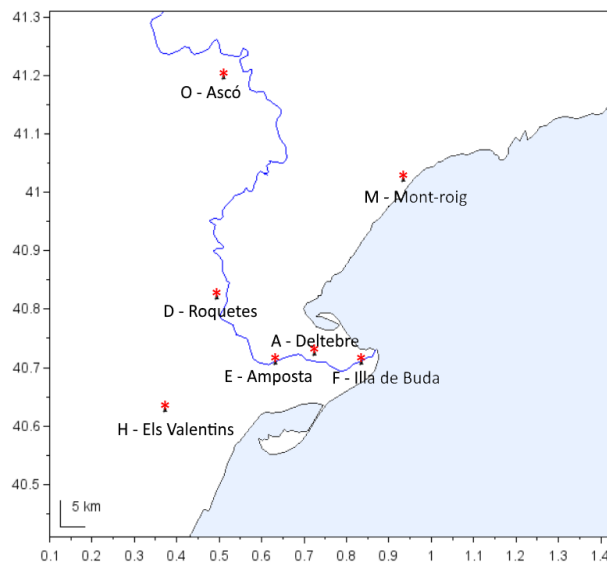


Figure 1.2.1 Location of the Ebro-LMA stations for the period 2017-2018.

The LMA system locates radio emissions in the very high frequency range (VHF, 60-66 MHz) in three dimensions by the time-of-arrival analysis using at least five stations.

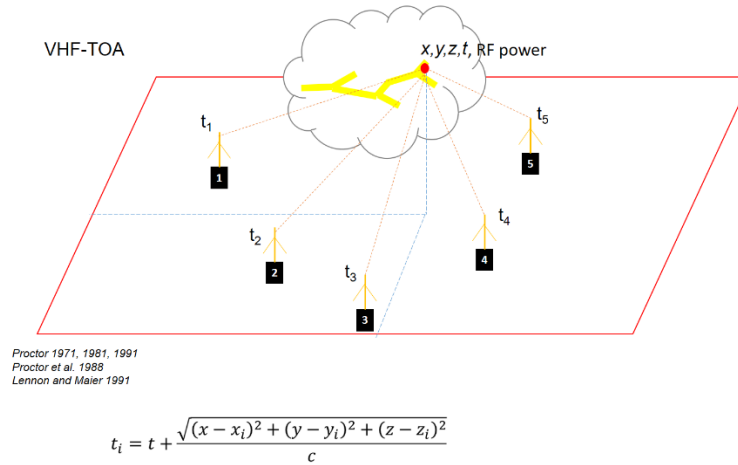


Figure 1.2.2 Principle of the VHF Time-of-Arrival (TOA).

Each station samples the maximum RF power signal amplitude and its GPS derived precise time over 80 μs intervals (figure 1.2.3).

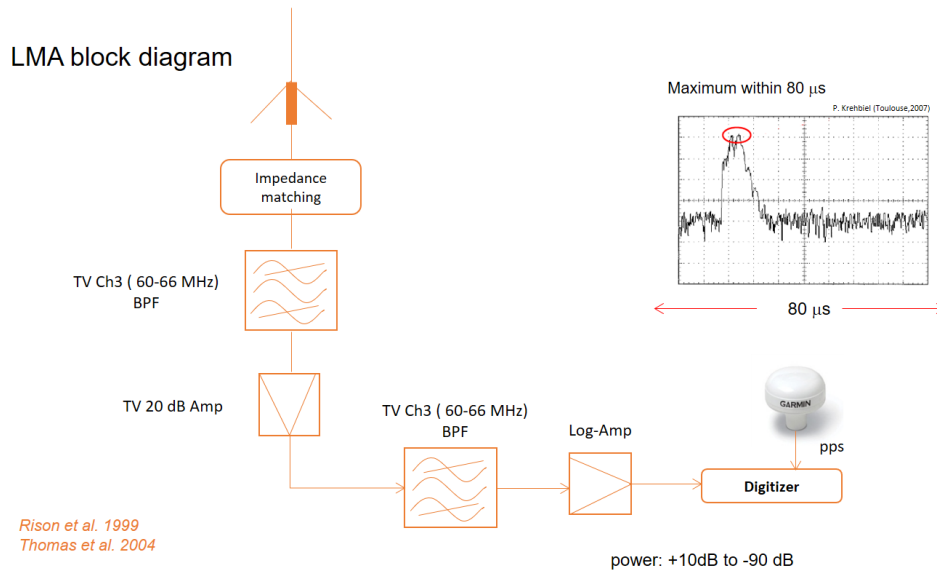


Figure 1.2.3 Diagram of a LMA station.

These located (x,y,z,t) emissions are named sources. Typically, two to three thousand sources per second can be located during lightning flashes.

Background noise level at the sites varies usually between -75 dBm to -60 dBm, although higher or lower levels do occur sometimes at some of the stations. Power in dBW is available for every located source (see *Thomas et al., 2001* for examples and discussion). The distance between adjacent sensors ranges between 6 and 17 km.

Located sources are mainly coming from negative leaders moving through regions of positively charged cloud particles, but typically weaker sources from positive leader traces inside the negative charge region are often detected as well. These are caused by negative recoil leaders (e.g. *Mazur, 2002*). So, effectively the LMA detects negative breakdown at both negative and positive leader sections.

### 1.2.1 E-LMA data processing

LMA raw data (Level 0) is collected from the stations and copied to a processing computer. Time-of-arrival reconstruction is performed by a script which accepts configuration parameters and a file with the station locations and their relative internal delays in nanoseconds (tuning). For the Ebro LMA, processing is done with the criterion of 5 stations as a minimum to find locations. If more stations can contribute positively, the software automatically adds these. The 5-station processing allows a better result when a network is small and has relatively high background noise levels at multiple stations. However, the 5-station processing is the minimum for 3D solution finding, without the redundancy to determine  $\chi^2$ , a metric for the precision of the solutions by which other LMA often filter the data. Thus, our current 7-sensor network produces relatively more scattered sources (local noise sources interfering with lightning sources to produce erroneous locations). This is handled by a spatial filtering round on the produced data.

The data files (Level 1, GNU-zipped .dat text format) include a header with information about the active stations, and the data [time in UT second of the day, latitude, longitude, altitude (m), reduced  $\chi^2$ , power (dBW), and mask (hexadecimal) which identifies the stations that participated in the solution]. These data files are usually processed before displaying the data, in order to identify and count separate physical events called “flashes”. A flash is the entire series of lightning processes from inception until the end of all leader channel growth.

Before we process flashes and assign flash numbers to data sources, we first determine which sources are considered scattered, noisy sources, and which of them are plausible lightning solutions by using proximity to other sources. For this, filtering is done by flagging any sources in a grid box per time step if there are only 2 or less of them. A typical size grid box used here is 5 by 5 km horizontally, 1.5 km vertically, and 50 ms in time. The rejected sources are not discarded, just flagged, and can be inspected when necessary.

Because ideally there are no LMA sources occurring between two subsequent flashes, the straight-forward way to determine flashes is to separate streams of sources whenever a break longer than 150 ms occurs (typical value). This is sufficient for most displaying purposes, and is the data used for this study (human interaction can judge the quality of the flash). However, an extra precision pass has been developed for automatically dealing with the case when there are multiple flashes occurring across the

domain at the exact same time. This analysis uses a 2D grid (e.g. 6x6 km cells) where per time-based “flash” it is determined if its grid cells are adjacent to each other. If this is not the case, e.g. a cluster of cells is separated by more than 2 cells from another, the “flash” is split, and sources of the flash are relabeled with different flash numbers.

The resulting Level 2 data, then, includes extra columns with the number of the flash the source belongs to, and its lightning or scatter (“noise”) status.

## 2 Data selection

In this part, the methodology of data selection and sensitivity analysis of the dataset due to the selection criteria are analyzed.

### 2.1 Methodology of data selection

As described in the section 1, the Ebro LMA (E-LMA) monitors continuously the target area whereas the ISS-LIS orbiting aboard of the ISS observes typically this area once or twice times a day during short periods (e.g. <90 s). The selection of the data will be based on the steps shown in figure 2.1.

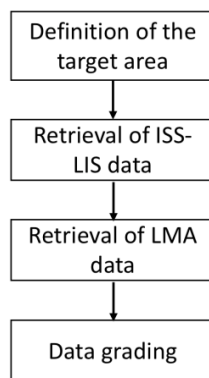


Figure 2.1 Flowchart of the data selection.

#### 2.1.1 Target area

The target area is defined by an area within the coverage area of the E-LMA where the performance of the E-LMA is suitable for data comparison. See section 2.3 and its subsections.

#### 2.1.2 Retrieval of ISS-LIS data

ISS-LIS data is retrieved from the ISS-LIS Space Time Domain Search

<https://lightning.nsstc.nasa.gov/isslisib/isslissearch.html>

A window larger than the monitoring area of the LMA has been selected.

The period selected corresponds from March 2017 to October 2018.

HDF-4 files have been downloaded from:

<https://ghrc.nsstc.nasa.gov/pub/lis/iss/data/science/nqc/hdf/>

Flash, group and event data from the *hdf* files is grouped in a single file: 'ISS\_LIS.txt'

In addition, data corresponding to the FOV information (*location*, *viewtime\_start* and *viewtime\_end*) is also retrieved from the *hdf* files for future use in the data comparison.

### 2.1.2 Retrieval of LMA data

E-LMA data is processed at the Technical University of Catalonia (UPC) processor. Processed data is organized in folders corresponding to individual days. Each folder contains files with data organized in 10 minute intervals.

For the 10 minute interval LMA data, a post-processing code is applied where sources are grouped into flashes. An ID is provided to each flash. Sources identified as 0 are sources with no assigned flash.

For future use, it is convenient to organize LMA data as follows:

- LMA level-0 data: This corresponds to row data at the sensor level: Time and RF power of each detection.
- LMA level-1 data: This is processed data composed by located sources: Time, latitude, longitude, altitude and RF power of sources.
- LMA level-2 data: This data corresponds to flash data, sources are grouped in flashes: Flash ID, time, latitude, longitude, altitude and RF power of sources.

## 2.2 Dataset

From the ISS-LIS point of view, figure 2.1 shows the distribution of the ISS-LIS flashes near the area of the E-LMA.

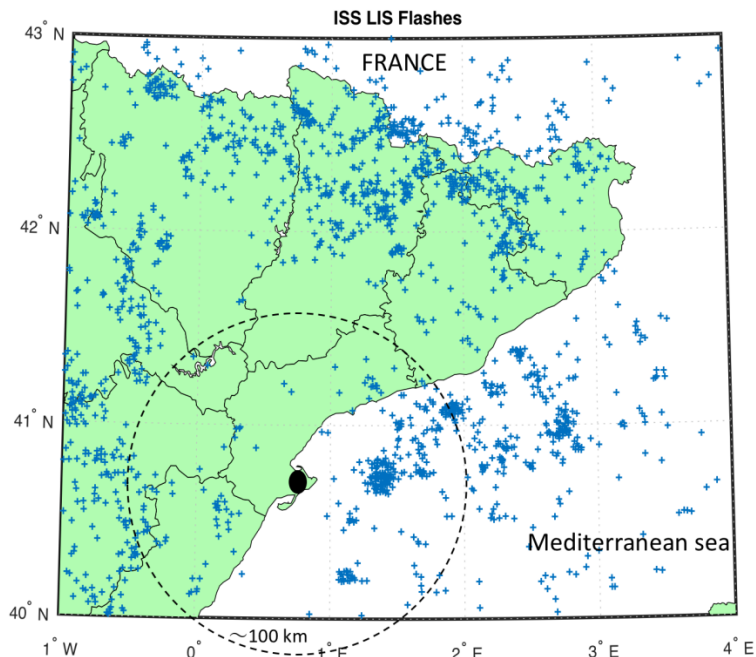
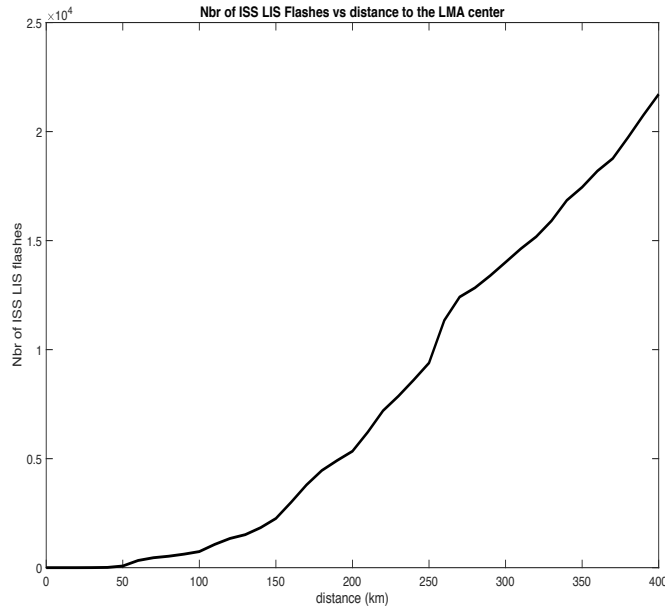


Figure 2.1 ISS-LIS Flashes for a period from March 2017 to October 2018. The black circle corresponds to the center of the E-LMA network and the dashed circle to a range of 100 km from the E-LMA center.

Figure 2.1 depicts the number of ISS-LIS flashes versus distance to the center of the E-LMA network. This plot will be helpful to decide the size of the target area.



**Figure 2.2** Number of ISS-LIS flashes occurred in a given distance from the E-LMA network.

Note that there are no ISS-LIS flashes in a distance below 25 km of the E-LMA. See the next table for a quick overview.

Distance to the center of the ELMA	Number of ISS-LIS flashes
25 km	0
50 km	76
75 km	495
100 km	738
125 km	1396
150 km	2256

Besides the number of flashes of the ISS-LIS in a given distance from the E-LMA, it is interesting to count the number of days with thunderstorms. This is depicted in figure 2.3.

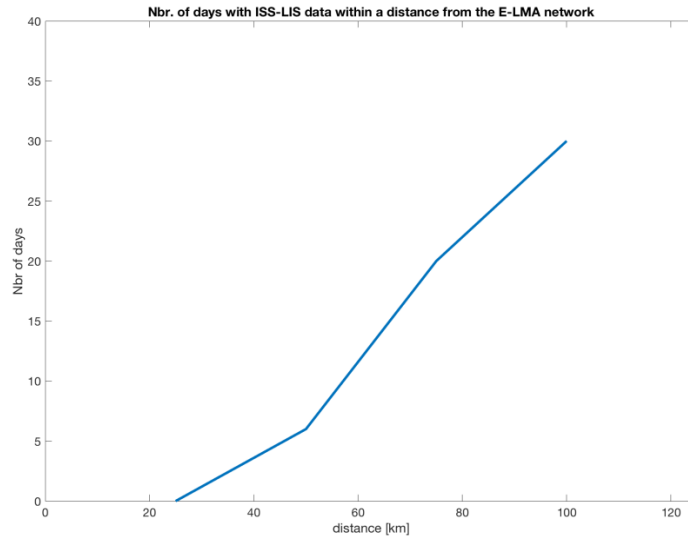


**Figure 2.3** Number of days with ISS-LIS flashes in a given distance from the E-LMA network.

Note from the graph that there are 5 different episodes corresponding to the ISS-LIS flashes within 50 km. The respective values for 75 km and 100 km are 20 and 30 days.

### 2.3 Sensitivity analysis

The sensitivity analysis is focused on the performance of the E-LMA with distance to its center and the number of flashes detected by the ISS-LIS at a given distance. In the subsection 2.3.1 the theoretical location accuracy is evaluated whereas in the section 2.3.2 the E-LMA is evaluated based on its data. Several parameters to represent the performance will be defined.

In the subsection 2.3.3 the sensitivity analysis of the E-LMA performance and the number of ISS-LIS flashes is presented. That will be used to define the target area to consider in the study.

### 2.3.1 Theoretical location accuracy

In the work of *Thomas et al. (2004)* the accuracy of the LMA is investigated. From this reference, we have calculated the location accuracy versus distance to the center of the network. The result is presented in figure 2.3.1.

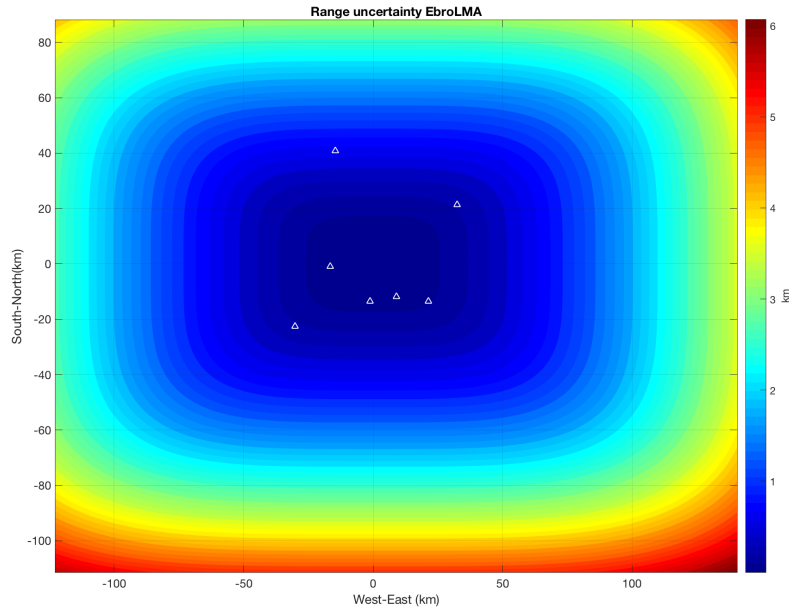


**Figure 2.3.1** Location accuracy (x,y) of the Ebro LMA (E-LMA). Triangles corresponds to the current E-LMA stations.

Note that the theoretical x,y accuracy of the E-LMA is better than 2 km below 100 km of the network. But the ELMA also provides altitudes z of the sources. This is evaluated in the next figure 2.3.2 and 2.3.3.

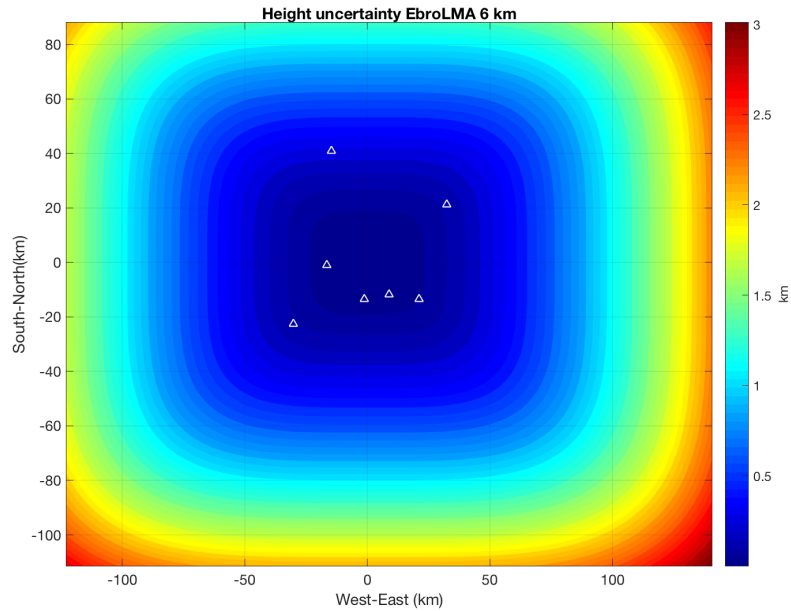


**Figure 2.3.2 Location accuracy (height) of the Ebro LMA (E-LMA) for a source located at 6 km altitude. Triangles corresponds to the current stations.**

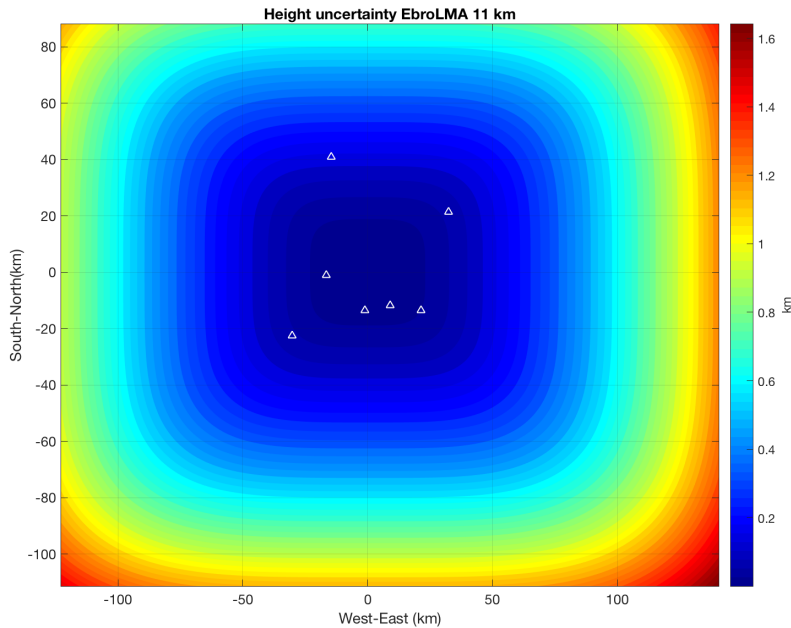


**Figure 2.3.3 Location accuracy (height) of the Ebro LMA (E-LMA) for a source located at 11 km altitude. Triangles corresponds to the current stations.**

In figures 2.3.2 and 2.3.3 the accuracy of locating sources occurring at heights of 6 km and 11 km, respectively are plotted. Note that at these altitudes, the accuracy is better than 1 km for ranges below 100 km. In this study it might be important the performance

of the E-LMA at high altitudes since the occurrence of leaders at these levels shall provide better conditions for ISS-LIS detections.

### **2.3.2 Experimental evaluation of the E-LMA performance**

The objective is to describe how E-LMA data quality drops off with distance from the stations. This information will be used to select the target area for the analysis.

Typically,  $\geq 5$  station time-of-arrival is performed for this relatively small Ebro Delta network of 5-7 active stations. Compared to 6-station minimum solutions, the resulting locations include more 'noise' (sources that are not assigned to flashes) and are less precise.

The spatial precision can be approximated by taking the median of x-y, z, and time differences between subsequent sources. Most often, subsequent sources belong to the same leader tip, and spatial scatter will therefore show up. The same for the time difference. With distance, as efficiency of detection above the noise level decreases, fewer sources per unit time will be detected, thus longer intervals.

With distance, also the lowest detectable altitude becomes higher with "line of sight" characteristic of VHF radio propagation over the horizon. This means downward negative leaders to ground (usually below 3-4 km in summer, 1-2 km in winter) may become undetectable. Furthermore, a wrong tuning can skew source altitude with distance as positioning errors become larger.

Additionally, low emission source power will start to become undetectable. For this we can determine the fraction of  $< 3$  dBW sources per flash. Close to the network center, if the station noise levels are low, positive leaders are mapped with low power. These leaders are often the only intracloud component of negative cloud-to-ground flashes (-CG), and missing these detections makes the entire flash undetectable at certain distance from the LMA center.

Statistics are derived from LMA data of 25 active thunderstorm days in mainly in 2018. Data has been divided in 10x10 km grid cells. A flash algorithm then separated groups of sources into flashes when a silent interval of  $> 150$  ms occurred. Of these sources, the statistics are summarized per flash. Over all flashes of all 25 days together, the following maps were computed. For most purposes, flashes with less than 50 sources were eliminated, to minimize noise contamination of results.

### 2.3.2.1 Median source-source time

The spatial precision can be approximated by the time differences between subsequent sources. With distance, as efficiency of detection above the noise level decreases, fewer sources per unit time will be detected, thus longer intervals.

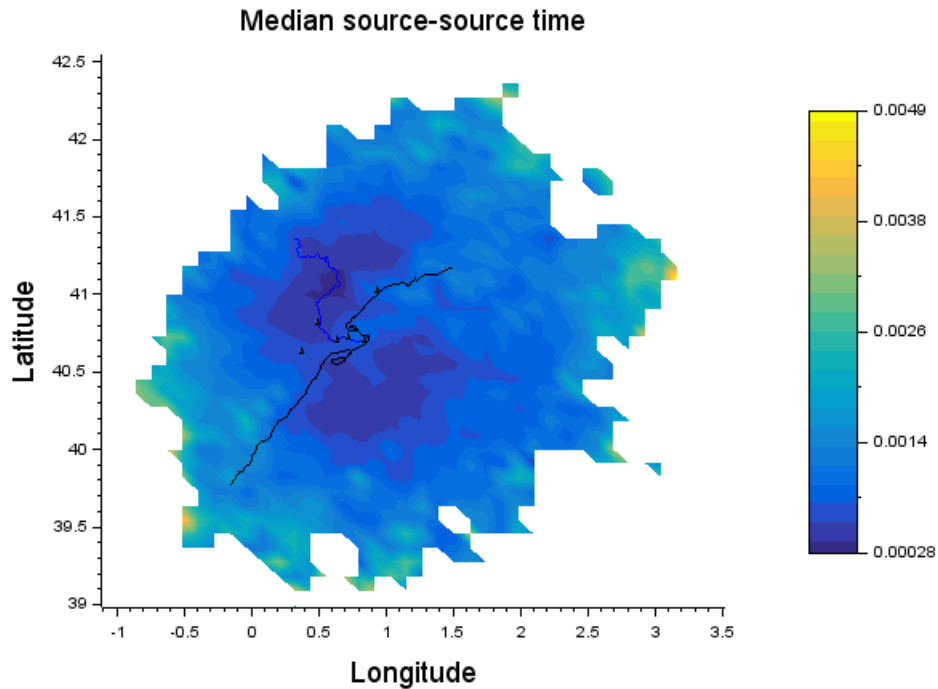


Figure 2.3.4 Median source-to-source time interval (s). Reference lines: costal border in black, Ebro river in blue, and LMA stations as black triangles.

Lower intervals are better, as it represents denser mapping in time. It appears that two zones NW and SE of the Ebro Delta show the most favorable values. An axis from WSW to ENE is somewhat less good.

### 2.3.2.2 Median source-source XY distance

The spatial precision can be approximated by taking the median of x-y differences between subsequent sources. Most often, subsequent sources belong to the same leader tip, and spatial scatter will therefore show up.

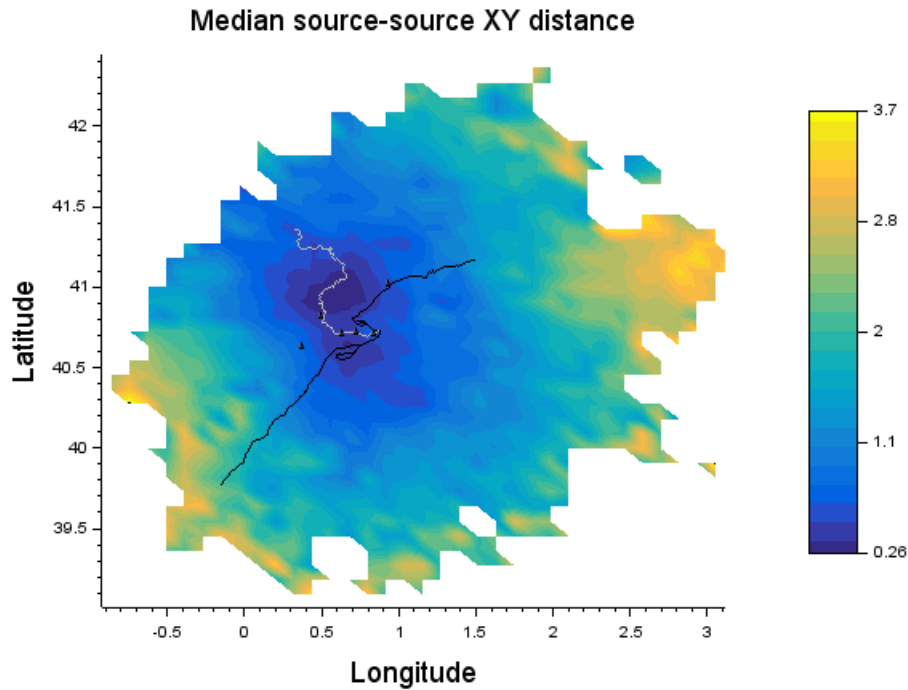


Figure 2.3.5 Median source-to-source XY distance (km).

The horizontal scatter in the mapping of channels is minimized in an area from the Ebro Delta to the lower Ebro Valley, which is the region within the perimeter of the LMA stations with less than 500 m horizontal scatter. But in a wide radius the scatter is less than 1.5 km.

### 2.3.2.3 Median source-source Z distance

In that case, the vertical spatial precision is evaluated by computing the distance along Z axis between consecutive sources.

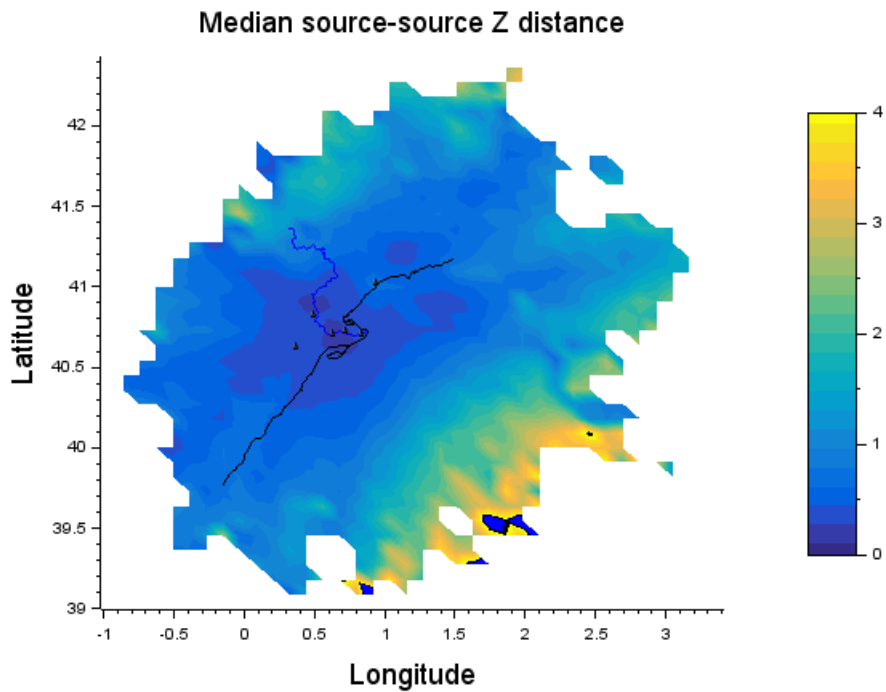


Figure 2.3.6 Median source-to-source Z distance (km).

Vertical scatter is best right over the Ebro Delta, where several sensors are clustered. It deteriorates to 1.5-2.0 km scatter over the Mediterranean almost 100 km from the network center, similar to the northwest sector.

### 2.3.2.4 Median flash duration

Now, the duration of lightning flashes is analyzed. In this analysis, only flashes with less than 50 sources are considered.

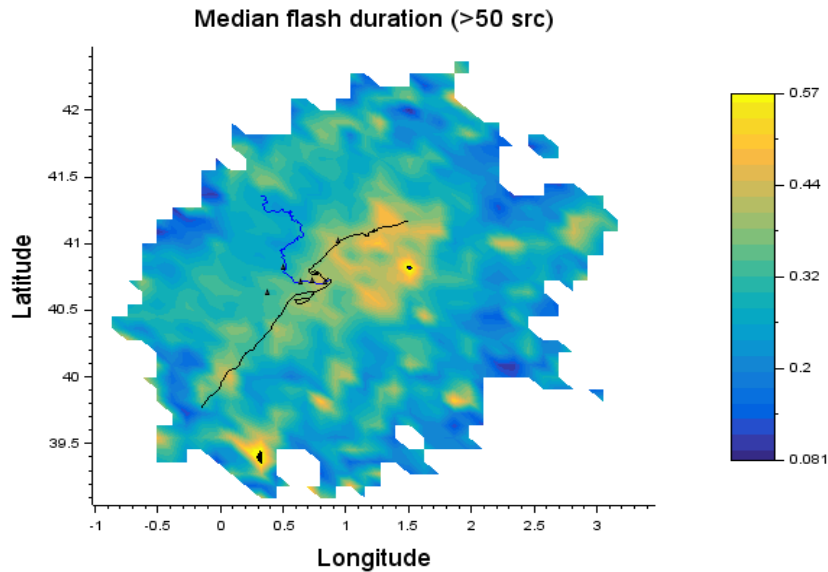


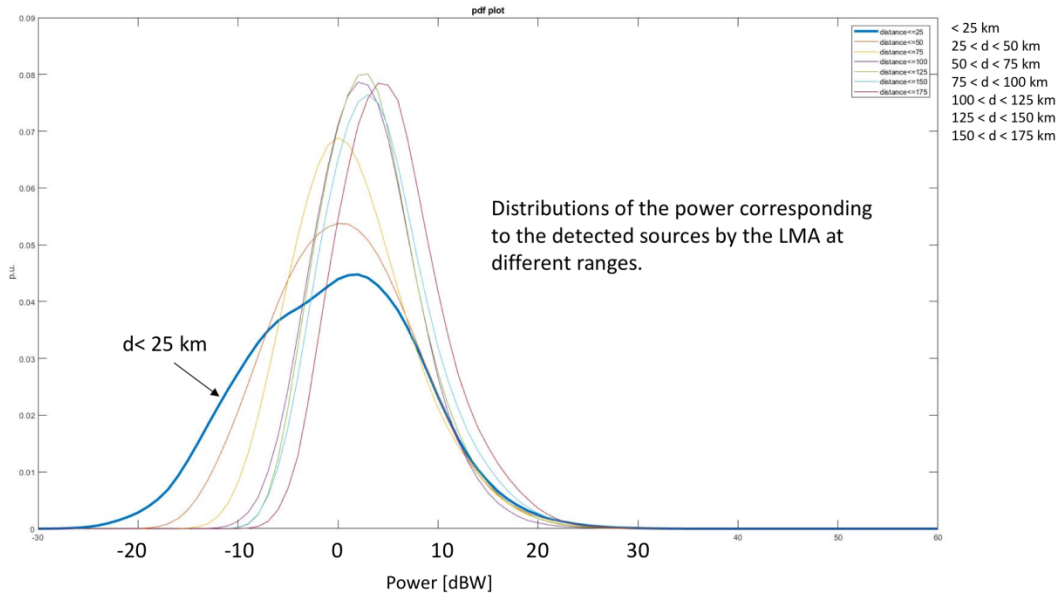
Figure 2.3.7 Median flash duration (seconds)

This map is showing more of a characteristic of the lightning flashes themselves, as the duration of a flash is less sensitive to the mapping quality. As result, the median flash duration cannot be used as a metric of the LMA performance.

### 2.3.2.5 Analysis of the source power

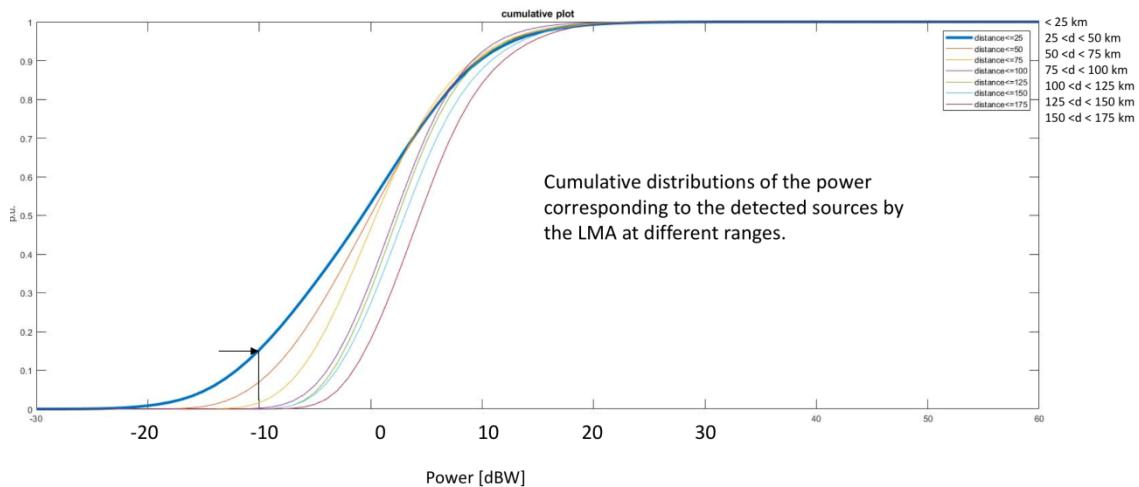
The LMA receives VHF radio emissions coming from lightning leaders. The sensitivity of each station depends on the radio noise at the location. That might limit the detection of low power sources. It is known that negative leaders produce more powerful emissions than positive leaders. That is one reason why LMA detects mostly negative leaders.

Figure 2.3.8 presents the distributions of the power of the detected sources of flashes at different ranges.



**Figure 2.3.8 Distribution of detected source RF power at several ranges.**

Note how the closest range sources with power of less than -10 dBW can be detected whereas at distances of 100 km these sources are not detected anymore. But to quantify the number of sources under a certain power level, cumulative distributions are more useful. From figure 2.3.9 we can see that the population of sources below -10 dBW represents about 15 % of the sources of those flashes detected at close range. The plot also shows that below 150 km the sensitivity is about -8 dBW and above. That means that a 20 % of the low power sources will not be detected at that range.



**Figure 2.3.9 Cumulative distribution of detected source RF power at several ranges.**

Adopting the threshold of 3 dBW where most of the sources are, figure 2.3.10 shows the spatial distribution of the fraction of the <3 dBW sources in flashes.

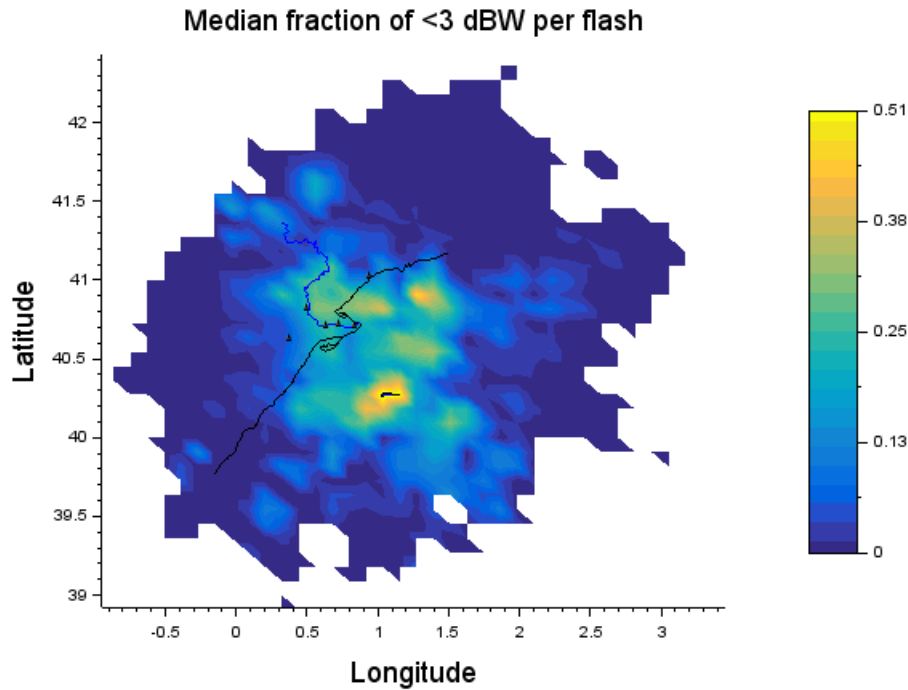
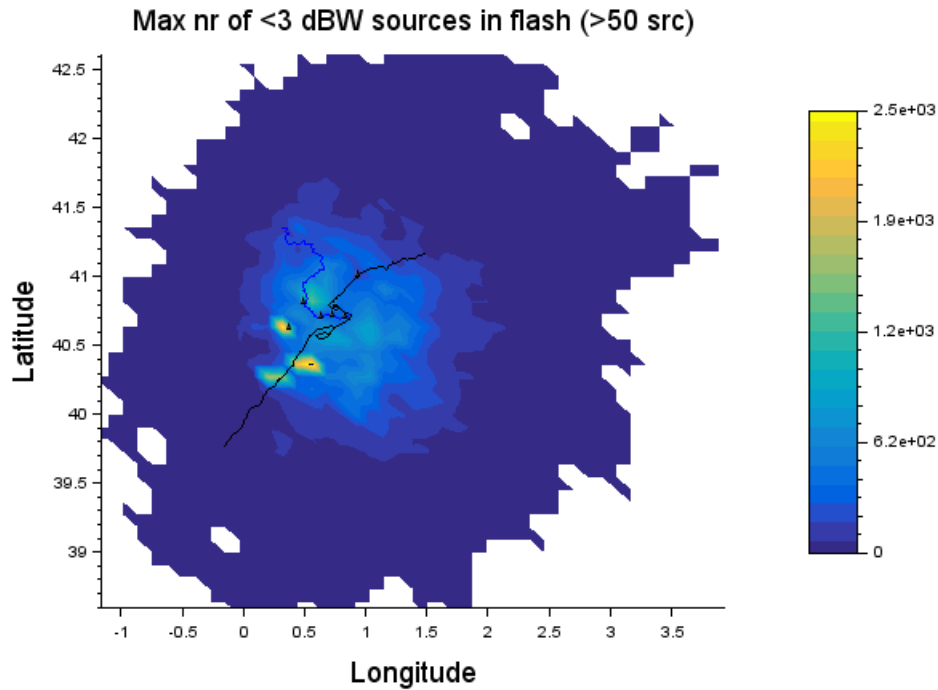


Figure 2.3.10 Median fraction of a flash with low power emissions (positive leaders).

The higher the fraction, the better detected is the contribution of positive leader activity with removes negative charge from the cloud. This can be important for detection efficiency of negative cloud to ground flashes. The quality appears good in the area directly northwest of the network center, as well as the nearby Mediterranean Sea, especially within about 60-80 km radius (but not toward the west). The result may be affected to some extent by the type of thunderstorms that occurred.



**Figure 2.3.11 Maximum number of low power sources in a flash (positive leaders)**

The plot in figure 2.3.11 shows how the number of sources with <3dBW are detected within 100 km from the center of the network.

A more useful map to define the best performance region of the E-LMA is computed by the sensitivity regions to certain power levels (figure 2.3.12). For each grid cell, the minimum detected power corresponding to the indicated levels is assigned. This map can be produced for long and short periods of time. Long periods would offer average sensitivity whereas short periods can include the effect of missing stations in a particular day/episode and noise variation.

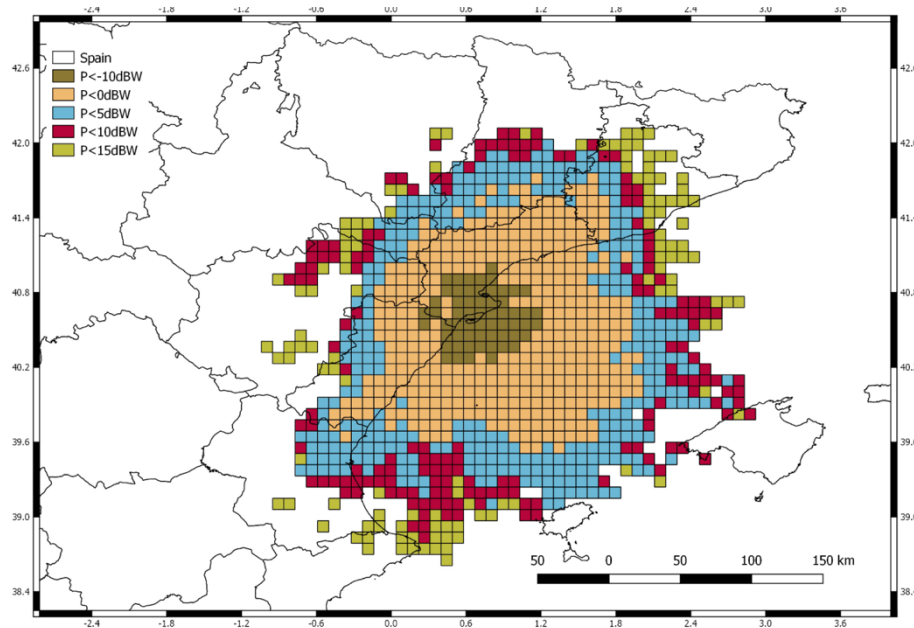


Figure 2.3.12 Sensitivity area of the Ebro-LMA for a specific dataset (5 days of data with 65262 flashes).

### 2.3.2.6 Maximum number of sources per flash

The number of sources per flash is probably the most important and relevant indicator of the LMA performance with distance.

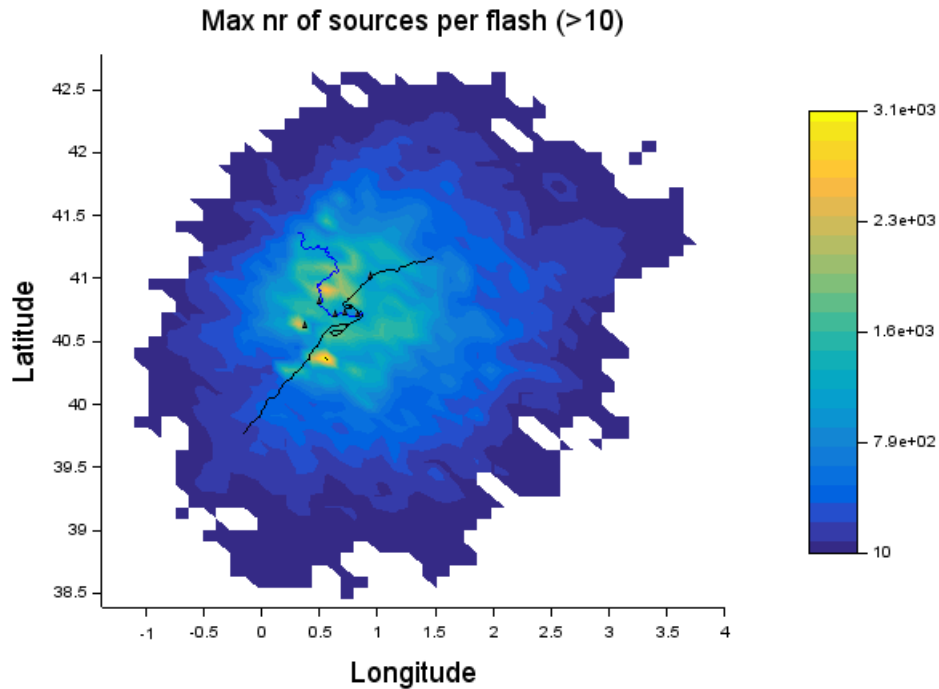
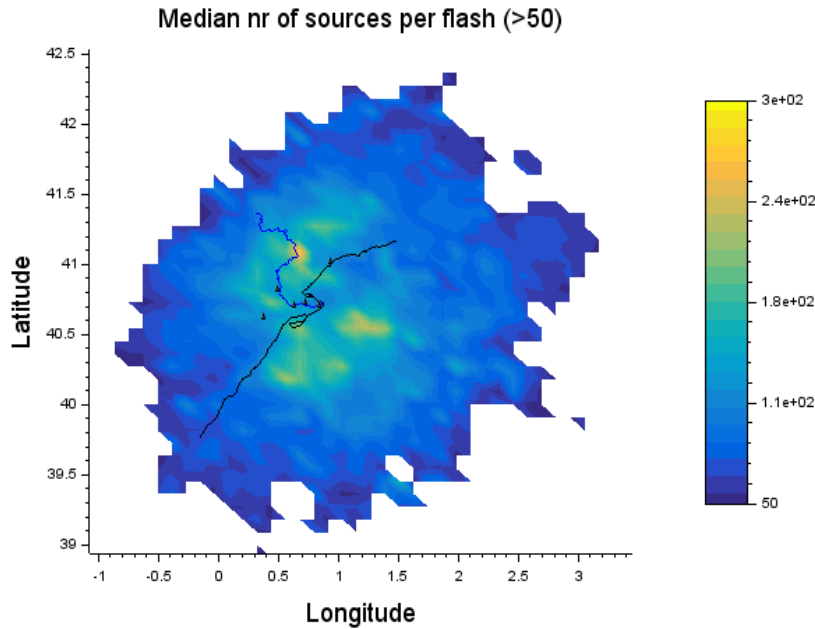


Figure 2.3.13 Maximum number of sources in a flash.

This map shows how many sources (per 10x10 km) can be detected at maximum. The closer the more detail can be provided, with zones of about 60 km radius, then 100 km, and beyond that, never more than a few hundred sources can be detected for a flash.



**Figure 2.3.14 Maximum number of sources in a flash.**

The median shows like a circle with exception of the north and northeast of the Ebro Delta, where numbers are low, but perhaps depends on thunderstorm characteristics that occurred with very small flashes, or more noise (less apparent in >50 src plot).

### 2.3.2.7 Minimum source altitude

It is well known that the minimum source altitude detectable for the LMA depends on the line-of-sight. That can be seen in figure 2.3.15.

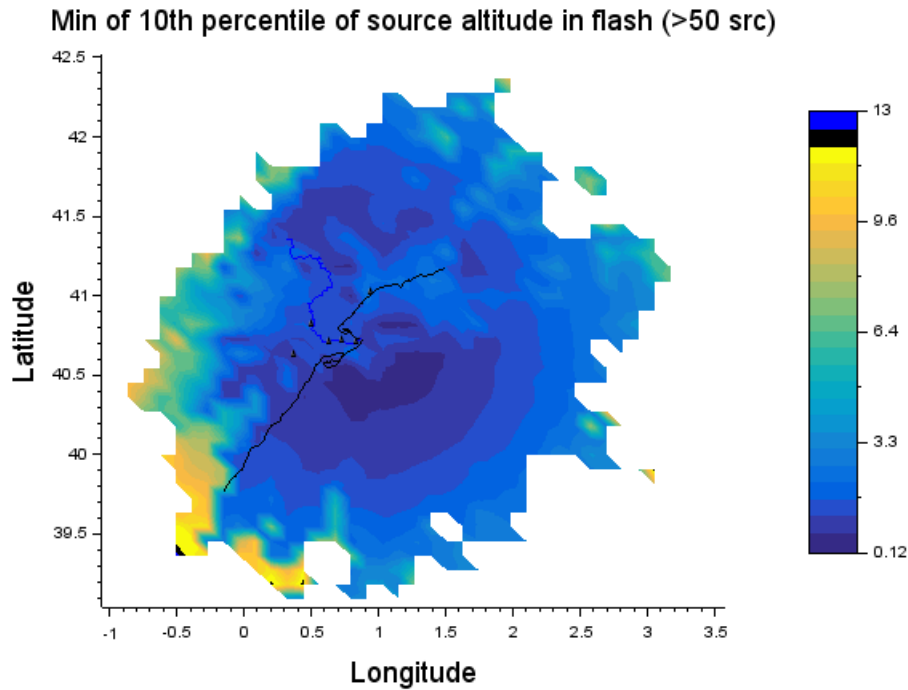
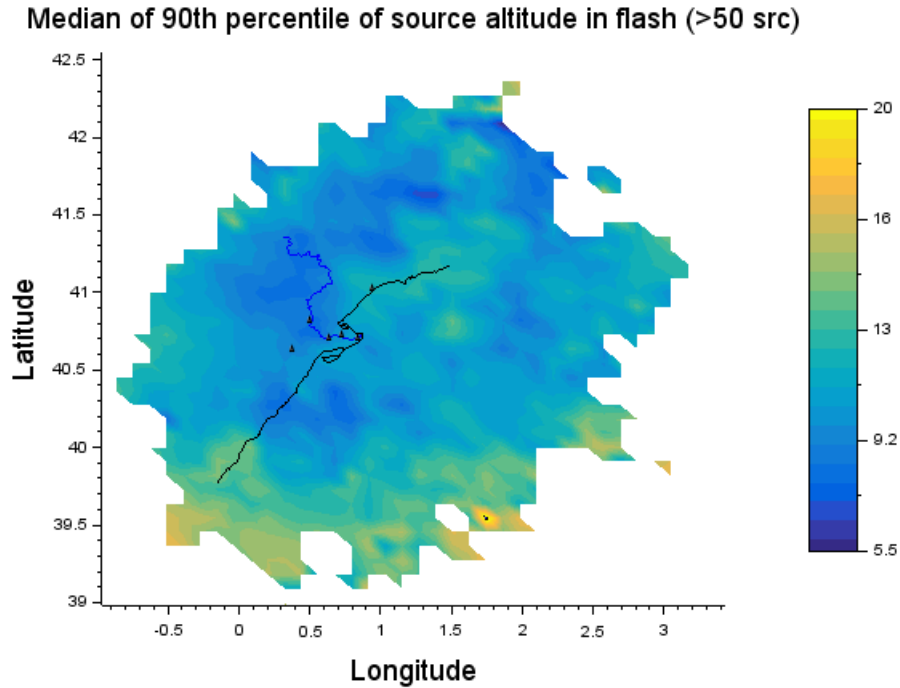


Figure 2.3.15 Minimum altitude of lowest part of flashes.

Here we see the absolute lowest source altitudes than can be seen by LMA. The circular part is due to horizon curvature. West and southwest are more blocked by mountains, while also the coast near Tarragona is more blocked for probably the westernmost stations.

### 2.3.2.8 Detection of sources at high altitudes

As theoretically calculated in the section 2.3.1, the highest the location of the source the better can be detected. Figure 2.3.16 shows the altitude analysis of the highest percentile of source altitude.



**Figure 2.3.16 Median 90<sup>th</sup> percentile of source altitudes.**

In the E-LMA region, most of the sources are typically located below 12 km and, in some cases they reach heights of 14 km. In the figure, we see how the altitude errors increase at distances of more than 100 km (S-E).

### **2.3.3 Sensitivity analysis**

From the plots presented in the previous section (2.3.2), averaged values at given distances have been determined. These are presented in the next figures.

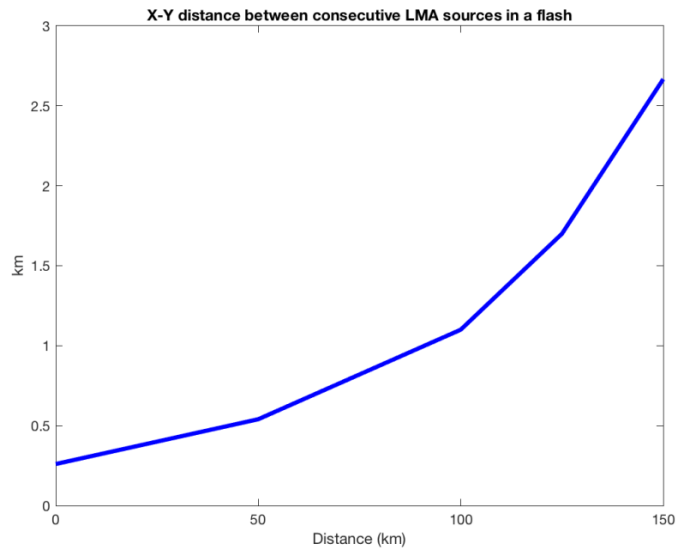


Figure 2.3.17 Distance X-Y between consecutive sources versus distance to the center of the E-LMA.

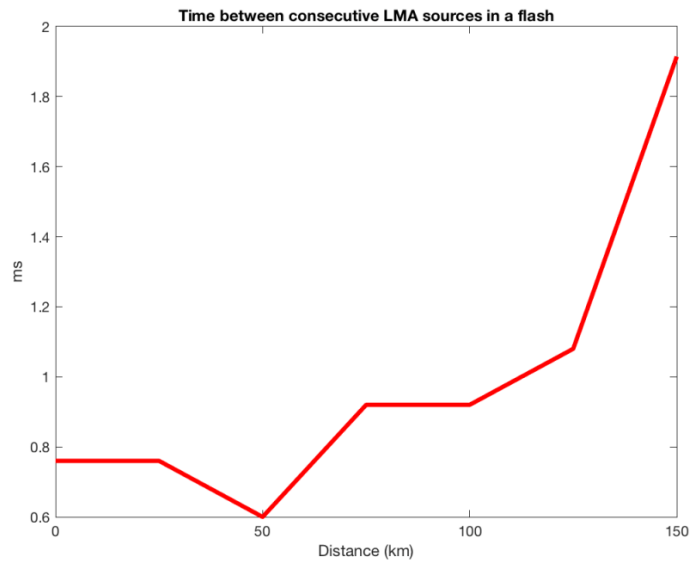


Figure 2.3.18 Time between consecutive sources versus distance to the center of the E-LMA.

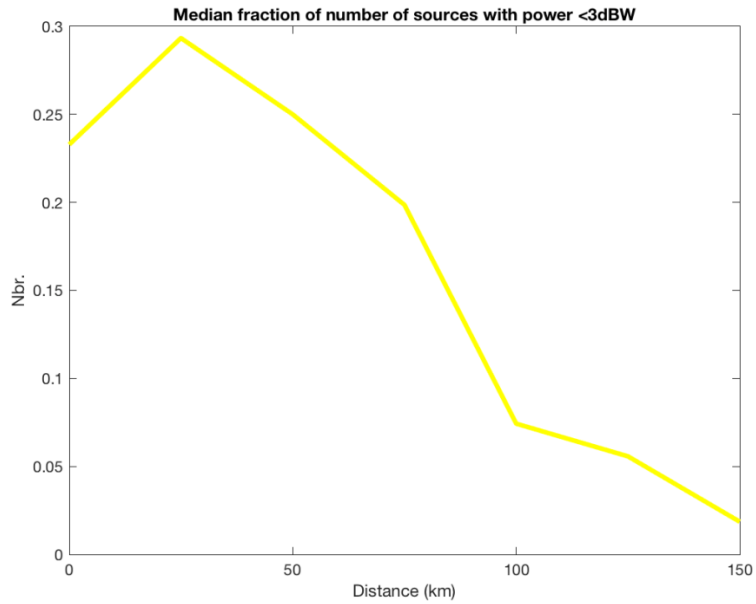


Figure 2.3.19 Median fraction of the number of sources with power levels <3 dBW versus distance to the center of the E-LMA.

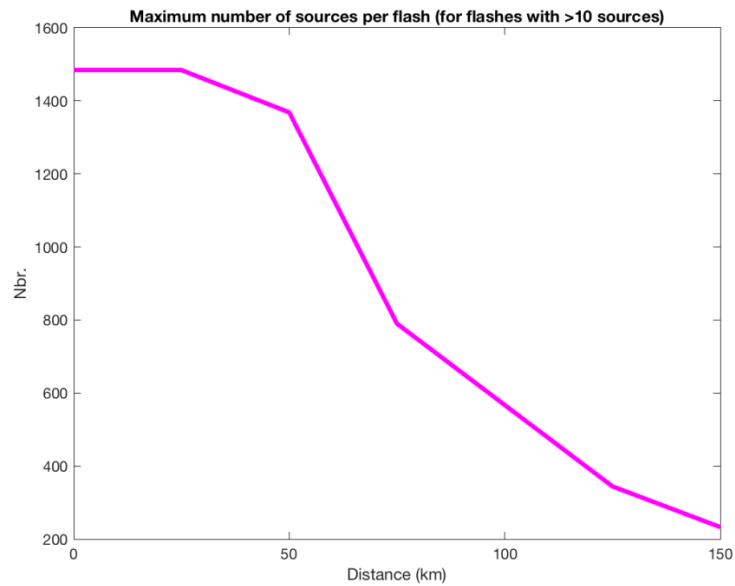


Figure 2.3.20 Maximum number of sources versus distance to the center of the E-LMA.

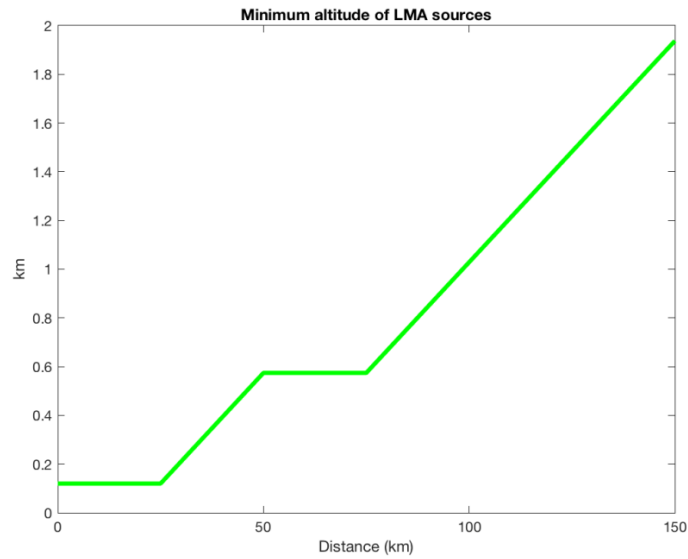


Figure 2.3.21 Minimum altitude Z of the LMA sources versus distance to the center of the E-LMA.

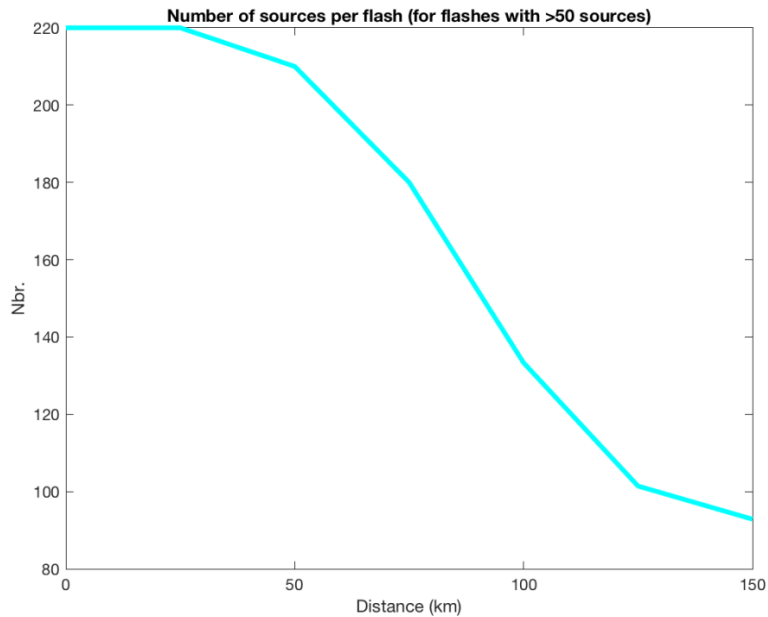
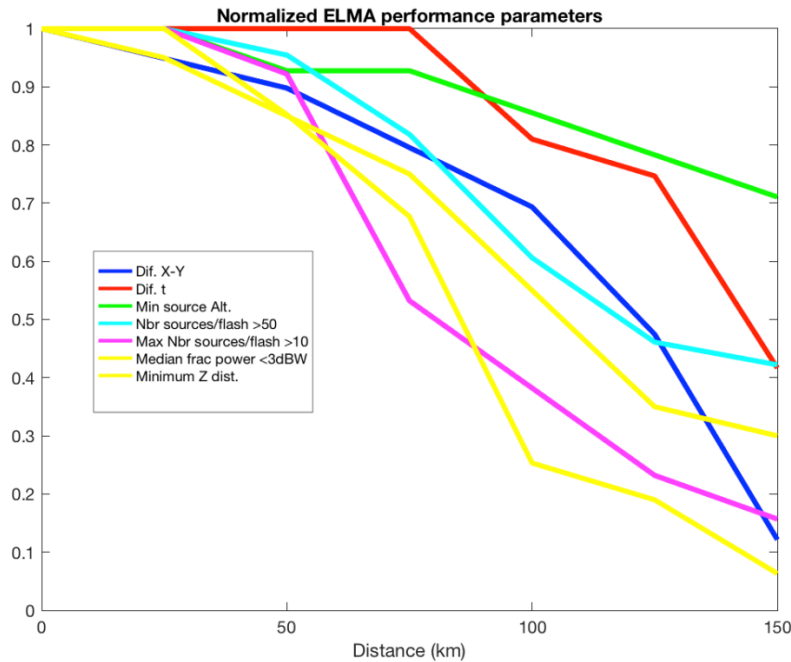


Figure 2.3.22 Number of sources per flash versus distance to the center of the E-LMA.

For each parameter that has been shown in the previous figures, the values at the center of the E-LMA network and the maximum values obtained in the plots of the previous section (2.3.2) are summarized in the following table.

Parameter	Value at the center	Maximum value
X-Y Distance between consecutive sources	0.26 km	3 km
Median Z distance between consecutive sources	0.167 km	3.5 km
Minimum Z altitude of LMA sources	0.120 km	6.4 km
Time difference between consecutive sources	0.001 ms	3 ms
Number of sources per flash	220	228
Maximum number of sources per flash	1484	2067
Median fraction of number of sources with power < 3dBW	0.23	0.51

The values at the center of the network are adopted as reference (or best). Now, the parameters are normalized respect the center values of the E-LMA network and their maximums. Figure 2.3.23 presents the normalized parameters.



**Figure 2.3.23 Normalized ELMA performance parameters versus distance to the center of the network.**

To determine the distance to consider in this study (target area) is necessary to add the ISS-LIS flashes (figure 2.3.24).

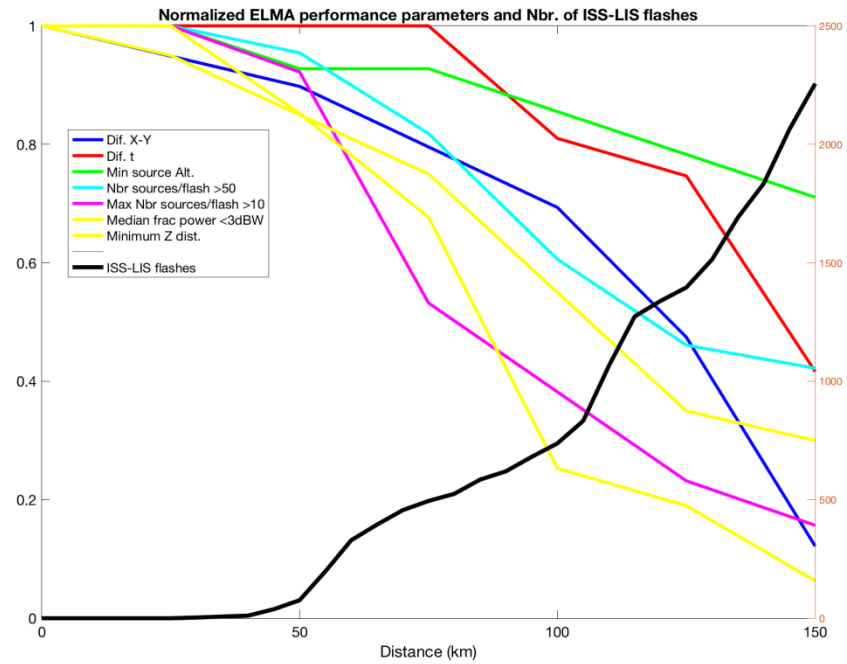


Figure 2.3.24 Normalized E-LMA performance parameters and the number of ISS-LIS flashes to the center of the network.

The seven parameters might be grouped forming the RMS performance of the network:

$$RMS = \sqrt{\frac{1}{N} \sum U_j^2}$$

where N is the number of  $U_j$  parameters. The resulted RMS performance is depicted in figure 2.3.25.

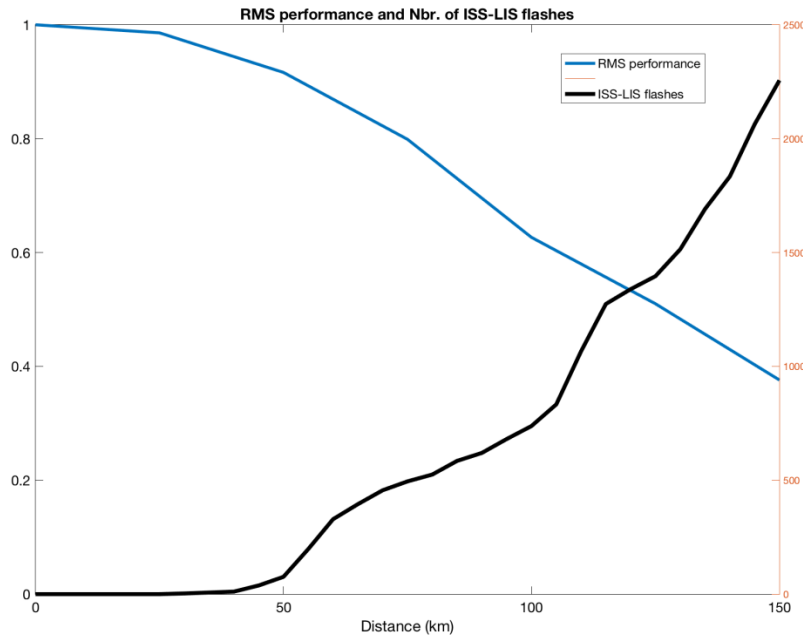


Figure 2.3.25 RMS performance of the E-LMA (all parameters) shown and the number of ISS-LIS flashes to the center of the network.

But the parameters included have not the same importance in the performance of the network. That is the parameter related to the power of the received sources. That decrease fast but the effect to the number of sources is not dramatic. Also, the location accuracy, although it decreases, its maximum values are at the range of the one or two km. To be conservative we decided to use the number of sources as the critical parameter. In such case the performance of the E-LMA and the number of ISS-LIS flashes are plotted in figure 2.3.26.

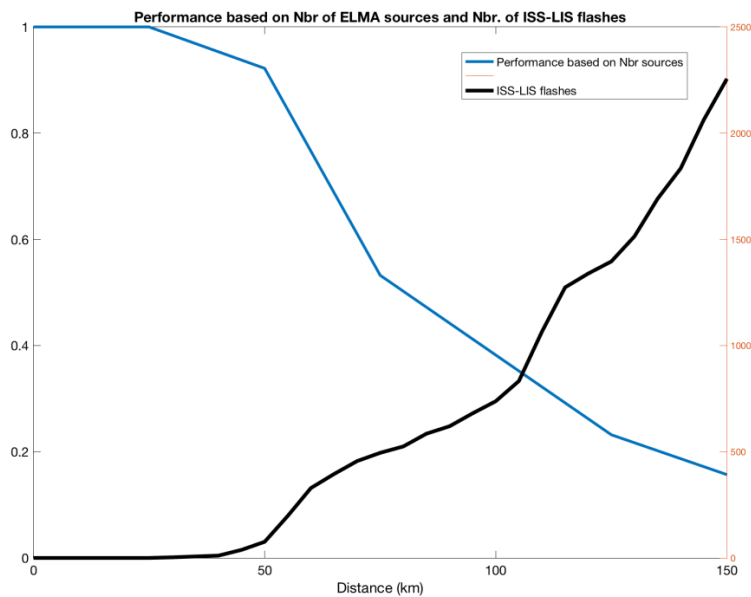
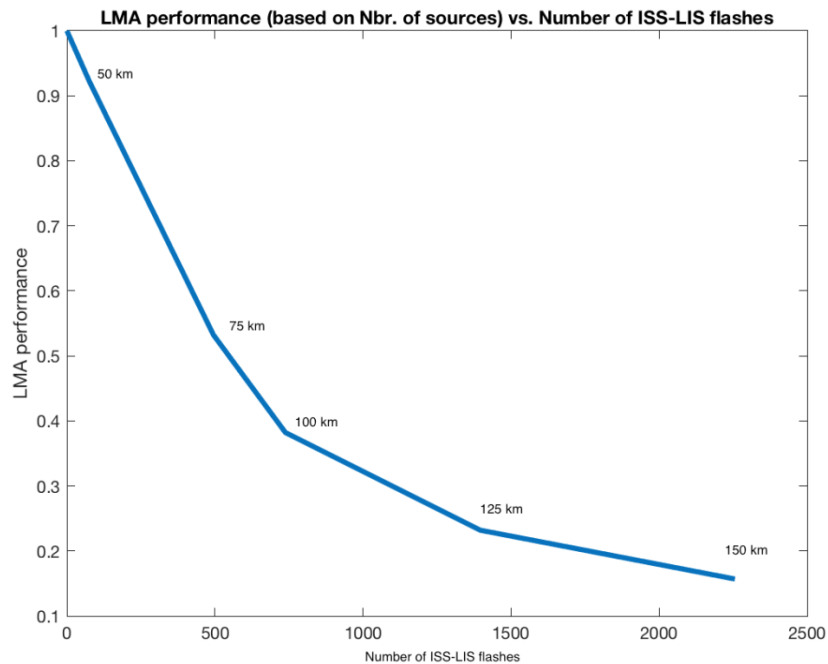


Figure 2.3.26 Performance of the E-LMA in terms of number of sources and the number of ISS-LIS flashes to the center of the network.

Finally, the sensitivity analysis concludes with a graph of the LMA performance versus the number of ISS-LIS flashes (figure 2.3.27).



**Figure 2.3.27 E-LMA performance based on the number of sources versus the number of ISS-LIS flashes.**

## 2.4 Conclusions

We have investigated the performance of the E-LMA based on several parameters:

- Distribution of source-source time.
- Distribution of source-source x-y distance.
- Distribution of source-source z distance.
- Distribution of flash duration.
- Distribution of source power.
- Number of sources per flash.
- Minimum source altitude.

These parameters have been evaluated using E-LMA data for the coverage area corresponding to the period of analysis with the same network configuration. Performance of the E-LMA is used to define the analysis area in order to maximize the number of ISS-LIS flashes:

- Considering a range of 50 km the number of ISS-LIS flashes is low (76) but the performance is over 90%.
- At 75 km the performance (conservative approach) of the LMA decays to 54 % but the number of ISS-LIS flashes grows to 498.

- Beyond 75 km, the most significant increase of ISS-LIS flashes occurs between 100 to 125 km where the number of ISS-LIS flashes reaches ~1400.
- Although a performance of 50 % might look dramatic, the high number of sources that the LMA provides is still good enough to evaluate the ISS-LIS.

In this study we define:

- From the performance analysis, the best performance region is defined by: longitude  $0.4^{\circ}$  to  $1.5^{\circ}$  and latitude  $40.1^{\circ}$  to  $41.4^{\circ}$ .
- To maximize the number of ISS-LIS events, the range shall be limited to <150 km. This extended range can be used for some analysis such as flash detection efficiency.

After the evaluation presented in section 4 and the methodology escribed in section 6, we propose the use of the power criteria as the most convenient performance indicator. The advantages that support the use of the power criteria (or sensitivity) are:

- A full picture of a lightning flash needs the detection of positive and negative leaders.
- VHF RF power of sources of negative leaders is typically higher than sources related to positive leaders.
- Sensitivity is highly related to the detection of positive leaders.
- Power levels might be characteristic of each LMA network. But the analysis of power levels produced by negative and positive leaders will allow the determination of the required sensitivity.
- The sensitivity of the LMA in a particular region depends on the network configuration and noise levels at a given moment.
- Regions of sensitivity can be easily produced using by a gridded approach.
- Sensitivity maps can be generated for each day or thunderstorm episode.

Figure 2.3.12 has shown an example of the sensitivity areas. Later, in section 6 the use of these maps as criteria to define the evaluation area is defined.

## 2.5 Description of the key properties of the dataset

The following table presents the number of ISS-LIS flashes for a given range to the center of the E-LMA and the available data.

Range	Number of ISS-LIS flashes	Dates of occurrence	Number of ISS-LIS flashes per date	Availability of ELMA data	Number of expected comparable flashes
<50 km	76	20170424	1	-	74
		20171018	15	20171018	
		20180917	1	20180917	
		20180918	40	20180918	
		20181010	2	-	
		20181018	17	20181018	
< 75 km	495	20170424	1	-	398  (402 including data to be processed)
		20170628	7	-	
		20170708	1	-	
		20170917	4	-	
		20171018	20	20181018	
		20180427	4	20180427	
		20180429	2	20180429 NP	
		20180525	1	20180525 NP	
		20180605	1	20180605	
		20180613	1	20180613 NP	
		20180716	1	-	
		20180809	15	20180809	
		20180822	2	20180822	
		20180831	3	20180831	
		20180917	8	20180917	
		20180918	322	20180918	
		20181010	2	-	
20181014	77	-			
20181018	23	20181018			
				NP: available but not processed	
< 100 km	738	20170424	1	-	578  (593 including data to be processed)
		20170615	5	-	
		20170628	7	-	
		20170708	2	-	
		20170805	3	-	
		20170917	7	-	
		20171018	22	20171018	
		20171129	1	-	
		20180427	8	20180427	
		20180429	2	20180429 NP	
		20180525	2	20180525	
		20180605	2	20180605	
		20180606	2	20180606	
		20180613	1	20180613 NP	
20180716	3	20180716 NP			

		20180807	5	20180807 NP	
		20180809	78	20180809	
		20180811	4	20180811 NP	
		20180822	2	20180822	
		20180823	2	20180823	
		20180831	68	20180831	
		20180904	4	-	
		20180910	27	-	
		20180917	14	20180917	
		20180918	349	20180918	
		20181008	7	-	
		20181010	2	-	
		20181014	79	-	
		20181018	29	20181018	
< 125 km	1396	20170424	1	-	1055
		20170529	10	-	
		20170604	220	20170604	(1144 including data to be processed)
		20170615	23	-	
		20170625	2	-	
		20170628	7	-	
		20170708	2	-	
		20170721	2	-	
		20170805	4	-	
		20170827	30	-	
		20170831	1	-	
		20170917	7	20170921 NP	
		20170921	1	-	
		20171018	47	20171018	
		20171110	4	-	
		20171129	1	-	
		20180427	36	20180427	
		20180429	2	20180429 NP	
		20180509	10	20180509 NP	
		20180525	6	20180525	
		20180530	2	20180530	
		20180604	1	20180604 NP	
		20180605	6	20180605	
		20180606	2	20180606	
		20180609	8	20180609 NP	
		20180613	1	20180613 NP	
		20180623	2	-	
		20180627	6	20180627	
		20180712	5	20180712 NP	
		20180716	3	20180716 NP	
		20180807	12	20180807 NP	
		20180809	82	20180809	
		20180811	4	20180811 NP	
		20180812	3	20180812 NP	
		20180822	2	20180822	
		20180823	2	20180823	
		20180831	252	30180831	
		20180904	5	-	
		20180905	4	20180905	
		20180910	57	-	

		20180915	2	-	
		20180917	15	20180917	
		20180918	373	20180918	
		20181008	14	-	
		20181010	2	-	
		20181014	82	-	
		20181018	33	20181018	

### 3. Definition of the evaluation of the ISS-LIS using the LMA

The parameters that will be computed to evaluate ISS-LIS are defined. ISS-LIS is evaluated versus the E-LMA which is assumed to be the reference network. The evaluation has two parts. The first part corresponds to the typical metrics of performance of lightning location systems whereas the second part is focused to understand lightning leader processes related to ISS-LIS detections.

The parameters that will provide the evaluation of ISS-LIS are introduced in the next table:

Parameter	Section	Method	Evaluation
Flash Detection Efficiency (FDE)	4.1	<p>LMA is the reference.</p> <p>A flash is detected by the ISS-LIS if there is at least one ISS-LIS event during the duration of the corresponding LMA flash. A distance criterion is also included.</p> <p>Only LMA flashes that have been located within the FOV of ISS-LIS are considered.</p> <p>The range to consider will be up to 150 km</p> <p>LMA flash data is used (LMA level-2 data)</p>	<p>Qualitative maps of ISS-LIS flashes and LMA flashes.</p> <p>Fraction of LMA flashes detected by ISS-LIS versus the total number of LMA flashes in the FOV of ISS-LIS.</p> <p>Flash Detection Efficiency versus maximum height of LMA flashes.</p> <p>Number of ISS-LIS flashes per LMA flash.</p> <p>Number of ISS-LIS events per LMA flash.</p> <p>Distribution of number, power and height of LMA sources for thus flashes detected and not detected by ISS-LIS.</p>
Flash False Alarm (FFAR)	4.1.6	<p>Flashes reported by ISS-LIS without corresponding LMA flashes.</p> <p>First, false alarm (FA) candidates are identified.</p> <p>FA candidates are then verified to LMA source data (LMA level-1 data).</p> <p>After comparison of LMA level-1 data, still remaining candidates will be analyzed in terms of distance to the network, status of the network and LMA level-0 data (raw data).</p>	<p>Number of ISS-LIS false alarm.</p>

Flash duration (FD)	4.2	Duration of LMA flashes. Duration of ISS-LIS flashes.	Statistics on the duration of LMA and ISS-LIS flashes.  Distribution of ISS-LIS events within LMA flashes.  Fraction of the ISS-LIS event at the start of the flash. Fraction of ISS-LIS duration versus LMA duration.
Radiance	4.4	Analysis of the radiance of ISS-LIS events versus LMA sources.	Radiance versus LMA height and LMA power.
Location Accuracy (LA)	4.5	Analysis performed using a gridded approach. Grid cell size corresponding to the ISS-LIS average pixel size.  LMA data is gridded. Each LMA gridded flash will be compared with the ISS-LIS events.	Offset of LMA flash and ISS-LIS flash centroids: lat, lon and absolute.  Statistics on the fraction of matched LMA and ISS-LIS cells per flash.  Statistics on the area of LMA flashes and ISS-LIS flashes.

To investigate what ISS-LIS detects within a lightning flash, the following parameters will be analysed:

Parameter	Section	Evaluation
Flash occurrence altitude	4.1.3	Height of LMA sources for those flashes detected and not detected by ISS-LIS
	4.3.2	Distribution of the height of the LMA sources related and not related to ISS-LIS events.
LMA power	4.1.3	Power of LMA sources for those flashes detected and not detected by ISS-LIS.
	4.3.3	Distribution of the height of the LMA sources related and not related to ISS-LIS events.
ISS-LIS radiance	4.2.3	Distribution within a flash of event radiance.

## 4. Evaluation of ISS-LIS

### 4.1 Flash detection efficiency

In this section the flash detection efficiency ( $DE_f$ ) of ISS-LIS will be determined based on the comparison with the Ebro-Lightning Mapping Array (E-LMA).

#### 4.1.1 Methodology for $DE_f$

The method for the  $DE_f$  compares the flash detections provided by the E-LMA with the detections of ISS-LIS. The diagram in figure 4.1.1 describes the methodology employed.

LMA flashes are adopted as reference, so a  $DE_f$  of 100 % is assumed. To evaluate  $DE_f$  of any lightning detection system it is important to define a lightning flash for each system. LMA solutions are called sources and these need to be grouped in flashes. The criteria employed here is the one used by *van der Velde and Montanyà* (2013). In this reference, LMA sources belong to a flash if they are detected in a group isolated at least 150 ms from the previous and the subsequent flash. Within a flash, sources are inspected and qualified to pertain to a flash if a distance criterion is met (see section 1.2.1).

The method starts with filtering the flashes of ISS-LIS and LMA outside a range. In this analysis a range up to 150 km has been considered. Once ISS-LIS and LMA are filtered, for each LMA source it is determined if it was visible (in the field of view, FOV) of ISS-LIS. To do that, the information within ISS-LIS *hdf* files of *Location* from the *View Parameters* are used. With that, for each 0.5 LAT x 0.5 LON grid cell the *view time start* and *view time end* are determined. A LMA source was in the FOV of ISS-LIS if its time of occurrence was within the *view time start* and *view time end* for the corresponding location within its 0.5 LAT x 0.5 LON cell.

An LMA flash is considered to have been detected by ISS-LIS if ISS-LIS have at least one event within  $\pm 0.1$  s (T) from the start and end of the LMA flash. To ensure that these ISS-LIS events belong to the same LMA flash, a distance criterion (D) of 50 km is used.

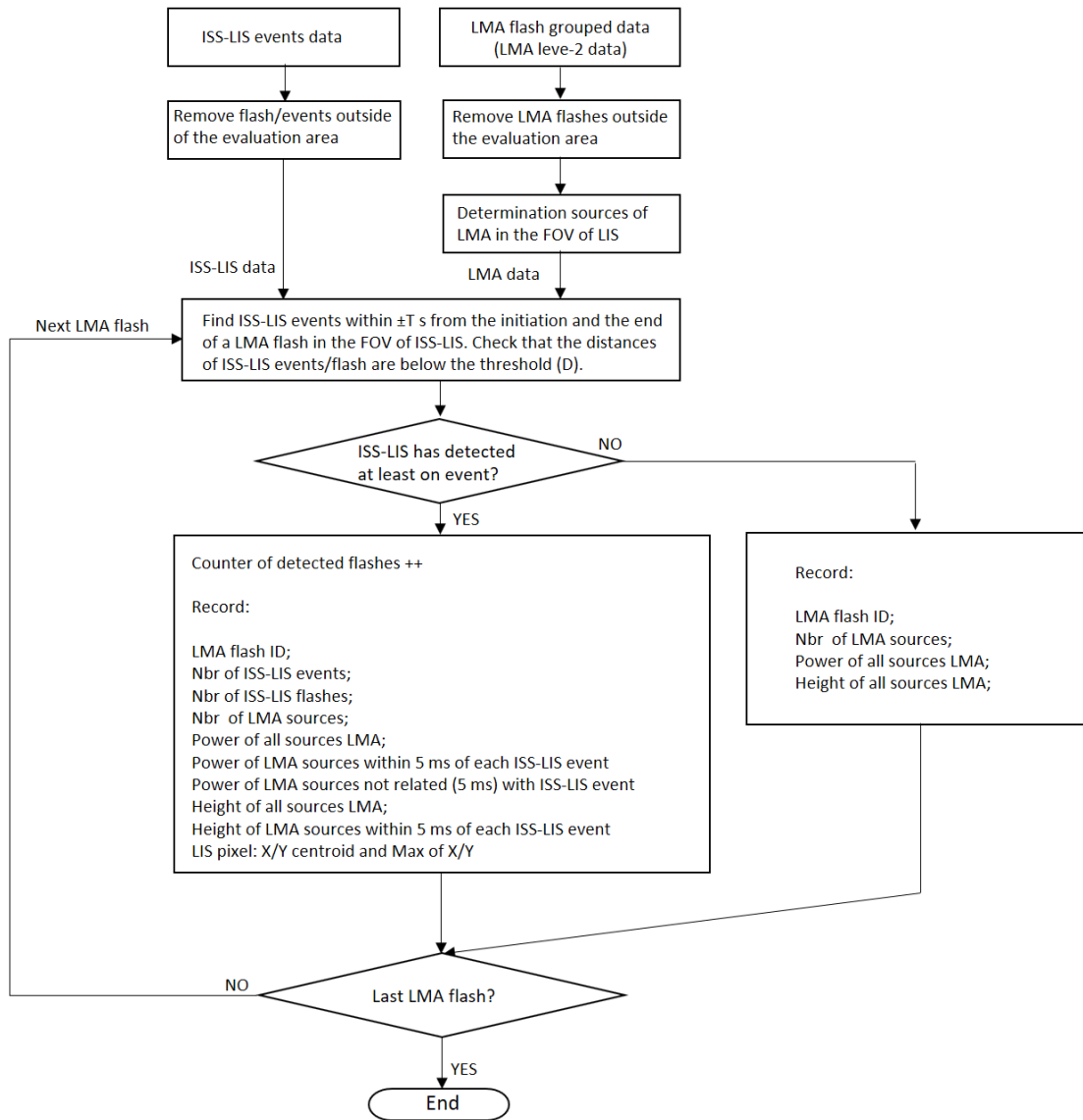


Figure 4.1.1 Diagram of the  $DE_f$  computation

In the case that ISS-LIS detected a LMA flash, a counter is increased (to compute the  $DE_f$ ). Data related to the VHF RF power, height, ISS-LIS pixels etc (see figure 4.1.1) is saved for analysis. In the case that ISS-LIS has not detected a LMA-flash, the counter is not increased and additional data is saved (see figure 4.1.1). Finally, the  $DE_f$  is computed as:

$$DE_f = \frac{\text{Nbr of LMA flashes detected by ISS - LIS}}{\text{Total number of LMA flashes}}$$

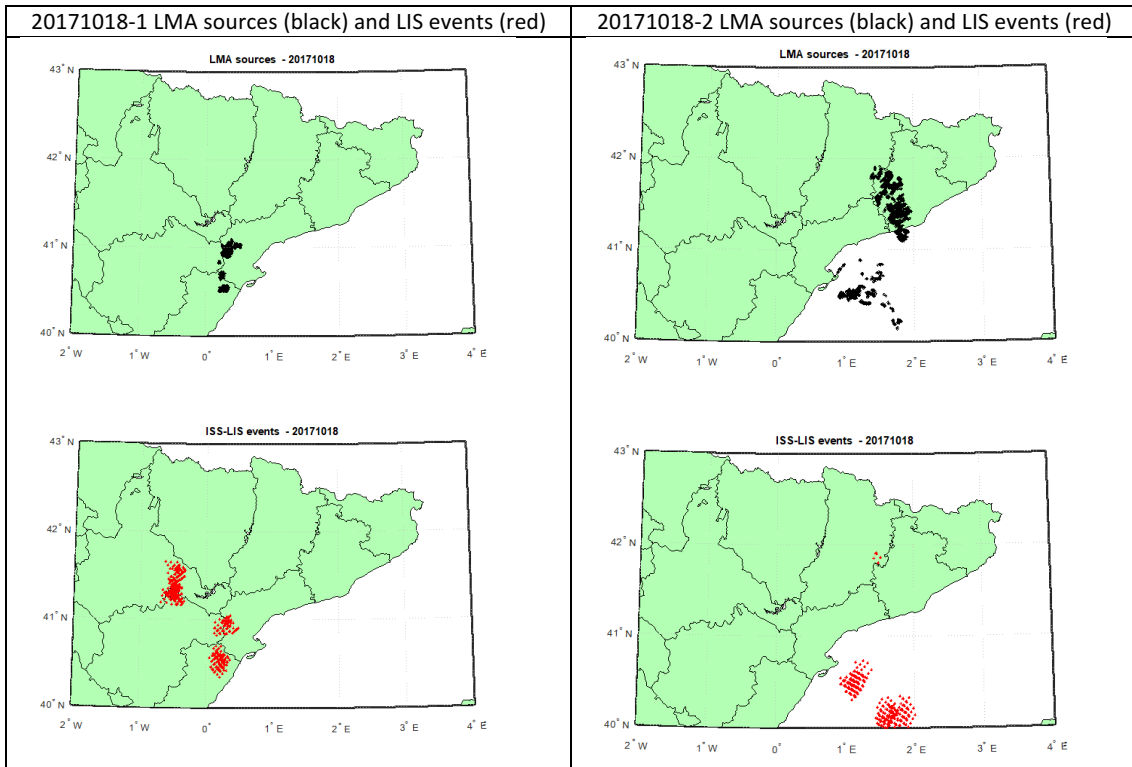
Output data of  $DE_f$  can be used later for post-processing and investigate other ISS-LIS parameters such as the flash grouping criteria, etc. In addition,  $DE_f$  output data will be useful and used as input to evaluate other parameters such as false alarms.

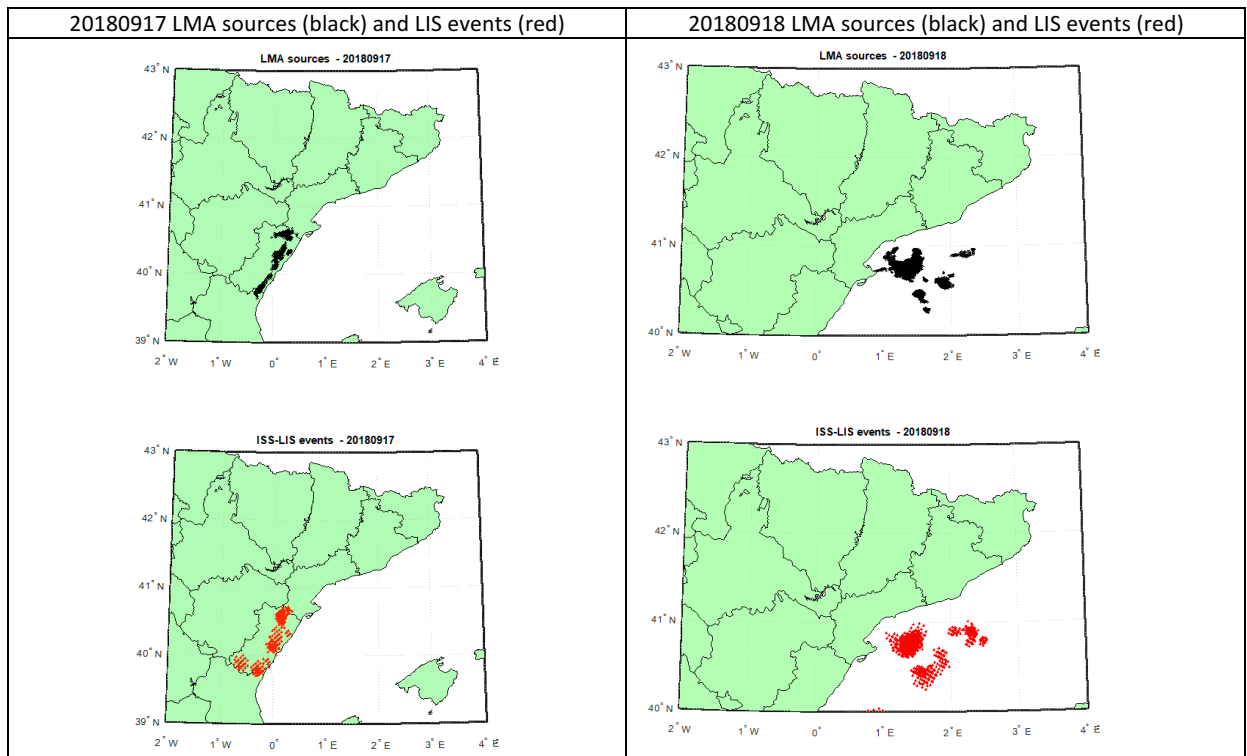
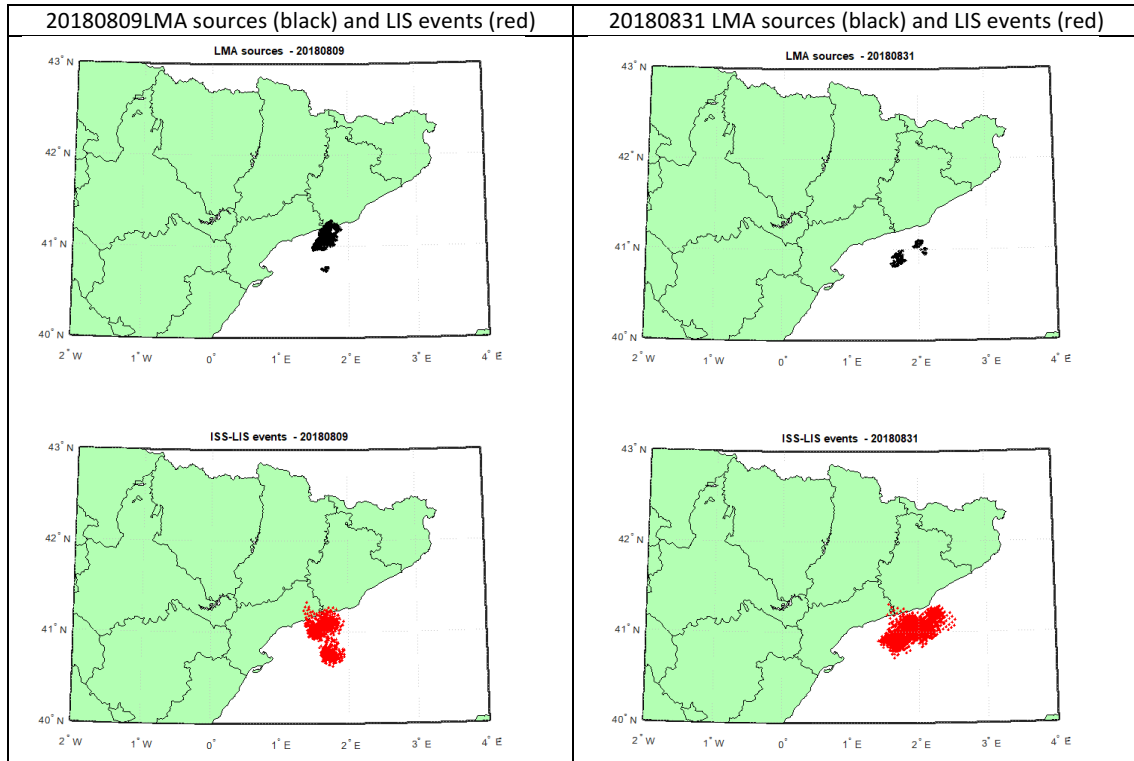
#### 4.1.2 Comparison criteria and data

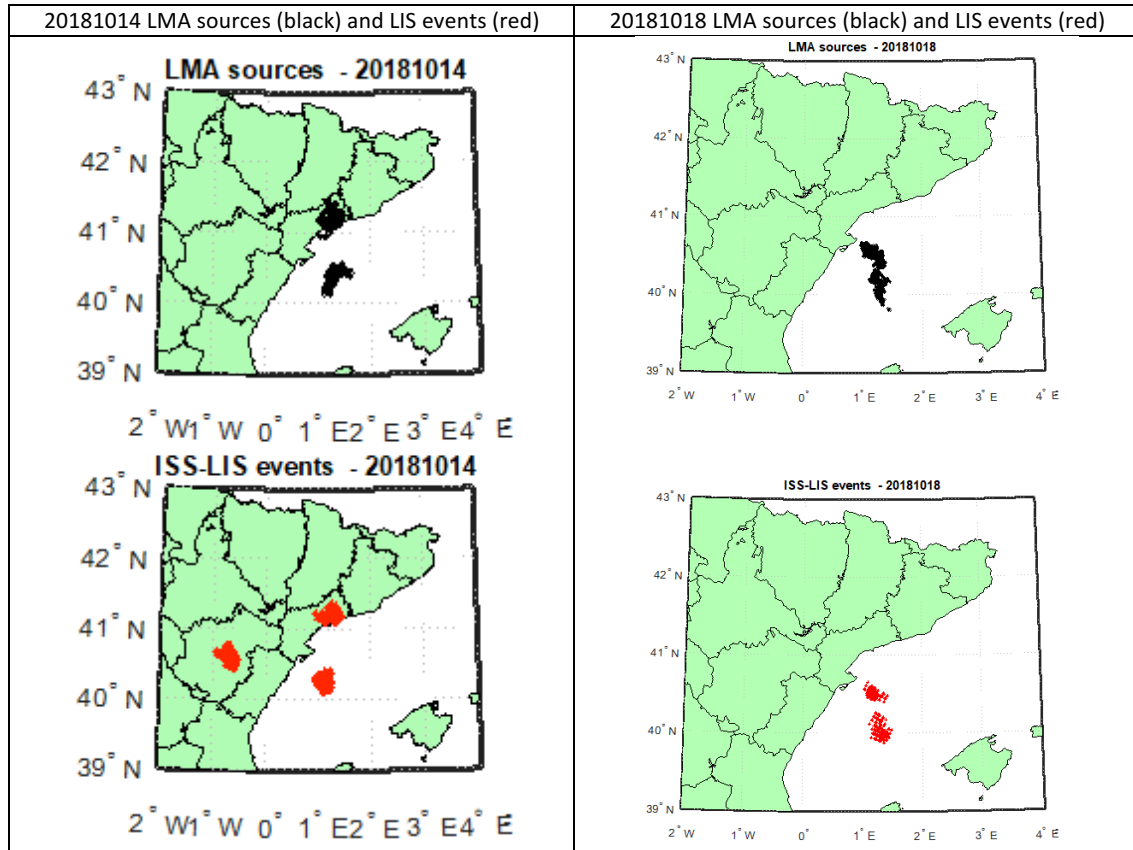
The following table summarizes the criteria for the determination of the  $DE_f$ .

Investigated range	$\leq 150$ km
Time tolerance (T)	$\pm 0.1$ s
Minimum number of ISS-LIS events to detect a flash	1
Total number of episodes	8
Number of episodes occurring at night time	1
Allowed distance between centroids of ISS-LIS and LMA flashes (D)	50 km

Qualitatively is convenient to inspect the maps of LMA and ISS-LIS detections. The maps below show the LMA and ISS-LIS detections for the 8 analysed episodes.





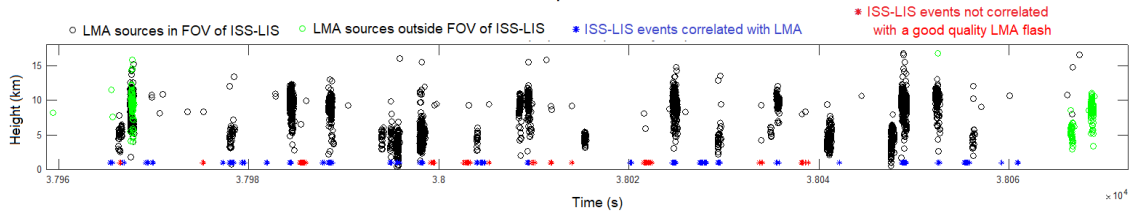


#### 4.1.3 Results of $DE_f$

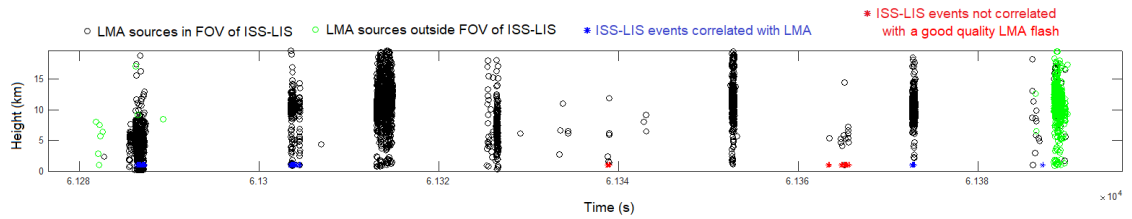
The previous maps have shown good agreement between the lightning locations provided by the ISS-LIS and the LMA. From a simple inspection we can see how some ISS-LIS detections (red), e.g. eastern storm cell on 20181014, are not reported by the LMA (black). The location of these ISS-LIS flashes is not resolved by the LMA because occur in a region out of the range of the LMA (e.g. see figure 2.3.12).

Figure 4.1.2 shows the time occurrence of the eight analysed thunderstorm episodes. LMA sources are plotted by circular markers. Black circles correspond to LMA sources that have occurred in time and location within the FOV of ISS-LIS whereas the green ones are those occurring in time and location outside the FOV of ISS-LIS. Events of ISS-LIS are plotted in asterisks where blue colour asterisks are associated to a LMA flash. Red asterisks are associated to LMA sources of flashes detected with poor quality. These flashes commonly occur at distances far from the LMA network (e.g. >100 km).

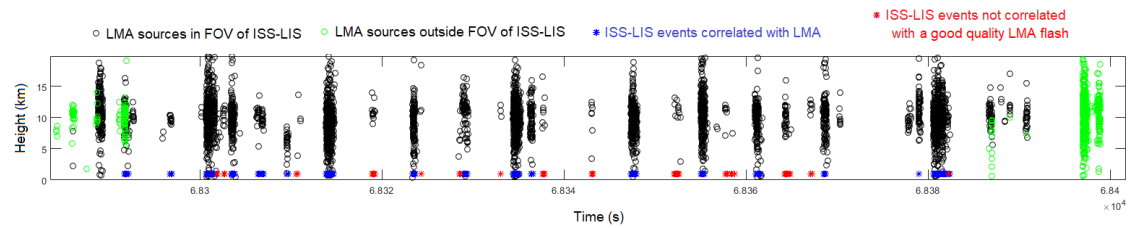
20171018 pass 1



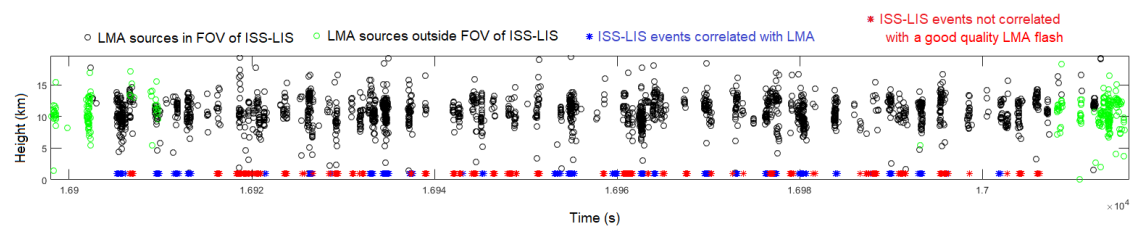
20171018 pass 2



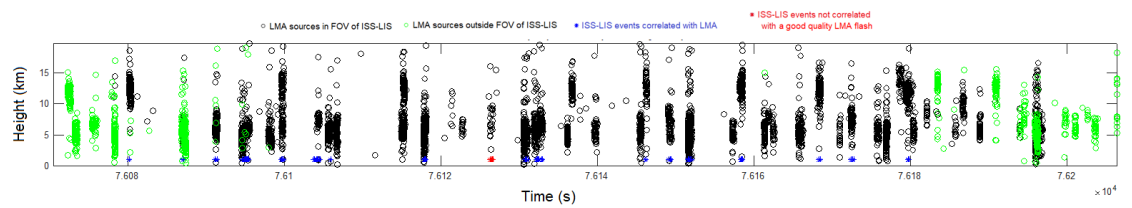
20180809



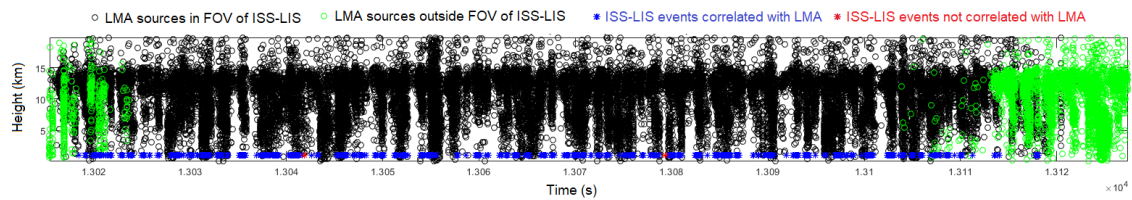
20180831



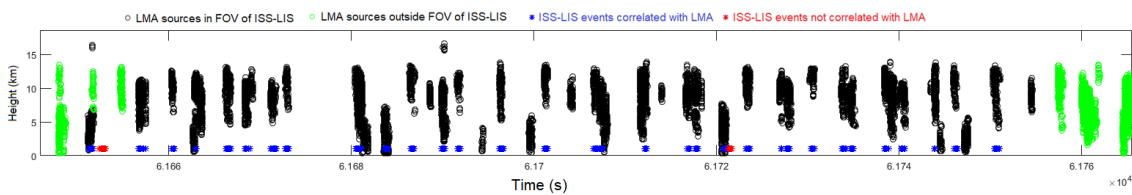
20180917



20180918



20181014



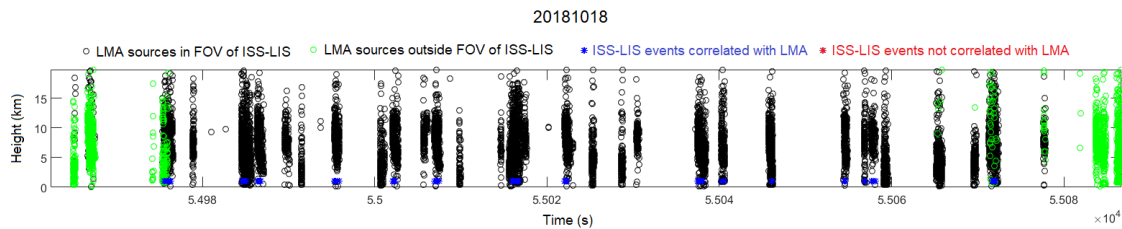


**Figure 4.1.2 Examples of the LMA sources and LIS events. LMA sources are colored in black if are within the FOV of ISS-LIS. Yellow LMA sources are those outside of the FOV of ISS-LIS.**

By visual inspection, the plots in figure 4.1.2 provides an idea of the detection efficiency of ISS-LIS for each episode as well some particularities. The episode of 20180918 presents extreme lightning activity that, in many cases, even the LMA cannot determine the start and end of an individual flash. The vertical flash extension of the LMA sources in 20181018, 20181014, 20180917, 20180918, 2018089 and 20171002-2 is indicative of the good quality of the LMA data in terms of lightning mapping because the close occurrence of the storms to the network. The case of 20180831 the LMA mostly detected the upper part of the flashes probably due to the distance of the storm (more than 100 km) or due to flashes occurring predominantly at high levels (unlikely).

The results for the individual episodes are summarized in the tables below. Each table presents the total number of flashes of the episode, the number of flashes that have been detected by ISS-LIS, the calculated  $DE_f$  and some comments. Results from three situations are presented:

- 1) All flashes in a range of 150 km with a minimum of 50 sources per flash. That restricts to high quality LMA flashes but, at the same time, it can remove small flashes.
- 2) All flashes in a range of 75 km with a minimum of 50 sources per flash. That restricts to high quality LMA flashes but, at the same time, it can remove small flashes.
- 3) All flashes in a range of 150 km without a minimum number of sources per LMA flash.

<b>Episodes with high quality LMA data: distance &lt; 150 km and more than 50 sources per flash</b>						
<b>Date</b>	<b>Number of flashes</b>	<b>Average flash rate [min<sup>-1</sup>]</b>	<b>Average LMA source rate [s<sup>-1</sup>]</b>	<b>Number of flashes detected by ISS-LIS</b>	<b>Detection Efficiency DE<sub>f</sub></b>	<b>Comments</b>
<b>20171018-1</b> ~10:30 UTC	13	8.7	41.5	9	0.69	
<b>20171018-2</b> ~17:00 UTC	8	4.6	49.8	3	0.37	The flashes occurred in the edge of the CCD.
<b>20180809</b> ~19:00 UTC	14	8.6	29.5	13	0.93	
<b>20180831</b> ~04:40 UTC	2	1.1	1.1	2	1	Not representative.
<b>20180917</b> ~21:10 UTC	24	12.3	32.4	15	0.62	
<b>20180918</b> ~03:30 UTC	62	35.1	301.4	57	0.92	Extremely active episode Night time. Average flash rates are not realistic since many flashes cannot be separated
<b>20181014</b> ~17:00 UTC	39	22.6	224.0	32	0.82	Moderate activity
<b>20181018</b> ~15:15 UTC	31	18.2	214.2	16	0.51	Moderate flash rate but quite active in terms of LMA sources
<b>Total number of LMA flashes: 193</b>						
<b>Total number of flashes detected by LIS: 147</b>						
<b>DE<sub>f</sub> = 0.76</b>						

<b>Episodes with high quality LMA data: distance &lt; 75 km and more than 50 sources per flash</b>						
<b>Date</b>	<b>Number of flashes</b>	<b>Average flash rate [min<sup>-1</sup>]</b>	<b>Average LMA source rate [s<sup>-1</sup>]</b>	<b>Number of flashes detected by ISS-LIS</b>	<b>Detection Efficiency DE<sub>f</sub></b>	<b>Comments</b>
<b>20171018-1</b> ~10:30 UTC	13	8.6	41.5	9	0.7	
<b>20171018-2</b> ~17:00 UTC	2	1,2	12.0	1	0.5	The flashes occurred in the edge of the CCD.
<b>20180809</b> ~19:00 UTC	4	2.4	3.5	4	1	
<b>20180831</b> ~04:40 UTC	0					No flashes at the given distance and quality
<b>20180917</b> ~21:10 UTC	16	8.2	25.0	9	0.56	
<b>20180918</b> ~03:30 UTC	56	31.7	276	51	0.91	Extremely active episode Night time. Average flash rates are not realistic since many flashes cannot be separated
<b>20181014</b> ~17:00 UTC	32	18.5	155	26	0.81	Moderate activity
<b>20181018</b> ~15:15 UTC	28	16.4	206.15	13	0.46	Moderate flash rate but quite active in terms of LMA sources
<b>Total number of LMA flashes: 151</b>						
<b>Total number of flashes detected by LIS: 113</b>						
<b>DE<sub>f</sub> = 0.75</b>						

<b>Episodes with high quality LMA data: distance &lt; 150 km NO minimum number of sources per LMA flash</b>						
<b>Date</b>	<b>Number of flashes</b>	<b>Average flash rate [min<sup>-1</sup>]</b>	<b>Average LMA source rate [s<sup>-1</sup>]</b>	<b>Number of flashes detected by ISS-LIS</b>	<b>Detection Efficiency DE<sub>f</sub></b>	<b>Comments</b>
<b>20171018-1</b> ~10:30 UTC	24	16.0	43.2	13	0.54	
<b>20171018-2</b> ~17:00 UTC	10	5.8	50.3	4	0.40	The flashes occurred in the edge of the CCD.
<b>20180809</b> ~19:00 UTC	20	12.2	30.7	18	0.90	
<b>20180831</b> ~04:40 UTC	28	15.7	4.5	24	0.85	Flashes occur far from the network
<b>20180917</b> ~21:10 UTC	42	21.61	36.3	18	0.43	
<b>20180918</b> ~03:30 UTC	73	41.3	303.4	60	0.82	Extremely active episode Night time. Average flash rates are not realistic since many flashes cannot be separated
<b>20181014</b> ~17:00 UTC	43	24.9	225.3	32	0.74	Moderate activity
<b>20181018</b> ~15:15 UTC	32	18.7	214.3	16	0.50	Moderate flash rate but quite active in terms of LMA sources
<b>Total number of LMA flashes: 272</b>						
<b>Total number of flashes detected by LIS: 185</b>						
<b>DE<sub>f</sub> = 0.68</b>						

For the cases within a range of 150 and 75 km and LMA flashes with a minimum of 50 sources, the resulted DE<sub>f</sub> is 76 % and 75 %, respectively. The case of 150 km has 42 more flashes than the case of 75 km. For the case of 150 km and no restriction in the number of LMA sources per flash, the DE<sub>f</sub> drops to 68 %. In this case, however, the sample is much higher. As exercise, if the area is restricted to 75 km without restriction in the number of LMA sources, the DE<sub>f</sub> results in 64 %. So, that is indicative that ISS-LIS might not detect some small flashes.

On 20180917 and 20181018 episodes flash detection efficiency is below 50 %. The storm on 20180917 was not very active. The storm on 20181018 was moderate in terms of the number or rates of lightning flashes. The quality of the LMA data for that day was high (e.g. see the rates of LMA sources). To verify if there is some effect between the DE and the position of the ISS. figure 4.1.3 depicts the centroids of the ISS-LIS flashes within the CCD.

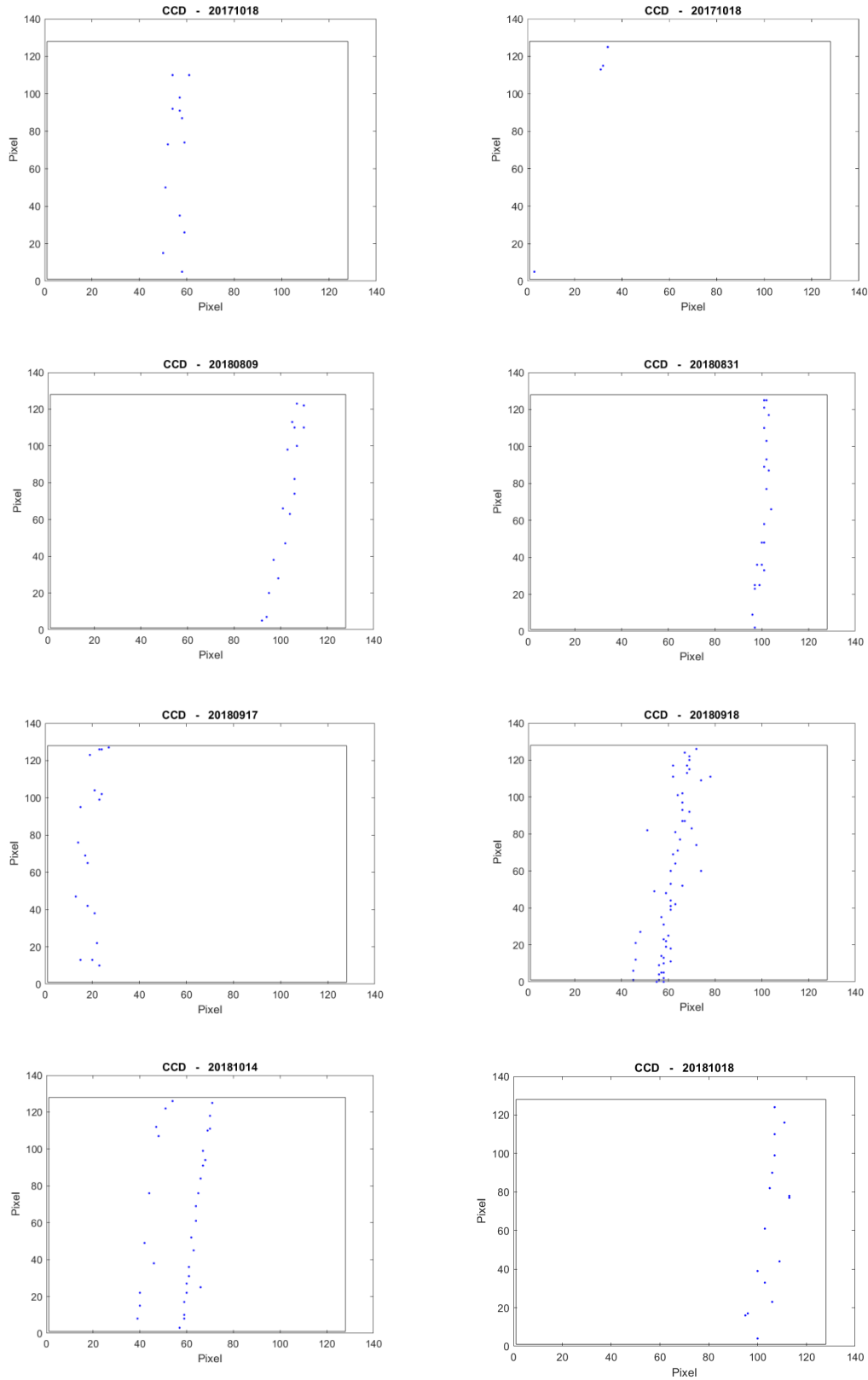


Figure 4.1.3 Location in the CCD of the ISS-LIS for each ISS-LIS flash (the location corresponds to the centroid of the ISS-LIS events in a flash).

From figure 4.1.3 we might explain the low DE (0.64) on 20171018-2 due to the flashes were observed at the top edge of the CCD. However, that not explains the lowest DE occurring in 20180917 and 20181018 ( $DE_f < 0.5$ ) episodes since the detections in the CCD are similar to the 20180809 ( $DE_f = 0.90$ ). Possible explanations:

- It is known that in some situations there is a shadowing effect of the ISS solar panels on ISS-LIS.
- Quality of ISS-LIS is indicated in the ISS-LIS *hdf* files. That shall be verified to investigate the reason.

Output data of the flash detection efficiency can be used to investigate other ISS-LIS performance. First ISS-LIS grouping can be evaluated by counting the number of ISS-LIS flashes assigned to each LMA flash. The analysis shoes that in 40 % of the cases, ISS-LIS assigns more than one flash for an individual LMA flash. Figure 4.1.4 shows the distribution of the percentage of ISS-LIS flashes per individual LMA-flash:

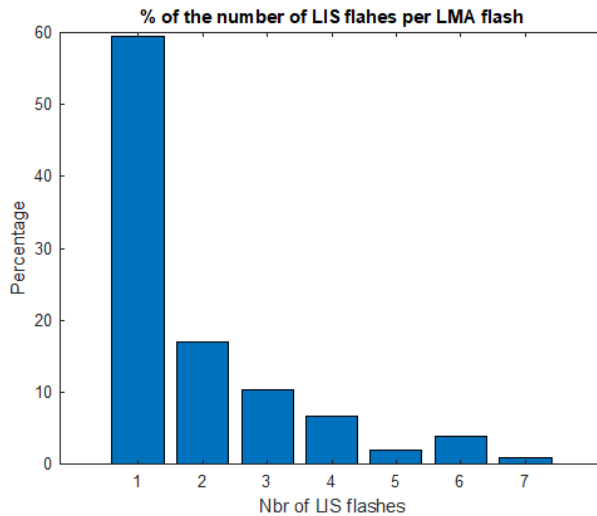
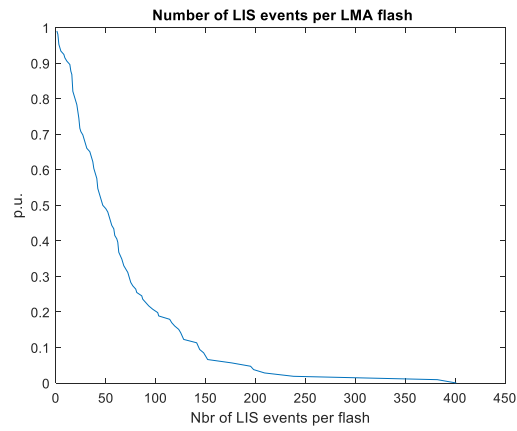


Figure 4.1.4 Distribution of the number of ISS-LIS flashes per individual LMA flash.

Regarding the number of ISS-LIS events per flash, figure 4.1.5 plots the distribution of the number of ISS-LIS events per single LMA lightning flash. More than 98 % of the LMA flashes are detected by 2 or more ISS-LIS events.

a)



b)

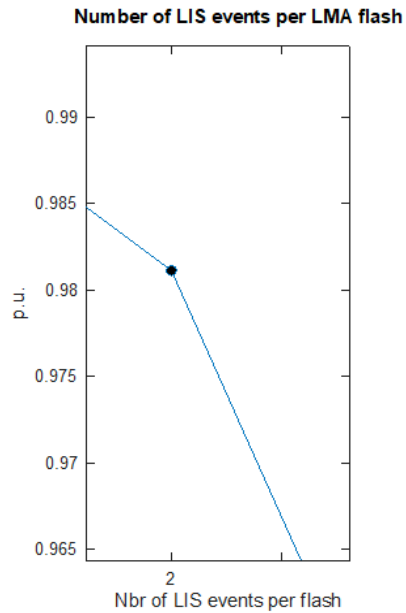


**Figure 4.1.5 a) Accumulated number of ISS-LIS events per single LMA lightning flash. b) Detail showing that more than 98 % of the flashes have 2 or more ISS-LIS events.**

Now some statistics in terms of number of LMA sources, height and power are depicted. Figure 4.1.6 shows two boxplots with the distribution of the number of LMA sources for flashes detected by ISS-LIS and for cases that ISS-LIS did not detected a flash.

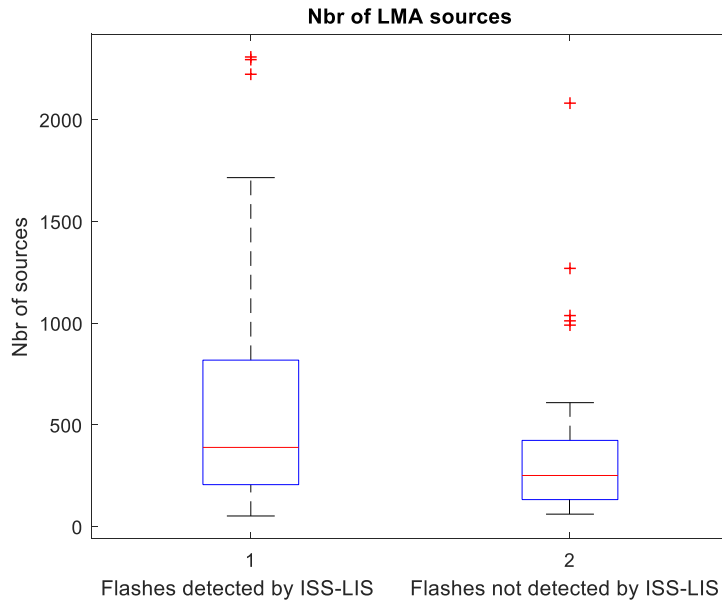


**Figure 4.1.6 Number of LMA sources for flashes detected and undetected by ISS-LIS.**

The figure shows how the median number of LMA sources is higher in those flashes detected by ISS-LIS. The number of sources per flash extends to higher values in those cases detected by ISS-LIS.

Now we compute the power of the events of ISS-LIS correlated with LMA sources and those LMA sources not correlated with ISS-LIS events.

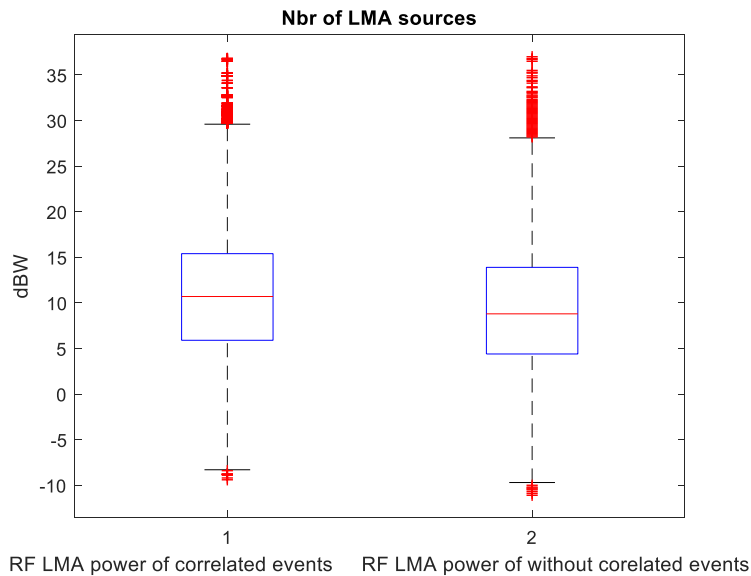


**Figure 4.1.7 VHF RF power for LMA sources correlated and uncorrelated with ISS-LIS events (within 4 ms).**

From figure 4.1.7 we can see that sources correlated with ISS-LIS events have slightly higher median power as well higher 25<sup>th</sup> and 75<sup>th</sup> percentiles. But there is not a clear evidence that the VHF RF power affects to the detection of ISS-LIS.

In relation to the heights of the LMA sources, figure 4.1.8 shows the boxplot for those LMA sources correlated with ISS-LIS and non-correlated events.

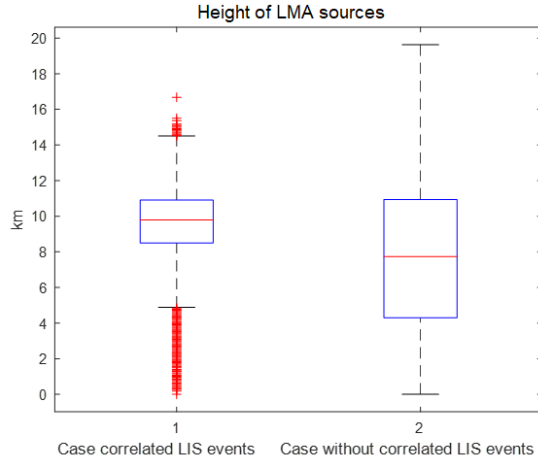


**Figure 4.1.8 Height of the LMA sources correlated (within 4 ms) with ISS-LIS events (left) and for those events not correlated with LMA.**

In that case, the median altitude of the sources tends to be higher as well the percentiles 25<sup>th</sup> and 75<sup>th</sup>. That can demonstrate the effect of the cloud depth. In the next section, we will investigate the  $DE_f$  for flashes reaching lower altitudes.

In the section 4.3 the investigation between the RF power and height of LMA sources and ISS-LIS events is extended.

#### 4.1.4 $DE_f$ by flash height

To investigate the effect of the lightning altitude to the  $DE_f$ , we have calculated  $DE_f$  versus flashes occurring below certain altitudes given by percentiles.

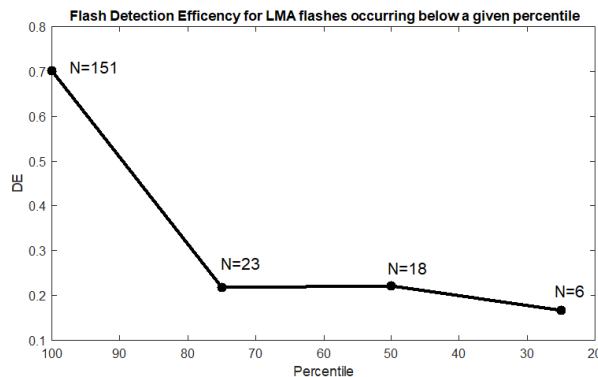


**Figure 4.1.9 Analysis the influence of the flash height to the  $DE_f$ . Detection Efficiency has been calculated for flashes below altitudes given percentile (100 %, 75 %, 50 % and 25 %). N is the number of flashes in the sample.**

The results show how the  $DE_f$  of ISS-LIS rapidly drops when the flashes do not reach high cloud altitudes. The decay is relevant (from 70 % to ~20 %) indicating how lightning luminosity is attenuated by the cloud.

#### 4.1.5 Flash false alarm (FFA)

The situations where ISS-LIS reports a flash and it is not detected by LMA will be named as a 'Flash False Alarm' candidate (FFA). These cases will need special treatment before being classified as false alarms. We suggest:

- Verification that these cases occur in thunderstorm episodes and not in 'fair weather' situations.
- Verification that these cases do not occur in areas of reduced detection efficiency by the LMA.
- Verification that these cases might be related to an existing flash but not reported by the LMA due to some technical issues, e.g.: not enough sensors to compute solutions, high noise at some of the stations, etc. In that case, LMA source data (LMA level-1) and raw data (LMA level-0) of single stations can be inspectional to confirm the existence of a flash.
- Additional data can be used such as: LLS data, satellite and radar to confirm the presence of a storm cell at the location of the false flash.

Figure 4.1.10 shows the obtained candidates of false ISS-LIS flashes as result of the Flash Detection Efficiency analysis. In this case, LMA level-2 data corresponding to flash data has been used up to a range of 150 km. But as shown in section 3, the general performance of the LMA significantly decays beyond 75 km and, in addition, some close locations have low performance due to the network geometry and orography (e.g. figure 2.3.12).

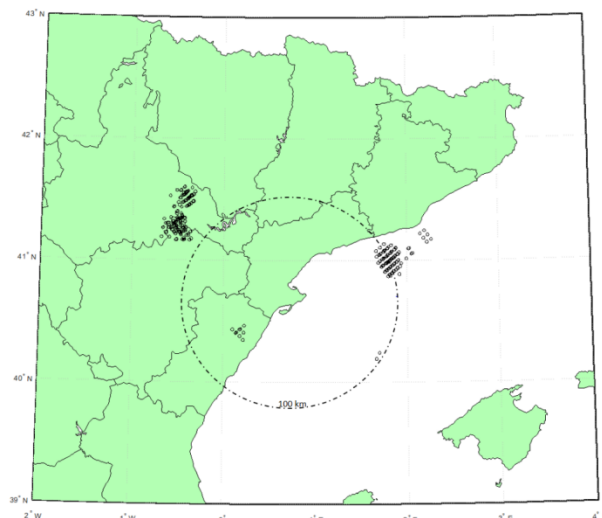


Figure 4.1.10 ISS-LIS events corresponding to candidates to flash false alarms (FFA).

By a post analysis of the ISS-LIS candidates to FFA, the majority occurred beyond a range of 100 km where the performance of the Ebro LMA is low. That corresponds to 23 of the 24 candidates. In these 23 cases LMA level-1 data showed the existence of at least of an LMA source corresponding to the FA candidates. Only one candidate of the 24 was not related to LMA level-1 data. This case occurred at a distance of about 50 km (case of south-west of the LMA). For this case, it was an existing cloud-to-ground flash that was not reported by the LMA (level-1 data), the reason was the low number of sensors for that particular day that reduced the coverage range.

#### 4.1.5 Conclusions of DE and FFAR

The conclusions can be summarized as follows:

- ISS-LIS  $DE_f$  has been evaluated using the LMA as reference.
- For the  $DE_f$  evaluation a time and distance criteria has been used.
- The study has considered 327 flashes in 8 episodes.
- In general, the  $DE_f$  of ISS-LIS is >70 %.
- In two cases,  $DE_f$  dropped below 50 %.
- This low  $DE_f$  might not be attributed to the day/night effect. Probably due to the ISS masking produced by solar panels or any other possible effect.
- For matched LMA - LIS flashes:
  - The flash grouping criteria of ISS-LIS matched in 60 % of the cases.
  - There are very few flashes detected by only one or few ISS-LIS events. When ISS-LIS detects a flash, the average number of events is ~38.
  - LMA flashes detected by ISS-LIS present a higher median number of sources. 75<sup>th</sup> percentile and extreme number of LMA sources are also high.
  - LMA sources associated to individual events occur at higher altitudes.
  - Power of LMA sources associated with individual events is slightly higher but no relation is obtained.
  - $DE_f$  drops when flashes occur lower in the cloud.
- No false ISS-LIS flashes have been identified.

#### 4.2 Flash duration

Flash duration is calculated as:

- LMA: time difference between the first and the last source (singletons sources will be ignored).
- ISS-LIS: time difference between the first and the last event.

Singletons are VHF sources not assigned to a flash in the flash data (LMA level-2 data).

#### 4.2.1 Duration Comparison

The first comparison on flash duration relies on general figures calculating the flash duration on the whole set of observations on the most relevant episodes. The following table presents the flash durations on both datasets. Besides, a third column presents flash duration on the sample of ISS-LIS flashes that are associated to LMA flash (collocated in time and space).

Date	Median duration (s) of		
	LMA flashes	ISS-LIS flashes associated to LMA flash	ISS-LIS flashes
20171018	0.206	0.181	0.185
20171018	0.356	0.318	0.185
20180809	0.308	0.3215	0.247
20180831	0.101	0.2145	0.256
20180917	0.200	0.217	0.216
20180918	0.923	0.836	0.184
20181014	0.530	0.395	0391
20181018	0.493	0.404	0.394
Average	0.370	0.356	0.238

Median ISS-LIS flash duration is around 70 % of the LMA flash duration, thus ISS-LIS flashes are 30% shorter. Contrarily, those flashes that were collocated by both remote sensing systems are larger, rather similar to the general LMA flash population, even slightly larger.

#### 4.2.2. Flash-by-flash comparison

Another way to compare flash duration recorded from both systems is on a flash-by-flash comparison approach. It focuses on the selection of flashes that occurred in three of the episodes with lightning within the close range of the LMA coverage (<50 km) (see section 2.4.).

Episodes and flashes used on the flash-by-flash comparison are summarized in the next table.

Day	LMA Flashes	LMA sources	LIS events
2017/10/18	4	2171	250
2018/09/18	20	10.432	1302
2018/10/14	22	7.943	1169
2018/10/18	10	11.327	813

Figure 4.2.1 shows an overview of the lightning activity detected by the LMA during one of those 2 min time interval when ISS-LIS was passing directly above the E-LMA. In particular, it shows several discharges occurring within the storm system on the 18<sup>th</sup>

October 2017 between 10:32 and 10:34 UTC aprox. Over 5.800 VHF sources were located by the LMA during the time interval of the figure.

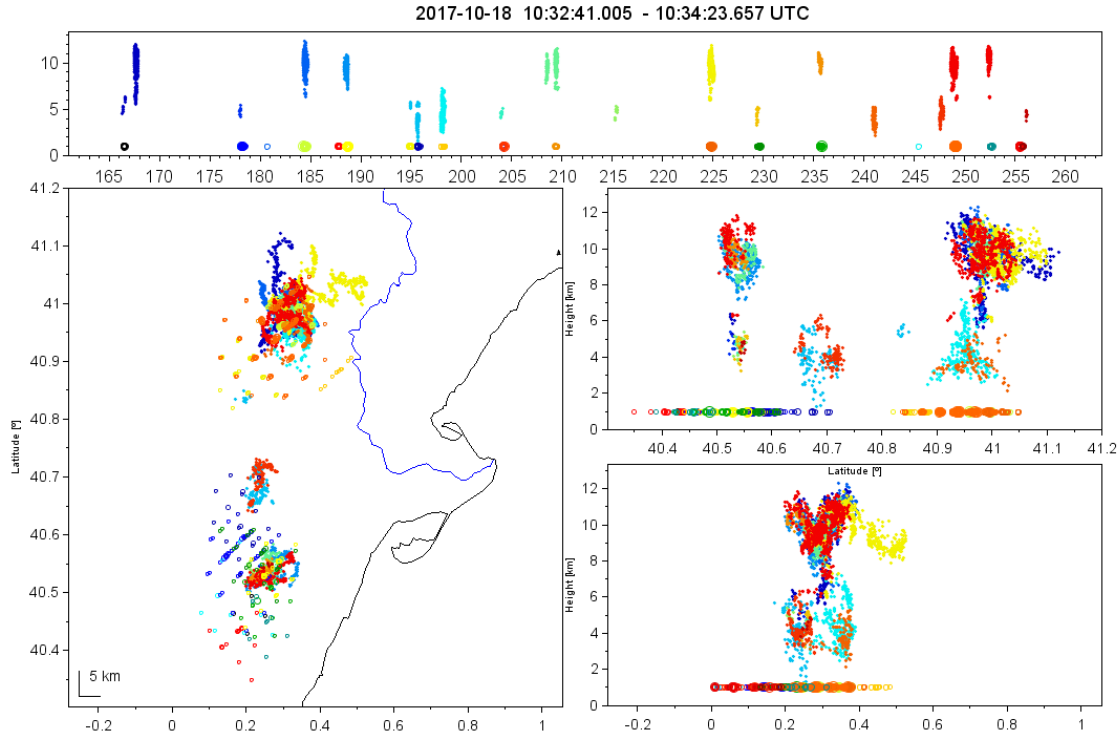


**Figure 4.2.1** Multipanel display of Lightning activity detected by the E-LMA during the 2 min time interval the ISS-LIS was passing directly overhead the E-LMA. The top panel is altitude above mean sea level (km) versus time (time in seconds regarding the ten-min period from 10:30 to 10:40). Black circles correspond to the LIS events corresponding to the same IC flash. The left panel is a plan view map. reference lines correspond to the coast line and the Ebro river. The panels at the right show altitude (km) versus latitude (top) and longitude (bottom).

The reference for this analysis are the LMA flashes detected by both systems. On this basis, the analysis developed in this section seeks to compare LMA and ISS-LIS detections on the same flash. At this point, it should be said that not all flashes have been selected, but only those having a good detection by LMA, where the cloud fraction predominates. An example is presented in figure 4.2.2. The figure displays one of the IC flashes detected by the E-LMA during the ISS-LIS overpass on 18th October 2017 at 10:33:04 UTC. The IC discharge was first detected by the LMA and is seen on the top panel of figure 4.2.2. ISS-LIS events corresponding to the same flash were detected shortly after the flash initiation as soon as the discharge reached the upper level. A series of ISS-LIS events followed, stopping before the end of the LMA sources.

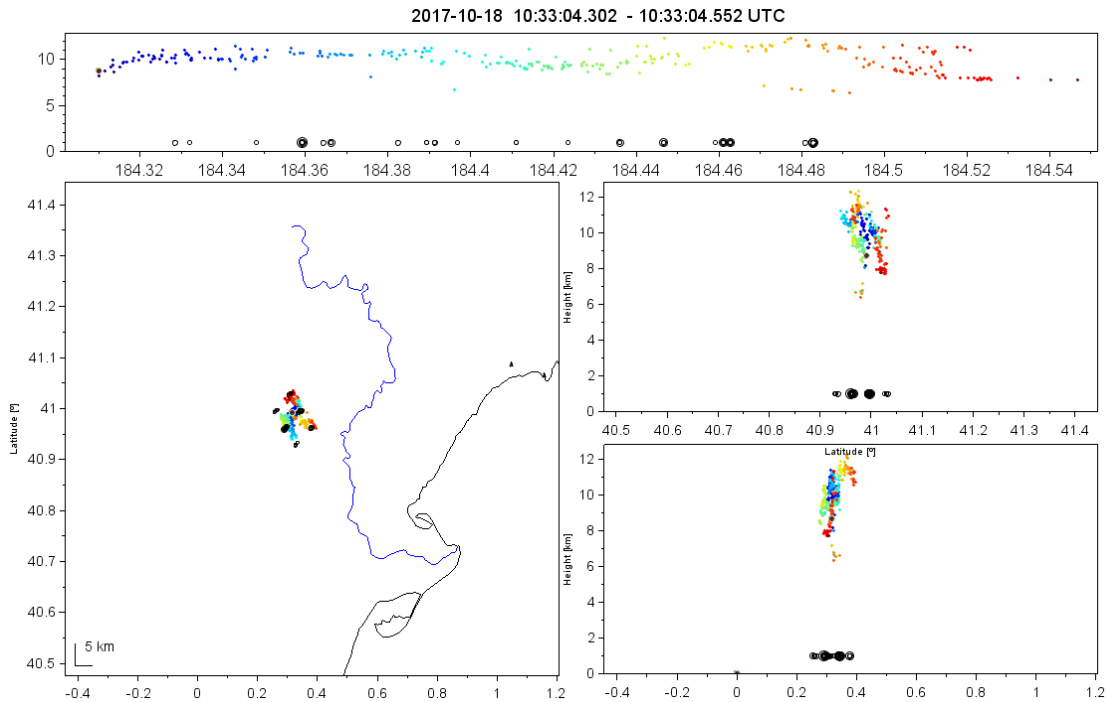


**Figure 4.2.2** Multipanel display of one of the intracloud lightning flash detected by the ELMA during the LIS overpass. 18th October 2017 at 10:33:04 UTC. The top panel is altitude above mean sea level (km) versus time (time in seconds regarding the ten-min period from 10:30 to 10:40). Black circles correspond to the LIS events corresponding to the same IC flash. The left panel is a plan view map. reference lines correspond to the coast line and the Ebro river. The panels at the right show altitude (km) versus latitude (top) and longitude (bottom).

First, a matchup is done so the information on the same event as seen by the two remote sensing systems is linked. The following table summarizes the minimum, maximum and average duration of the selected sample:

Duration (s)	ISS-LIS	LMA
average	0.691	0.860
min	0.107	0.167
max	2.405	2.272

### 4.2.3 Normalization procedure

After the matchup procedure, there is a normalization process: the duration of the LMA flash is normalized to [0.1]. This way, the comparison can be done on the whole sample in spite of the different flash durations. The LMA flash is therefore considered as “ground truth”, the analysis focuses on which fraction is seen by ISS-LIS in terms of position and duration within the normalized duration. In particular, two different aspects are analyzed:

- start and end;
- and total duration are compared.

The duration on the LMA is the time between the first and the last source of a flash. In the ISS-LIS flash is the time between the first and the last event. The starting time, duration and ending time of the ISS-LIS flash are compared to the normalized LMA flash. These concepts are represented in figure 4.2.3.

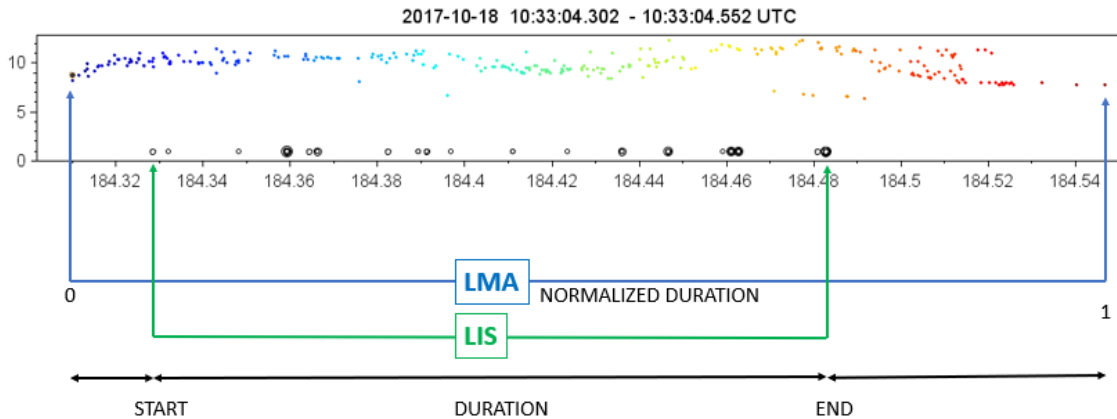
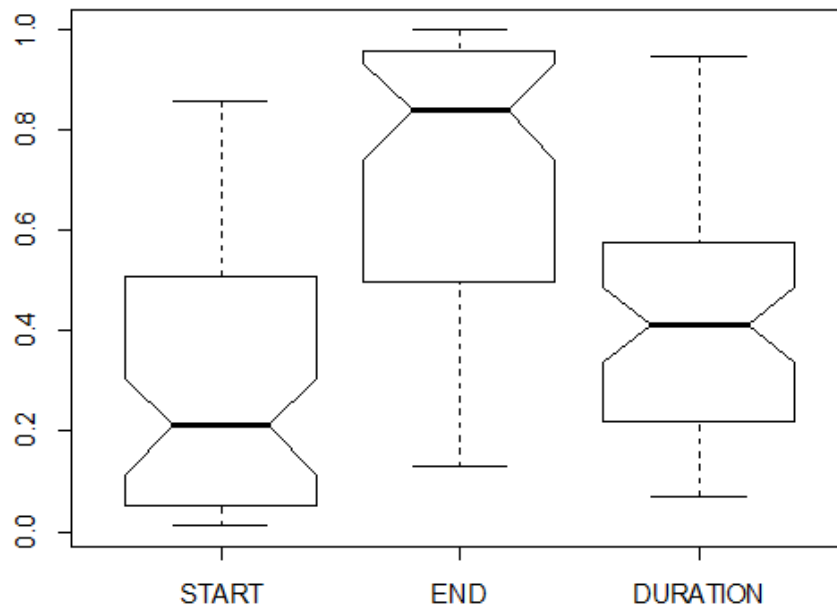


Figure 4.2.3 Scheme on flash normalization. start. end and duration

Results are represented in figure 4.2.4. The boxplot corresponds to the normalized starting time (INI), the end of the flash (END) and the normalized duration of the ISS-LIS flash in relation to the duration of the LMA flash.



**Figure 4.2.4** Boxplot for the start, end and duration of the LIS flash, in relation to the normalized LMA flash.

Regarding the initiation, the boxplot shows that, in most of the cases, the first ISS-LIS event is detected before the 20% of the normalized flash duration. Besides, almost all analyzed flashes start before the middle of the normalized flash duration. Focusing on the end of the LIS flash, it can be observed on the boxplot that the last ISS-LIS event is generally detected around the 85% of the normalized flash duration. Moreover, in most of the cases, the last 10% of the LMA flash is poorly detected by ISS-LIS. Finally, regarding the total duration, the median of the ISS-LIS flash duration is around 40% of the total flash duration (assuming LMA sees all the flash). In most of the cases, the ISS-LIS flash duration is, at least, 60% of the total duration.

On the following, the normalized LMA flash duration is divided into ten segments: each of the ISS-LIS events along the normalized flash duration are assigned to one of the time segments. Frequencies on each bin are represented in the following figure 4.2.5.

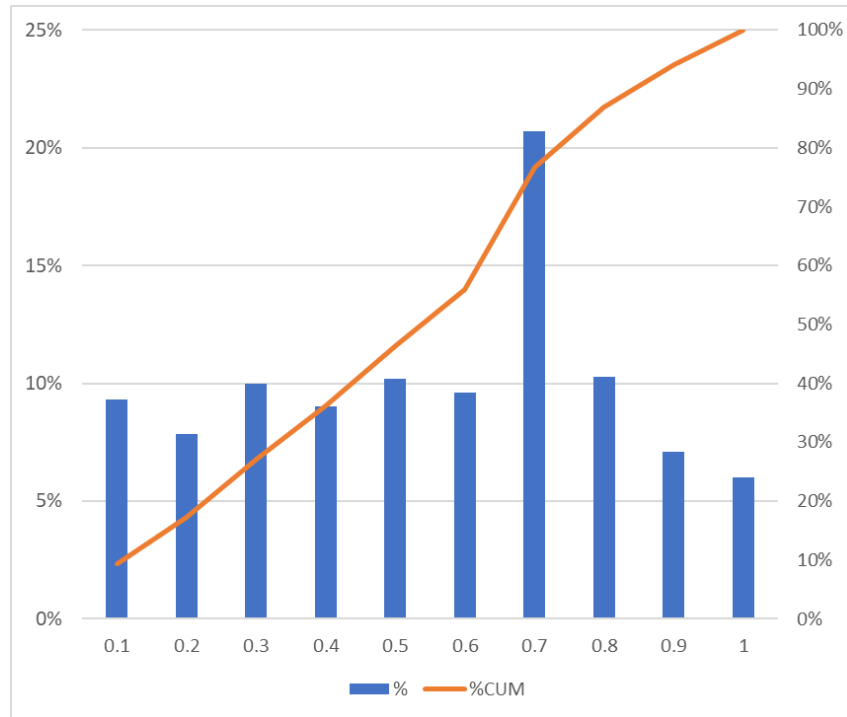


**Figure 4.2.5 Frequency of ISS-LIS events along the normalized LMA flash duration, in bins of 10%. The line (right axis) represents the accumulation.**

Figure 4.2.5 shows a rather regular distribution of ISS-LIS events along the first 60% of the flash. Surprisingly, the seventh 10% bin accumulates more than a 20% of the ISS-LIS events. After that, the frequency decays. In fact, the two last bins only have the 13% of the recorded events. In order to complement this result, the next figure presents the radiance of the events on the same bins.

Regarding the ISS-LIS event radiance along the normalized bins, figure 4.2.6 shows that, in general, it is rather constant along the flash duration. However, there are also some characteristics to notice: it shows a higher radiance in the first bin, radiance that progressively decreases until the fourth bin. On the following, it gently increases to present, until the end of the duration, values close to the average.

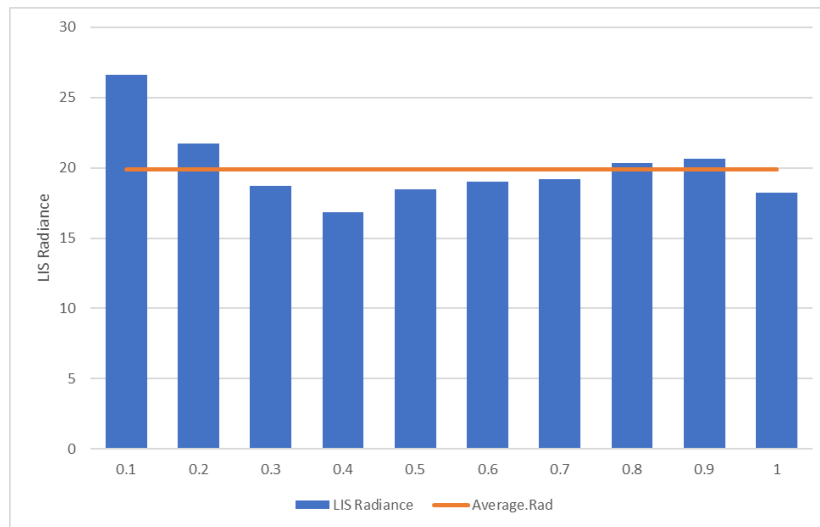


Figure 4.2.6 Distribution of radiance of ISS-LIS events within the normalized flash.

Figure 4.2.7 presents the height and the power of the LMA sources in each of the ten bins of the normalized flash. Boxplots on the height show an increment of the interquartile distance with time. This would mean that cloud channels on the mid regions are more frequent at the end of the flash. This could be an explanation for the lowering on the ISS-LIS detections. However, higher channels keep occurring on this stage. On the other hand, the power of the sources stays more or less the same throughout the flash durations, it does not look like the decay on the number of events at the end of the flash is related with a power weakening.

*Thomas et al.* (2000) found that the brightest optical events tended to occur at the end of intra cloud discharges, when a large number of pixels covering the full horizontal extent of the flash were impulsively illuminated. These observations do not match with ours, where ISS-LIS events are more frequent in the first  $\frac{3}{4}$  of the flash. This weakening of events on the final stage of the flash deserves further investigation.

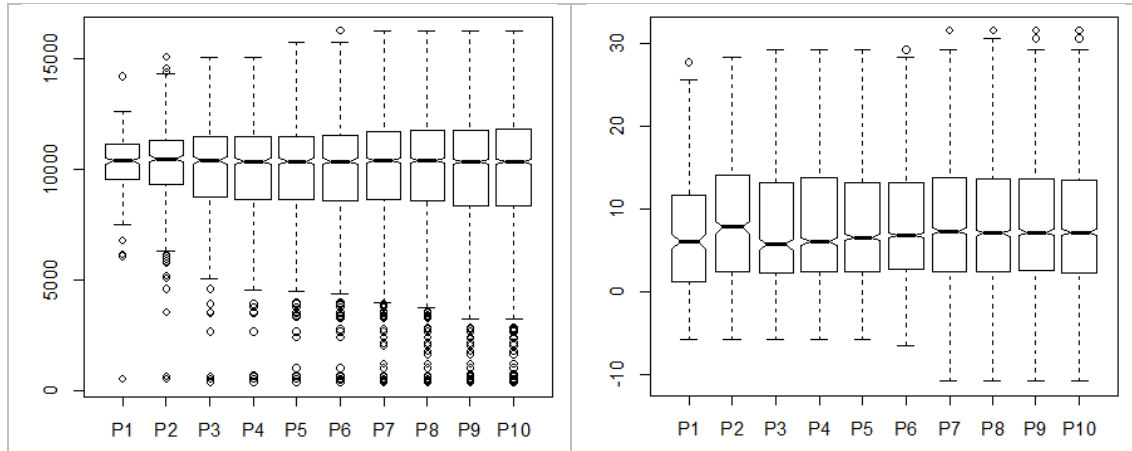


Figure 4.2.7 Boxplots for LMA height (m) (left) and power dBW (right) along the normalized flash duration. The duration is divided into ten bins (P1 to P10).

#### 4.2.4 Conclusions of the flash duration

Conclusions are summarized as follows:

- In general, the duration of ISS-LIS flashes is about 30 % shorter than the duration of an LMA flash.
- The ISS-LIS flash criteria resulted that about 40 % of the LMA flashes have more than two ISS-LIS flashes (section 4.1). That strongly influence the difference pointed in the previous point.
- For the selected cases with good quality in both LMA and ISS-LIS, the time difference in duration decreases to 20 %.
- After the normalization of the LMA flashes. we have shown that:
  - In most of the ISS-LIS cases (>75 %), the first event is detected before the 20 % of the normalized flash duration.
  - Almost all of the analyzed flashes start before the middle of the normalized flash duration.
  - The last event of ISS-LIS occurs generally around the 85 % of the normalized flash duration (median value).
  - In most of the cases, the last 10% of the LMA flash is poorly detected by ISS-LIS.
  - The median of the ISS-LIS flash duration is around 40 % of the total flash duration (remember that LMA has been taken as reference for normalization).
  - In most of the ISS-LIS cases, the duration is, at least, 60 % of the total duration.
- Location in time of the ISS-LIS events:
  - A rather regular distribution of the occurrence of ISS-LIS events is found in the first 60 % of a flash.

- Surprisingly, the seventh 10% bin accumulates more than a 20% of the LIS events, almost doubling adjacent bins
  - The last 20 % of the flash only contains the 13 % of the ISS-LIS events.
  - The radiance of the events is rather constant along the flash durations, even though it is above the average on the first two 10% bins
  - From the distribution of LMA source heights during the normalized flash duration, the interquartile distance (from 25<sup>th</sup> to 75<sup>th</sup> %) gently increases with time. That might explain that in the last part of a flash it contains a higher fraction of sources at low levels (cloud channels on the mid regions seem to be more frequent at the end of the flash).
  - However, occurrence of higher channels keeps active at this stage (e.g. recoil leaders).
  - There is not a significant variation in the power of the LMA sources along the flash duration.
- 
- We have not found that brightest optical events tended to occur at the end of intra-cloud LMA discharges as ‘might’ have been suggested by *Thomas et al.* (2000). (Note to verify that the flash end corresponded to LMA and not to ISS-LIS).

### 4.3 Distribution of ISS-LIS events with height and power

This section deals with the relationship of the ISS-LIS events with the height of the cloud channels (LMA sources). To this end, we used the same sample of flashes from section 4.2.

Here, we try to answer these questions: “Does the LMA sources corresponding to ISS-LIS detections have different characteristics? (compared to the whole set of LMA sources)

Are those sources at higher altitudes? Are those sources more intense in terms of power?

To this, a match-up procedure has been applied, making pairs of events LMA-LIS. The “one-to-one” match-up assigns to each LIS event the closest LMA source in time. An example is presented in figure 4.3.1. Two restrictions apply:

- a maximum time difference of ten milliseconds
- a maximum distance (surface projection) of 10 km between potential pairs

Therefore, at the end of the match-up process only LIS-LMA pairs with a good time correspondence and, at the same time, which are not far away from each other, remains. Once the set of pairs is obtained, the analysis compares this sample of “ISS-LIS-corresponding” LMA, to the whole LMA source population (all sources). This comparison is made in terms of height and power of the LMA sources.

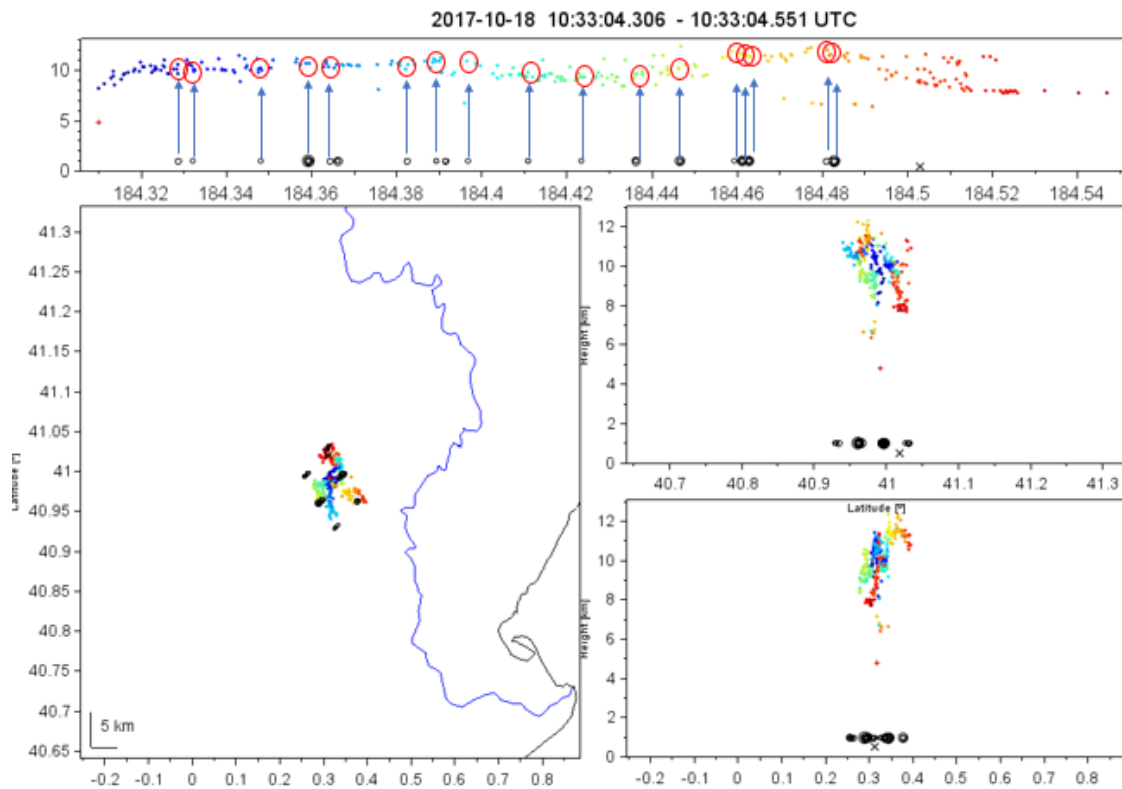


**Figure 4.3.1** Multipanel of an LMA flash with the corresponding LIS events as in 4.2.1. A scheme of the matchup procedure is represented in the top panel.

#### Possible time offset (ISS-LIS timing accuracy)

Albeit the relation between the ISS-LIS events with lightning processes like the CG strokes is discussed later on, we shall mention here a possible time offset between ISS-LIS events corresponding to CG strokes and LLS CG stroke detections. *Ushio et al. (2002)* noticed a time delay of the optical pulse from the ground LLS first return stroke detection of about 10 ms. This time is considered to be the propagation time for the optical signal to reach the LIS in space. Accordingly, *Ushio et al. (2002)* suggested that there is a systematic time bias of about 10 ms. We raised this question to Doug Mach, who said that time on ISS-LIS is corrected for transit time and is now very close to UTC. According to him, the delay should be within one ms.

On the basis of these considerations, we have analyzed the data looking for an apparent delay. We have checked this delay in flashes where ISS-LIS events clearly correspond to CG strokes, like the example in figure 4.3.2

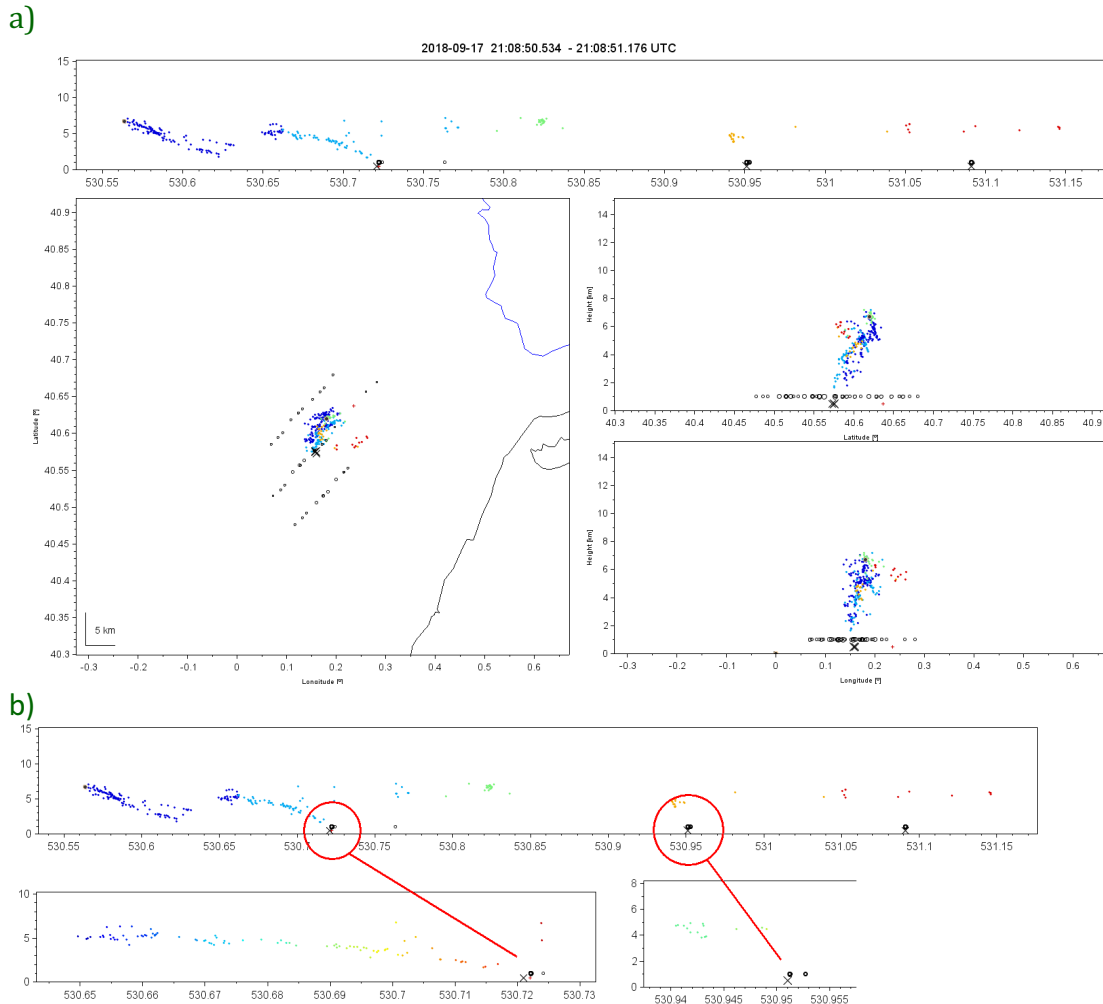


**Figure 4.3.2 a) As in 4.2.1. but for a CG flash with three strokes 17th October 2017 at 10:33:04 UTC b) Zoom on the CG strokes.**

Figure 4.3.2 shows a CG flash with three CG strokes, all detected by ISS-LIS. In this kind of flashes, the cloud activity is little. Accordingly, there are few LMA detections, most of them corresponding to the stepped leaders as shown in the beginning of the figure 4.3.2. In these cases, it is important to rely on CG detections, as ISS-LIS events are collocated with the CG strokes as shown in the top panel of figure 4.3.1.

A systematic delay of 1 ms has been observed in a set of flashes similar to the example in figure 4.3.2. The accuracy of the time records on both remote sensing systems did not allow a more accurate calculation of the delay. Besides, when the ISS-LIS events correspond to cloud lightning, it is not possible to assess a delay like in the CG cases. Therefore, the match up procedure has been carried on twice, considering two cases:

- LMA and ISS-LIS observations coincide in time.
- A certain delay of  $\pm 1$  ms exists between datasets.

This way, the first match-up procedure looks for the closest LMA source (in time), whereas the second one looks for all sources in the time period of  $\pm 1$  ms for each ISS-LIS event. If more than one LMA source is found on this time bin, the average is taken.

### 4.3.1 Geographical distance

A secondary outcome of the match-up process, that generates the LIS-LMA pairs, is the geographical distance between the LIS-LMA pairs. This output (figure 4.3.3) gives information on the location accuracy. The figure presents a frequency distribution of the distance between the ISS-LIS events and the LMA sources corresponding locations (longitude/latitude). Indirectly, the geographical accuracy of the ISS-LIS instrument can be inferred from this outcome. The median distance on the pairs is of 4.5 km.

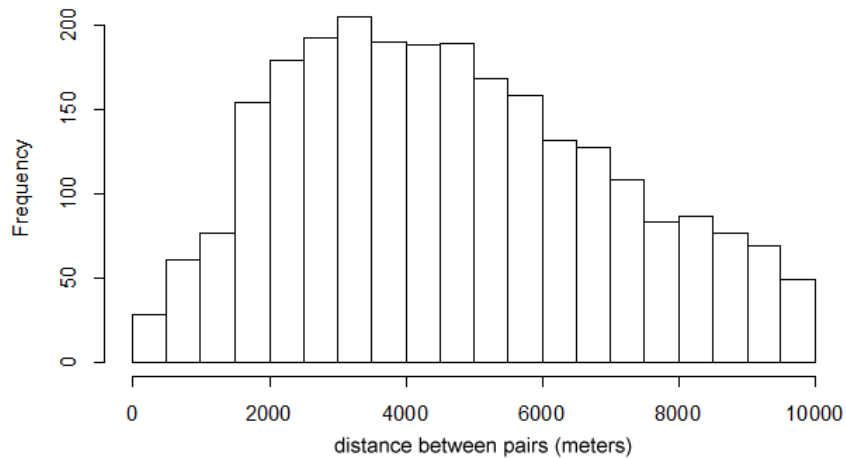
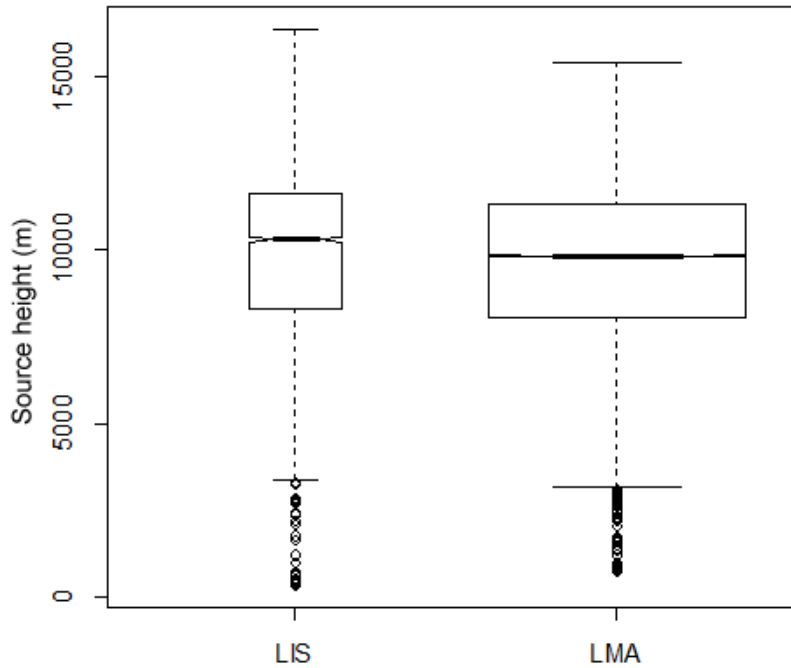


Figure 4.3.3 Frequency distribution of the distance between the ISS-LIS and the LMA corresponding locations (longitude/latitude).

### 4.3.2 Height

Going to the relationship of the ISS-LIS events with the height of the LMA sources, figure 4.3.4 presents the difference on the height of the sample LIS-LMA pairs (“LIS” boxplot in the figure) in comparison to the whole LMA source population height (LMA boxplot in the figure). It can be seen that the height of the LIS-LMA pairs (median 10172 m ASL) is slightly higher than the height of the rest of sources (9843 m ASL). Regarding the  $\pm 1$  ms time window, the median for the LIS-LMA pairs is of 10034 m ASL.



**Figure 4.3.4** Boxplot on the height of the LMA sources for the LIS-LMA pairs (LIS) and all the LMA sources (LMA). Case with nearest source (left) and average of  $\pm 1$  ms (right). Boxes are drawn with widths proportional to the square-roots of the number of observations in the groups.

Note that in the analysis of heights in figure 4.1.8 there is significant differences when the population of the LMA sources related to ISS-LIS events is compared to the population of LMA-sources non-related to ISS-LIS events. In the case of figure 4.3.4 the related LMA sources are compared to the overall LMA sources.

Another way to present this result is with frequencies, as displayed in figure 4.3.5. It presents the frequency distribution of LMA sources by height, both for the LIS-LMA selection and the whole LMA sources. It can be seen that frequencies above the 11 km are higher for the LIS-LMA sample (58% versus 47%), whereas this tendency is reversed below the 11 km.

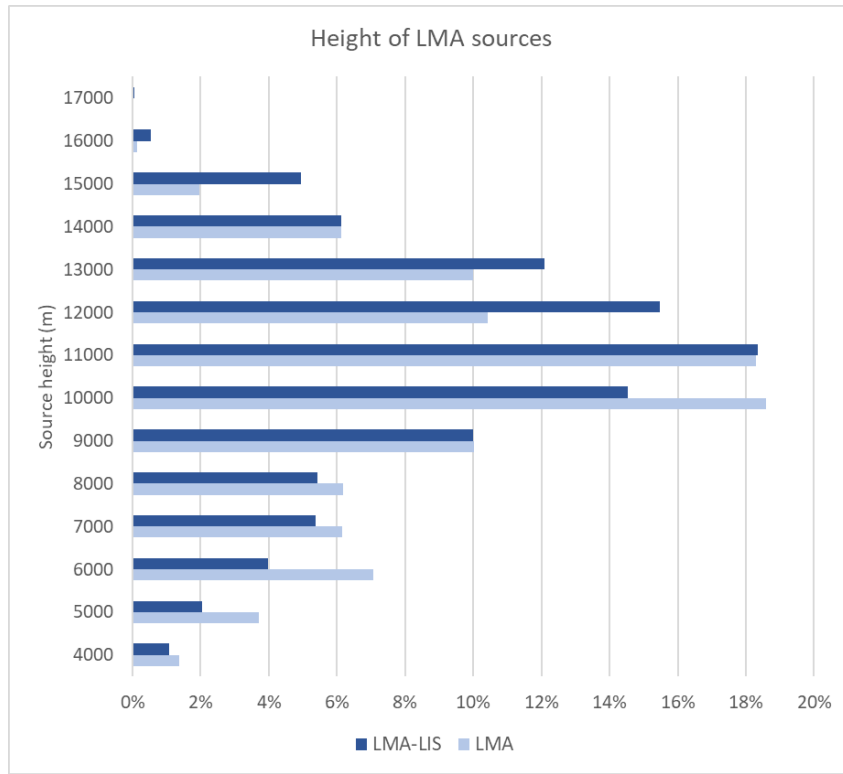


**Figure 4.3.5** frequency distribution of LMA sources by height. Both for the LIS-LMA selection and the whole LMA sources.

These results show that discharges which extend into the upper part of the cloud are better detected by the ISS-LIS. On the other hand, discharges confined below 11 km altitude were less well detected. These results are similar to those presented by *Thomas et al.* (2000). Results for the  $\pm 1$  ms time window are similar. Sources above 11 km represent the 58% of the sample in the LIS-LMA pairs (and 53% in the  $\pm 1$  ms time window), whereas this percent on the whole LMA sample is of 47%.

### 4.3.3 Power

To end this section, the results on power comparison are presented. Figure 4.3.6 presents the difference on the power for the sample LIS-LMA pairs in comparison to the whole LMA source population. It can be seen that the power of the LIS-LMA pairs (median 8 dBW) and for the  $\pm 1$  ms time window (median 9.75 dBW) is slightly higher compared to the whole population of LMA sources (median 6.5 dBW)

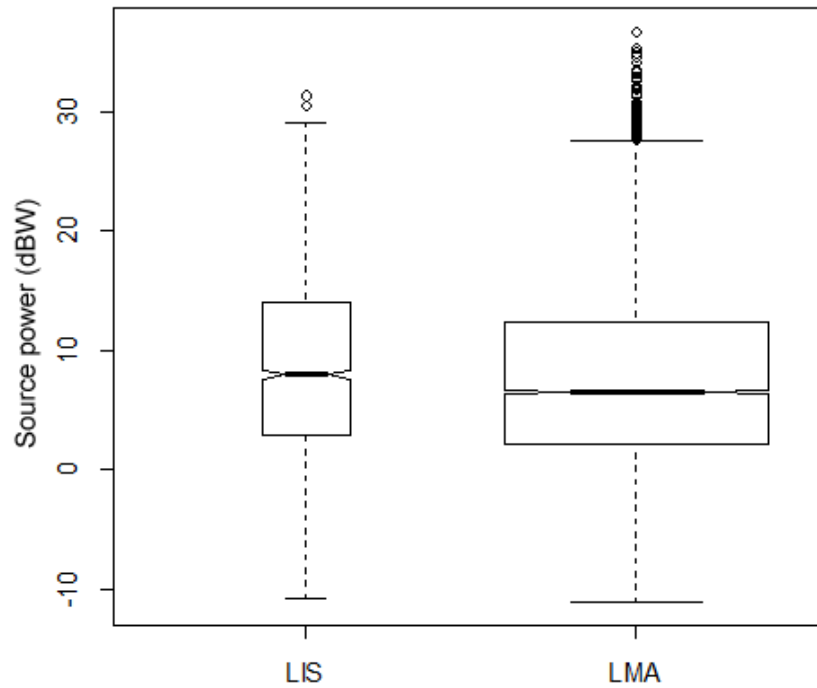


**Figure 4.3.6** Boxplot on the power of the LMA sources for the LIS-LMA pairs (LIS) and all the LMA sources (LMA). No delay (left) and delay 1 ms (right). Case with nearest source (left) and average of  $\pm 1$  ms (right). Boxes are drawn with widths proportional to the square-roots of the number of observations in the groups.

These results on the power of the sources indicate that intense discharges which extend into the upper part of the cloud are better detected by the ISS-LIS.

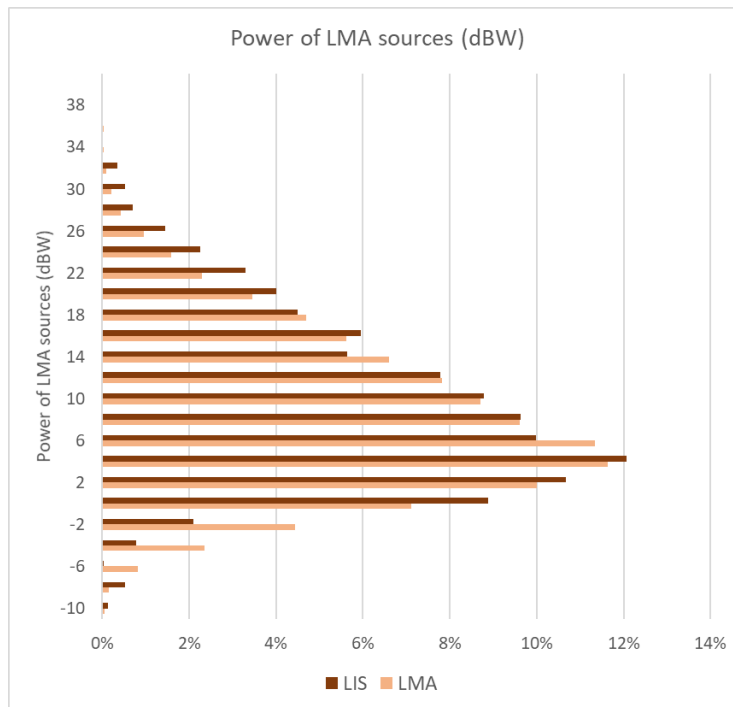


**Figure 4.3.7 Frequency distribution of LMA sources by power. The LIS-LMA selection (LIS) is compared with the whole dataset of LMA sources (LMA).**

Like with height, figure 4.3.7 displays the fraction of LMA-LIS sources (labeled as LIS) with the whole population (labeled as LMA). It can be seen that sources with power above 16 dBW are slightly higher for the LIS-LMA sample (23% versus 19%). Contrarily, there is a clear difference in the lowest power, with few LIS-LMA on the range between -2 and -10 dBW

#### 4.3.4 Conclusions on the relation of ISS-LIS events with LMA source height and power

Summary of the main conclusions:

- A time and location criteria has been used to match ISS-LIS events and LMA sources.
- To take into account the possible time delays between the time records on both datasets, we applied a second match-up procedure, considering a time window of  $\pm 1$ ms for each ISS-LIS event. Results are similar to those of the direct match-up.
- A secondary output of the match-up procedure is the geographical distance between sources, which is an approximation to the location accuracy. The median distance on the pairs is of 4.5 km.
- For those paired event-sources, the median height of the LIS-LMA sources (10172 m ASL) is slightly higher than the height of the overall sources (9843 m ASL).
- The height difference is more apparent when analyzing the frequency distribution, showing that frequencies above the 11 km are higher for the LIS-

LMA sample (58% versus 47%), whereas this tendency is reversed below the 11 km. Therefore, it looks like the discharges that extend into the upper part of the cloud (> 11 km) are better detected by ISS-LIS.

- Regarding the power of the sources, the median for the LIS-LMA pairs (median) is slightly higher compared to the whole population of LMA sources (8 dBW and 6.5 dBW respectively). As with height, it looks like the IC sources with powers above 16 dBW are better detected by ISS-LIS.

#### 4.4 ISS-LIS radiance

A “flash” identified by ISS-LIS has, besides duration and spatial extent, information on the emitted optical radiance ( $\text{J m}^{-2} \text{sr}^{-1} \mu\text{m}^{-1}$ ). One could expect this optical lightning radiance detected by ISS-LIS to be related with the height of the lightning channel, or with the power of the sources recorded by the LMA.

On the following, results on this comparison are presented. We shall notice, at this point, that we keep working here with the pairs “ISS-LIS event – LMA source” obtained in the previous section. Figure 4.4.1. shows the relation between ISS-LIS event radiance and LMA source height. There seems to be no clear relationship between the radiance detected by ISS-LIS and the height of the associated sources detected by the LMA. However, the scatterplot shows that events with radiances above  $30 \text{ J m}^{-2} \text{sr}^{-1} \mu\text{m}^{-1}$ , are generally in the upper part of the cloud.

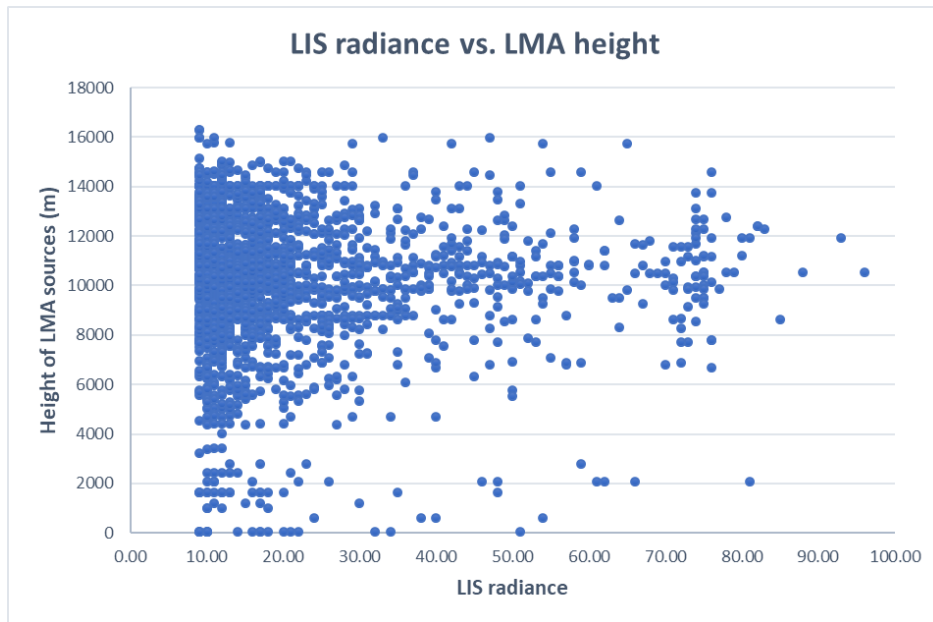
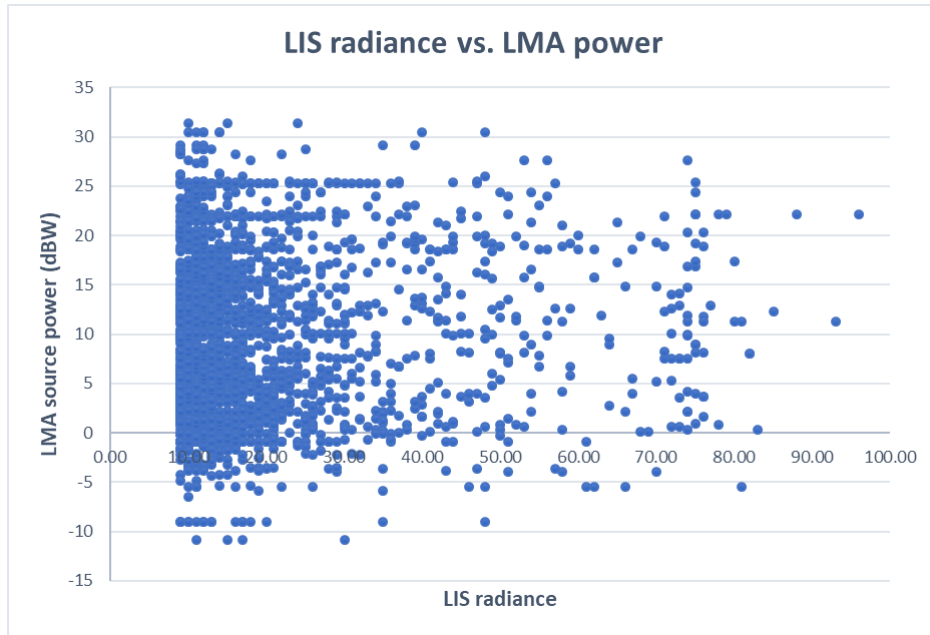


Figure 4.4.1 Scatterplot of the ISS-LIS event radiance ( $\text{J m}^{-2} \text{sr}^{-1} \mu\text{m}^{-1}$ ) and height (m ASL) of the LMA associated source (LIS-LMA pairs).

On the other hand, figure 4.4.2. shows the relation between LIS event radiance and LMA source power. Like with height, there seems to be no clear relationship between the

radiance detected by ISS-LIS and the power of the associated sources detected by the LMA.



**Figure 4.4.2 Scatterplot of the ISS-LIS event radiance ( $\text{J m}^{-2} \text{sr}^{-1} \mu\text{m}^{-1}$ ) and power (dBW) of the LMA associated source (LIS-LMA pairs).**

A closer look to the radiance of the events, in the context of the whole flashes, showed a wide range of radiance in most of the analyzed flashes. In the same way that events are grouped into flashes, radiance can be integrated for the whole flash. Although this means a significant reduction of the sample (from events to flashes), the analysis on flashes may be more robust.

On the following, the analysis focuses on the integrated radiance per flash, rather on the individual events. Figure 4.4.3 ISS-LIS integrated radiance per flash ( $\text{J m}^{-2} \text{sr}^{-1} \mu\text{m}^{-1}$ ) and average height of the LMA associated flash. Figure 4.4.3 reminds of figure 4.4.1, in the sense that there is a wide range of altitudes for the lower radiances, whereas higher radiances tend to concentrate around 9 to 10 km height.

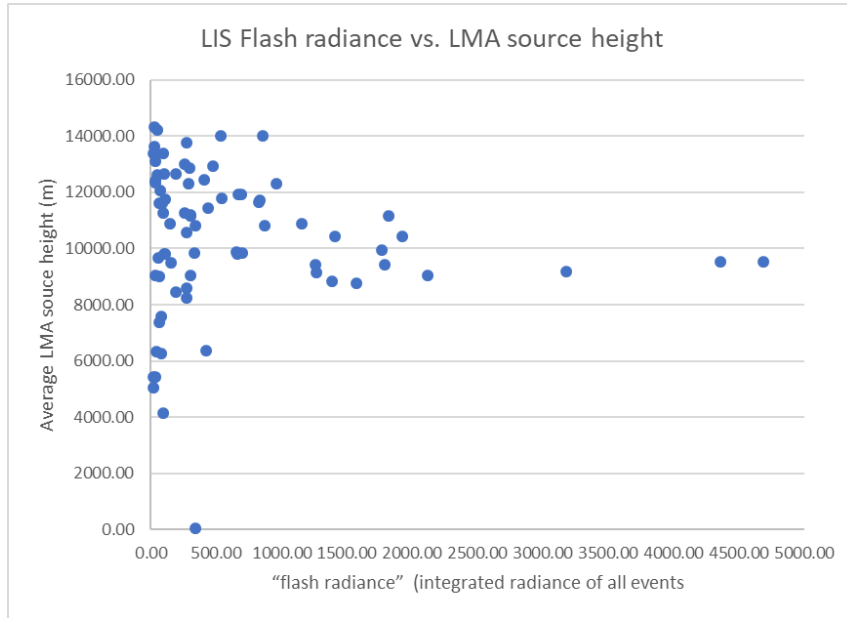


**Figure 4.4.3** ISS-LIS integrated radiance per flash ( $\text{J m}^{-2} \text{sr}^{-1} \mu\text{m}^{-1}$ ) and average height of the LMA associated flash.

In figure 4.4.4, flash durations have been added to the plot. One would expect to find a relationship between integrated radiance and flash duration. However, flashes with high integrated radiance are not especially long lasting. On the contrary, some of those having high integrated radiance are quite short. We also expected to find short durations in the higher flashes, which is not always the case.

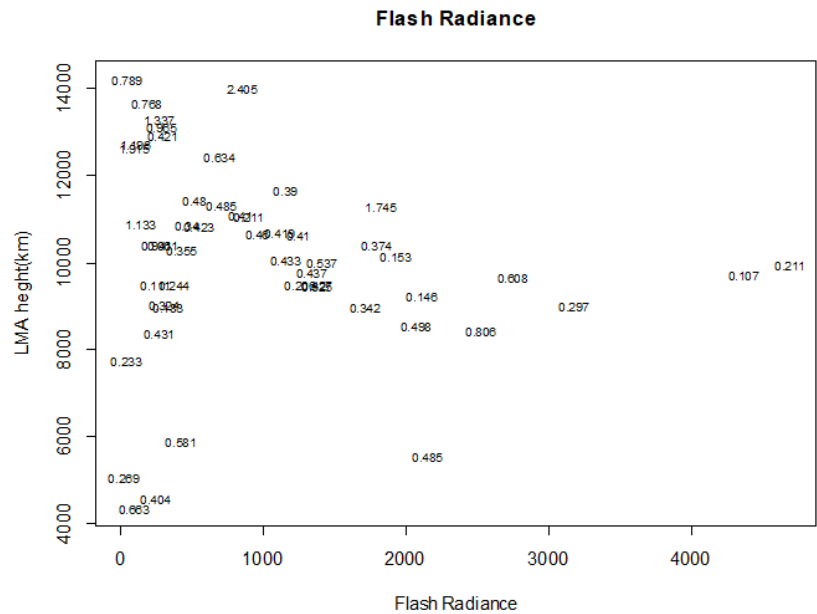


**Figure 4.4.4** ISS-LIS integrated radiance per flash ( $\text{J m}^{-2} \text{sr}^{-1} \mu\text{m}^{-1}$ ) and average height of the LMA associated flash. Dots have been replaced with numbers, which correspond to the flash duration (s).

Contrarily, there seems to be some correlation between the integrated flash radiance and the LMA source power, as shown in figure 4.4.5.

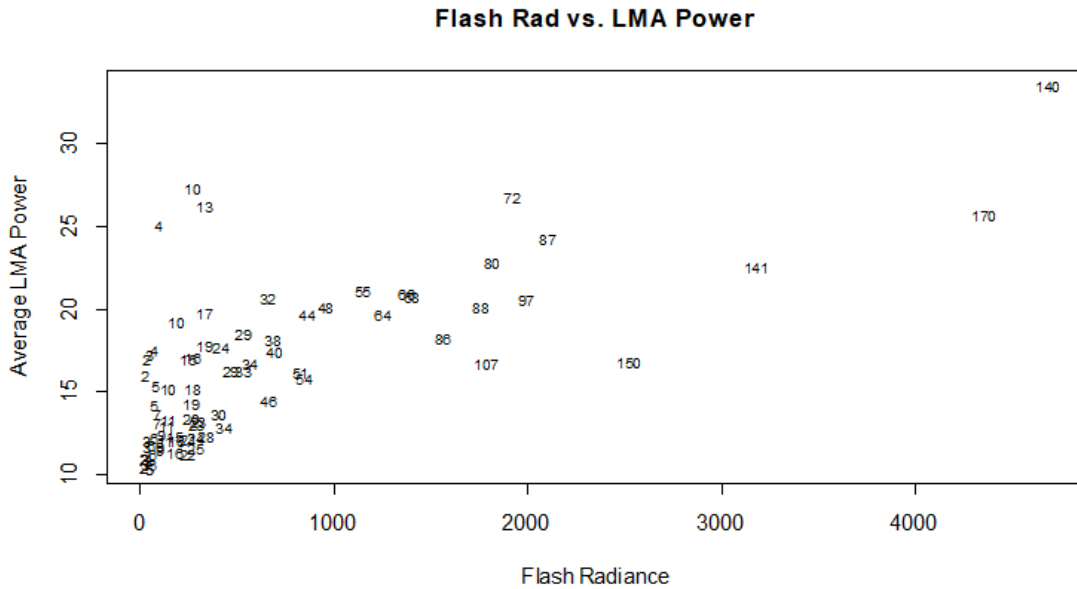


Figure 4.4.5. ISS-LIS integrated radiance per flash ( $J m^{-2} sr^{-1} \mu m^{-1}$ ) and average power of the LMA associated flash. Dots have been replaced with numbers, which correspond to the LIS events per LMA flash.

According to *Beirle et al. (2014)* clouds have a strong impact on the propagation of the optical pulse. Essentially, they cause a spatial smearing of the optical pulse via cloud multiple scattering, and the effect is more pronounced for flashes embedded more deeply below cloud top (*Thomason and Krider, 1982; Koshak et al., 1994*). In this regard, we think that, as future work, the cloud top and cloud optical depth should be taken into account to analyze event radiance (see annex A).

#### 4.5 Location accuracy

Location accuracy can be thought of as the offset between LMA and ISS-LIS detections, as well as the differences in size and overlap of the detections.

The location accuracy is tested with two methods. The first method determines the central latitude and longitude of LMA and ISS-LIS flashes, resulting in an absolute offset and the bias in  $x$  and  $y$  directions. These values can be compromised when two storm cells are active at the same time, with only part of them detected by ISS-LIS. Doing this for many flashes, histograms and statistical values are obtained.

The second method divides the LMA detection region into grid cells of 6 by 6 km (roughly the pixel footprint of ISS-LIS at the surface in mid latitudes). Both LMA sources and ISS-LIS events are mapped to this grid. In most cases, the ISS-LIS and LMA will not map exactly into the same pixels, so some ISS-LIS pixels will exist beyond the LMA contours, and vice versa. A grid cell can be expressed as “hit”, “false” or “miss” and the ratios  $hits/(hits+misses)$ : the percentage of the LMA cells correctly mapped by ISS-LIS; and  $false/(hits+false)$ , the fraction of all ISS-LIS cells not corresponding to an LMA cell.

The statistics can be assembled from the perspective of LMA flashes looking for corresponding ISS-LIS events, or from the perspective of ISS-LIS flashes, looking for corresponding LMA sources within 10 ms of the flash start and end times. The former is preferred as the ground-truth provided by LMA against which the performance of ISS-LIS is measured. Ideally, the ISS-LIS maps the flash with the same location and extent. The ISS-LIS perspective allows to be more specific to the LMA activity at the time of a ISS-LIS flash. Here we are getting closer to the process during a flash that emits light (except return strokes and currents which the LMA cannot detect).

The LMA flash algorithm looks for >150 ms of silent time between bursts of sources, after elimination of scattered sources, and additionally in this section, the algorithm was refined to identify clumps of simultaneous 6 km cells into different flashes if far enough apart. Only LMA sources at that time in the field of view of ISS-LIS were considered.

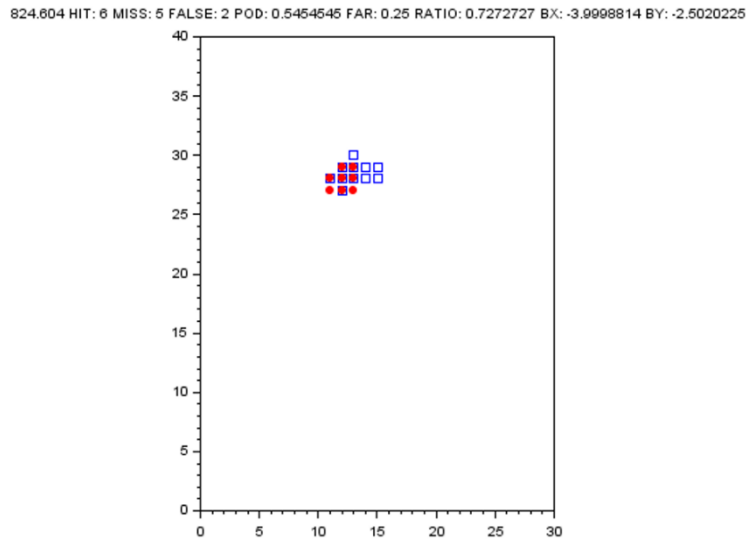


**Figure 4.5.1. LMA flash pixels (blue squares) versus corresponding ISS-LIS events (red circles). The fraction of LMA detected (POD) is 54.5%, while 25% of ISS-LIS pixels did not have LMA sources. The X and Y bias of the center of ISS-LIS relative to the center of the LMA flash was -4 km (longitude) and -2.5 km (latitude).**

The results for the 7 most active ISS-LIS passes (6 different days) are displayed in Table 4.5.1. The analysis was run for the area 0 – 2 degree longitude, 39.6 – 41.4 degrees latitude. This is larger than the area of the best LMA detection quality, because of the limited ISS-LIS numbers closer to the center of the LMA network. It can be expected that some LIS flashes may not be paired with an LMA flash. It could also affect the percentage of LIS unmatched by LMA, as parts of the LMA flashes will be poorly detected at great distance from the array. In case of the future LI, orbit no longer limits the number of matching events, and the area of study should be constricted to the area of best LMA performance only (see section 2).

<b>Table 4.5.1. Results from the LMA flash perspective.</b>							
Mean	171018/1	171018/2	180809	180831	180918	181014	181018
Abs offset, km	5.2 (stdv 2.8)	8.0 (1.5)	3.2 (2.4)	5.0 (2.9)	4.6 (2.9)	4.4 (3.6)	3.0 (2.2)
E-W bias, km	-1.5	-3.5	-0.9	-2.6	-1.2	-2.8	0.8
N-S bias, km	-1.5	-6.5	-0.3	0.5	1.0	-1.3	-1.3
LMA area, cell	3.6	11.6	4.9	1.8	5.7	5.8	5.4
LIS area, cell	3.7	5.4	11	5.4	5.3	5.9	3.6
% cells LMA matched	41	19	77	58	46	54	31
% cells LIS unmatched	55	36	67	77	38	50	30
LMA flashes	25	9	21	26	102	49	38
LIS flashes matching	13	3	19	19	65	33	16
Comment				Too far east			

<b>Table 4.5.2. Results from the ISS-LIS flash perspective.</b>							
Mean	171018/1	171018/2	180809	180831	180918	181014	181018
Abs offset, km	4.6 (stdv 3.1)	8.1 (4.5)	8.0 (12.3)	8.7 (9.8)	11 (22)	9.8 (25)	3.3 (3.7)
E-W offset, km	-1.0	-3.1	0.3	1.4	-2.0	-3.2	0.6
N-S offset, km	-1.1	-2.4	-2.9	4.1	2.0	-1.4	-2.0
LMA area, cell	3.7	10.8	4.7	2.3	4.5	5.7	6.7
LIS area, cell	7.1	12.8	11.1	12.9	4.6	8.7	7.6
% cells LMA matched	80	55	70	81	48	78	73
% cells LIS unmatched	62	53	71	82	57	54	40
LIS flashes	17	6	43	64	139	35	17
LMA matching	14	5	27	19	136	35	17

Table 4.5.1 shows the results from the LMA flash perspective. The absolute offset of ISS-LIS center to the LMA flash center varies between 3 and 8 km for different cases. Figure 4.5.2 is an example of a histogram displaying the distribution of error and x-bias for many flashes across multiple storm cases. It shows also that the mean offset in the table is larger than the median.

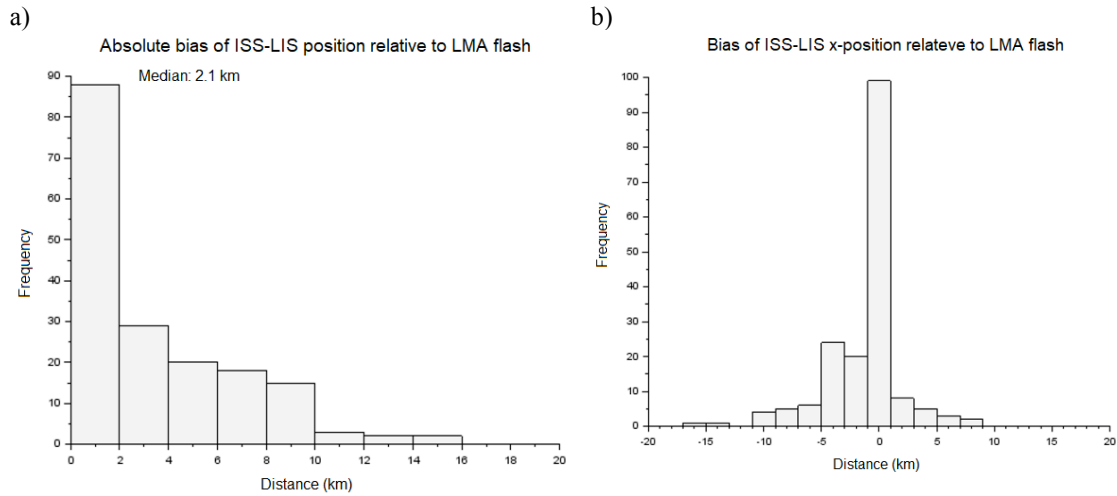


**Figure 4.5.2 (a) Absolute offset (km) between LMA flash and LIS activity center. (b) Bias in the x-direction (km). Individual flash offsets (x,y) are calculated by the differences on the median of the (x,y) location of the LMA sources and the median of the (x,y) location of the ISS-LIS events (not weighted).**

ISS-LIS activity is typically slightly biased to the west and south compared to the LMA flash. The scores for overlap between the two systems vary a lot from case to case. Typically, 30-60% of the LMA flash extension is covered by LIS pixels. Some of this comes from LMA flashes entirely not detected by LIS (this could be separated in future verification). Conversely, also 30-60% of LIS pixels are not corresponding to LMA activity underneath.

Some days have atypical LMA-LIS size ratios. 171018/2 shows on average ~11 grid cells  $(6*6) = 400 \text{ km}^2$  large LMA flashes, the largest of all studied passes. Most of these flashes have significant stratiform cloud (lower altitude) leaders, and may then not be detected as efficiently by ISS-LIS. The 180831 case had many flashes far from the LMA, so that the system misses parts or entire flashes.

The ISS-LIS flash perspective (Table 4.5.2) looks only at leader activity in LMA during just the ISS-LIS detections, but apparently results in greater offsets (typically 8-10 km) – these leaders may not be the producers of the light detected. On the other hand, it results in more of the LMA activity matched by ISS-LIS pixels (50-80%) while not improving the LIS excess pixels (50-70%).

Mean	<b>171018/1</b>	<b>171018/2</b>	<b>180809</b>	<b>180831</b>	<b>180918</b>	<b>181014</b>	<b>181018</b>
Abs offset, km	6.8 (stdv 3.0)	4.2 (3.8)			4.9 (2.6)	7.9 (3.9)	4.7 (2.8)
E-W bias, km	-0.9	-0.6			0.1	-4.9	2.5
N-S bias, km	-0.6	-4.1			1.0	-1.6	-2.5
LMA area, cell	2.7	6.5			3.4	4.9	4.0
LIS area, cell	2.0	11.5			4.1	5.0	2.9
% cells LMA matched	23	47			37	33	30
% cells LIS unmatched	81	66			73	71	59
LMA flashes	16	7	0	0	29	26	29
LIS flashes matching	5	3			13	14	12

Mean	<b>171018/1</b>	<b>171018/2</b>	<b>180809</b>	<b>180831</b>	<b>180918</b>	<b>181014</b>	<b>181018</b>
Abs offset, km	5.7 (stdv 3.0)	12.8 (8.4)	4.2 (3.4)	4.2 (1.3)	4.6 (2.8)	4.4 (3.5)	3.5 (2.4)
E-W bias, km	-1.8	-11	-0.6	-1.4	-1.5	-2.9	0.4
N-S bias, km	-2.8	-6.5	0.1	1.1	-0.5	-1.8	-0.8
LMA area, cell	2.8	9.5	3.2	1.7	3.6	4.7	4.7
LIS area, cell	4.3	7.8	11.8	5.0	5.7	6.1	4.1
% cells LMA matched	44	78	80	55	52	59	<b>37</b>
% cells LIS unmatched	66	13	78	75	65	55	36
LMA flashes	23	9	20	11	81	46	35
LIS flashes matching	12	3	18	8	56	31	16

Lastly, the effect of LMA altitude on ISS-LIS location accuracy was investigated. Here, only the parts of flashes were analyzed between 0-5, 5-10 and 10-15 km ranges. In the 0-5 km range low percentages of LMA matched by LIS can be noted (23-47%), while ISS-LIS pixels were also frequently not matched (~60-80%). The other altitude layers perform better without improvement over the general result (slightly best in the 10-15 km range, with numbers of 50-70% and 40-60% respectively, while in 5-10 km altitude range, they are 40-80% and 55-75% generally).

<b>Table 4.5.4. Results from the LMA flash perspective. 10-15 km</b>							
Mean	<b>171018/1</b>	<b>171018/2</b>	<b>180809</b>	<b>180831</b>	<b>180918</b>	<b>181014</b>	<b>181018</b>
Abs offset, km	4.0 (stdv 2.5)	7.0 (0.7)	2.7 (2.0)	5.4 (3.2)	4.9 (3.2)	4.0 (3.8)	2.9 (2.0)
E-W bias, km	-1.8	-3.5	-0.5	-2.3	-1.5	-1.7	0.5
N-S bias, km	-2.5	-5.1	-1.0	0.3	1.5	-1.8	-1.1
LMA area, cell	4.3	6.3	4.5	1.6	5.3	3.8	3.7
LIS area, cell	5.7	3.0	10.9	5.5	5.6	6.6	4.8
% cells LMA matched	60	18	85	64	53	67	51
% cells LIS unmatched	46	41	62	79	39	61	46
LMA flashes	9	7	19	26	83	40	25
LIS flashes matching	7	2	17	19	60	29	15

#### 4.5.1 Conclusions (Location Accuracy)

LIS activity is typically slightly biased to the west and south compared to the LMA flash. The mean absolute offset between ISS-LIS and LMA flash centers is 4.8 km. The mean x and y bias are -1.7 and -1.3 km, respectively. This means the overall calibration is really correct, much smaller than the pixel size.

The scores for overlap between the two systems vary a lot from case to case. On average 47% of the LMA flash extension is covered by ISS-LIS pixels. Some of this comes from LMA flashes entirely not detected by ISS-LIS (this is better separated in future verifications, to optimally separate flash detection efficiency from location overlap). A similar percentage of LIS pixels are not corresponding to LMA activity underneath, but it is to be expected that diffusion of light through cloud will lead to some overestimation of flash size.

A more puzzling result is that ISS-LIS flashes are apparently larger than LMA flashes, when using the ISS-LIS own flash algorithm, than the area of ISS-LIS events during an LMA flash. LMA flashes are on average 200 km<sup>2</sup>, corresponding ISS-LIS events 207 km<sup>2</sup>, but ISS-LIS flashes are 333 km<sup>2</sup>. This, perhaps, could be explained by cloud-to-ground strokes which, if far from the LMA, are poorly detected.

The ISS-LIS flash perspective looks only at leader activity in LMA during just the ISS-LIS detections, which would appear to be suitable for verifying the source in the lightning flash of the emitted light. However, the horizontal offsets actually are almost twice as

large (mean 7.6 km). So, these leaders may not be the producers of the light detected, but instead currents and return strokes.

Lastly, the effect of LMA altitude on ISS-LIS location accuracy was most marked for low altitude activity, where ISS-LIS matches less of the flash in position (mean 5.7 km for 0-5 km versus 4.4 km) and coverage (mean 34% at 0-5 km versus 57%). Besides that, often the flash parts below 5 km were not detected (42% detection efficiency versus 65%).

## 5. Model of lightning for test cases

In this section, statistical data useful to produce stochastic lightning flashes is provided. Lightning flashes can be parametrized in terms of duration, size, inter-flash time, the relation between duration and size and the maximum reached altitude.

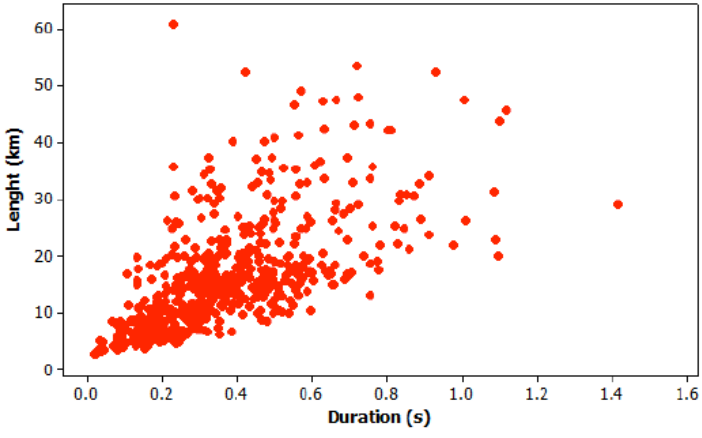
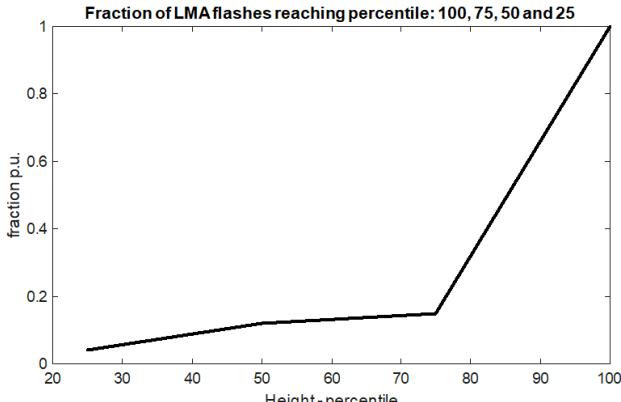
From the ISS-LIS (or LI) perspective, the number of events per flash, distribution of number of ISS-LIS flashes per LMA flash and the distribution of the ISS-LIS events within a flash are presented.

### 5.1 Statistics of lightning flashes derived from the LMA

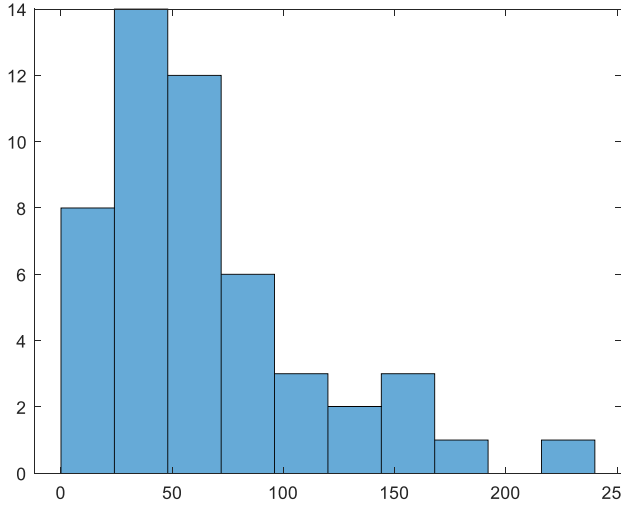
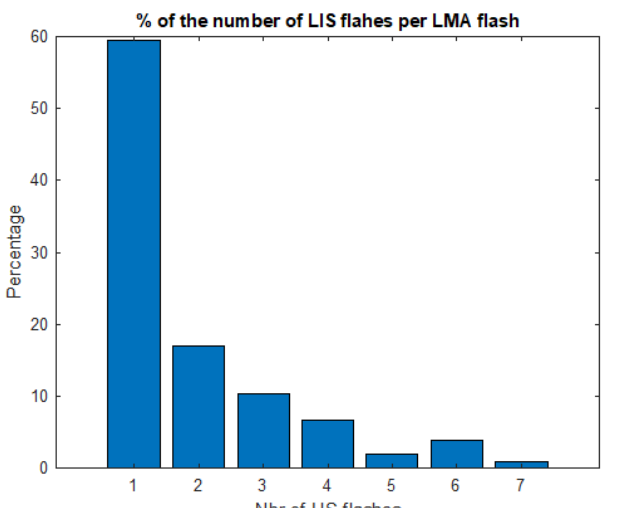
Parameter	
<b>Duration</b>	Summer: Median: 0.35 s Stdev: 0.31 s  Winter: Median: 0.41 s Stdev: 0.25 s  Maximum 2.39 s  Distribution is log-normal Source: López et al. (2016) based on the LMA in Spain.

<b>Size</b>	<p>Summer:</p> <p>Median: 10.3 km                  Stdev: 13.9 km                  Maximum 143 km</p> <p>Ellipse excentricity                  minor/major axes                  Median: 0.75                  Stdev: 0.154</p> <p>Winter:</p> <p>Median: 15.6 km                  Stdev: 10.9 km                  Maximum 70 km</p> <p>Ellipse excentricity                  minor/major axes                  Median: 0.75                  Stdev: 0.147</p> <p>Distribution is log-normal.                  Source: <i>López et al.</i> (2016) based on the LMA in Spain.</p>
-------------	--

Parameter	
<b>Inter-flash time</b>	<p>Summer:</p> <p>Median: 2.691 s                  Stdev: 14.51 s                  Min: 0.315 s (this can be as low as few tens of ms for some particular storms)                  Max: 150 s (the analysis was time limited up to 150 s)                  Number of samples for the statistics: 17526</p> <p>Winter:</p> <p>Median: 24.75 s                  Stdev: 29.692 s                  Min: 0.55 s                  Max: 150 s (the analysis was time limited up to 150 s)                  Number of samples for the statistics: 299</p> <p>Distribution is log-normal.                  Source: <i>J. López</i> (UPC).</p>

<p><b>Duration and size</b></p>	<p>In Montanyà et al. (2014, ICLP conf) flash size versus duration of the flash was analysed.</p>  <p><b>Figure 5.1. Lightning flash size versus duration (from Montanyà et al. 2014, ICLP).</b></p> <p>In that case the median relationship between distance and time corresponds to the speed of positive leaders <math>2 \cdot 10^4</math> m/s.</p> <p>Source: <i>Montanyà et al.</i> (2014) ICLP conference.</p> <p>It has been shown that the size of lightning flashes is also related to the intensity of the storm. Storms with high lightning flash rates tend to produce smaller flashes than storms with lower flash rates (<i>Bruning and MacGorman, 2013</i>)</p>
<p><b>Maximum flash height</b></p>	<p>Obtained from the analysis conducted in section 4.1.4. The sample is 151 flashes.</p>  <p><b>Fraction of LMA flashes reaching percentile: 100, 75, 50 and 25</b></p>

### 5.2 ISS-LIS statistics useful for simulate lightning

Parameter	
<p><b>Number of events per flash</b></p>	 <p><b>Figure 5.2 Number of ISS-LIS events per LMA flash.</b></p> <p>Median: 55 events per flash                      Stdev: 47.18                      Number of samples: 50</p>
<p><b>Number of ISS-LIS flashes per flash</b></p>	<p>See section 4.1</p>  <p><b>Figure 5.3 (same as 4.1.4) Distribution of the number of ISS-LIS flashes per individual LMA flash.</b></p>

**Distribution of ISS-LIS events within a flash**

**Distribution of ISS-LIS events on a normalized duration flash.**

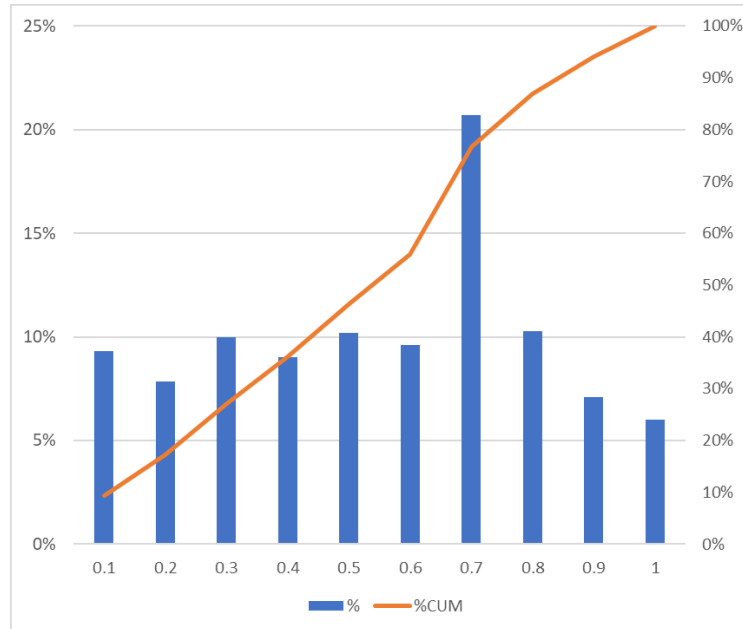


**Figure 5.3 (same as 4.2.5) Frequency of LIS events along the normalized LMA flash duration. in bins of 10%. The line (right axis) represents the accumulation.**

## 6. Validation of LI and routine monitoring

### 6.1 Introduction

In this section, we propose the strategy of using the LMA to validate the MTG-LI. Based on the analysis and results from the previous sections, we propose methods and we evaluate their applicability:

- Flash Detection Efficiency (FDE)
- Flash False Alarm (FFAR)
- Absolute Sample Position Knowledge Error (ASPKE)
- Time Accuracy (TA)
- Pulse detection efficiency (PDE)
- Pulse detection false alarm (PFAR)

### 6.2 Definition of the performance evaluation

#### 6.2.1 Flash Detection Efficiency

##### Summary (FDE)

Flash Detection Efficiency (FDE) correspond to the ratio between the flashes detected by LI versus the total number of LMA flashes. A time and distance criteria is considered to exclude flashes occurring at different time as well simultaneous flashes occurring at different storms. This is a flash by flash approach.

Flashes detected by the LMA are used as reference so LMA level-2 data is used. LMA flashes will be restricted to an area defined by sensitivity of <P dBW ensuring that LMA flashes will keep their properties.

##### Input data (FDE)

- LI level-2 data: events, groups and flash information.
- LMA level-2 data: VHF sources grouped in flashes.

LMA level-2 data format:

Date (YYYYMMDD) - Time UTC (s) – LAT – LON – Height (m) – Power (dBW) – Source ID – Flash ID – LAT centroid- LON centroid

### Configuration parameters (FDE)

- Time tolerance (T) corresponding to the extension of time at the start and at the end of a LMA flash.
- Distance tolerance (D) corresponding to the distance between LMA flash centroid and LI weighted centroid. This is used to discriminate LI flashes occurring at the same time as the reference flash in the LMA but corresponding to another storm.
- Area of evaluation for a given LMA power sensitivity (P): This area will correspond to the area where the LMA can detect lightning sources with power  $< P$  dBW. Because this area depends on the status of the network at a given moment (e.g. number of sensors, noise level at each station, etc), this shall be determined for each particular day or episode. The area of  $< P$  dBW will be provided in a gridded format.

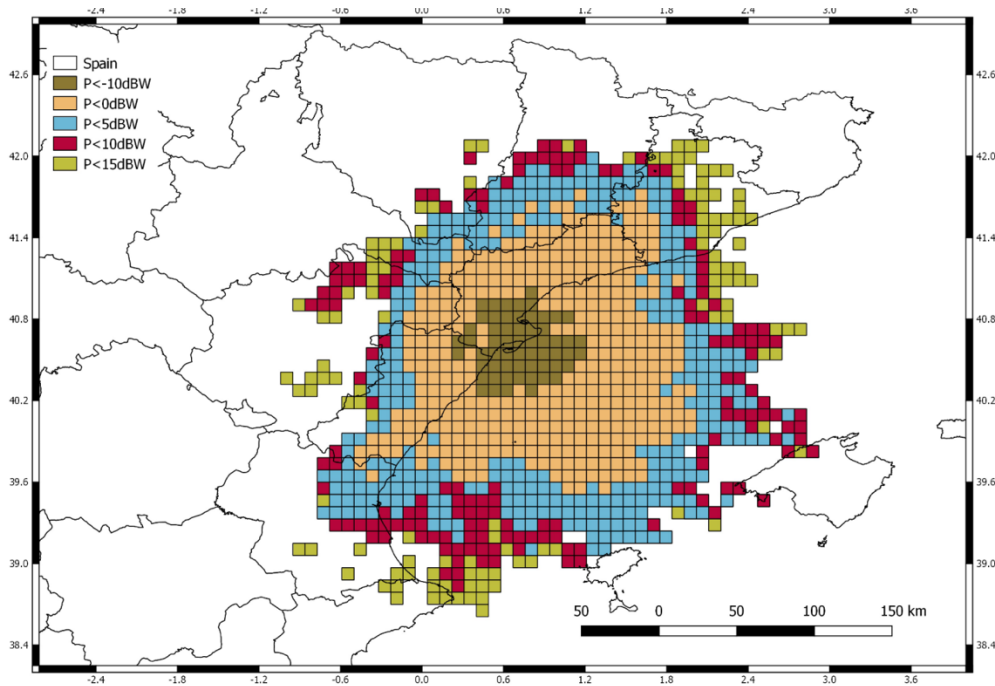


Figure 6.2.1 Example of  $< P$  dBW area ( $P = -10, 0, 5, 10, 15$  dBW) used to determine the area to consider for the analysis.

In theory, all LMA networks shall be comparable in the calibration of the determination of the power emitted by the VHF sources. However, due to the use of different antennas, frequency bands and preamplifiers the calculated powers can be different. So the power sensitivity level  $P$  can be different as well. This level can be obtained by analyzing the sources within LMA lightning flashes. The area defined by the sensitivity of  $< P$  dBW shall correspond to an area where the LMA is sensitive enough to detect positive leaders. Positive leaders are known to radiate less VHF power, so they require

higher sensitivity. As example, figure 6.2.2 shows the time-distance plot of a LMA lightning flash. In the time distance-plot, the indicated slopes (dashed lines) corresponds to the typical speeds of positive leaders and negative leaders. In this example it is clear that the sources that belong to positive leaders are organized along the lower slope ( $2 \cdot 10^4$  m/s) and are characterized by lower power emissions <5 dBW.

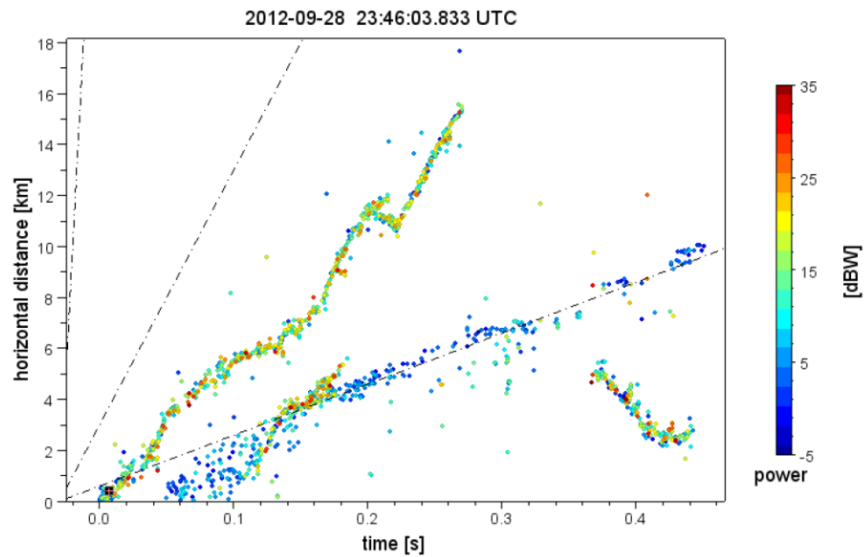


Figure 6.2.2 Time-distance graph of LMA sources, mapped by the Ebro Lightning Mapping Array. In this plot a location is selected as reference (e.g. first LMA source) and sources are plotted according to the time and distance from the reference source. Sources are coloured by power. Dashed lines indicate slopes corresponding to speeds of  $2 \cdot 10^4$  m s<sup>-1</sup> typical of positive leaders,  $10^5$  m s<sup>-1</sup>, and  $10^6$  m s<sup>-1</sup>, both typical of negative leaders. Source *van der Velde and Montanyà (2013)*.

By analyzing a representative number of flashes, a LMA data operator shall determine the power thresholds of the network that characterize positive leaders. This will define the sensitivity level P required for the analysis area.

## Output data (FDE)

- Flash detection efficiency.
- Flash detection efficiency as a function of the maximum height of LMA flashes expressed in percentiles: 90, 75, 50 and 25.
- LI FDE output data indicating these LI flashes that have been associated to LMA flashes. That can/will be used for further analysis, e.g. DE vs. LMA flash duration.
- LMA FDE output data indicating these LMA flashes that have been associated to LI flashes. That can/will be used for further analysis, e.g. DE vs. LMA flash duration.

The following figure summarizes the inputs and outputs for the analysis.

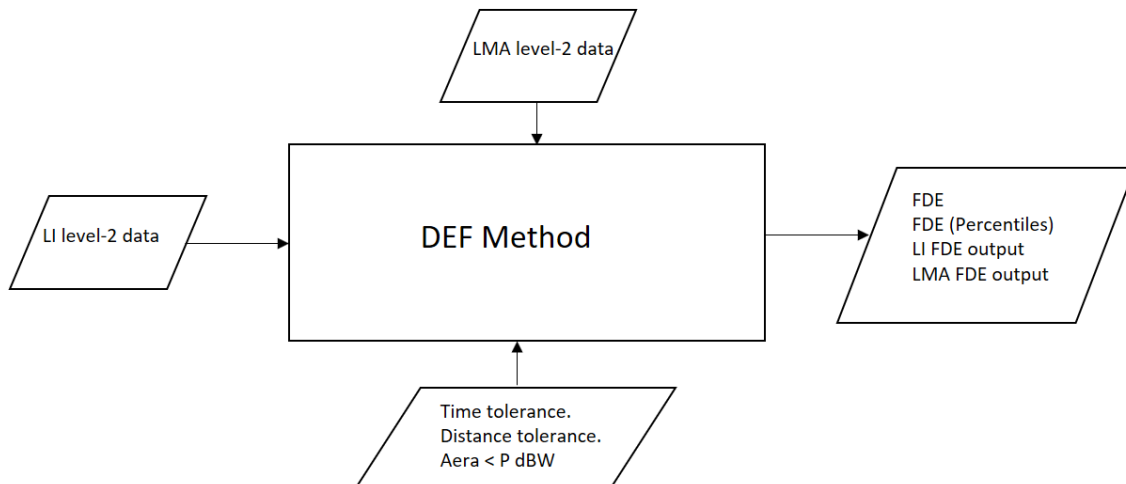


Figure 6.2.3 Summary of the input/output for the evaluation of the FDE.

## Method (FDE)

- Identification of LMA flashes within the sensitivity <P dBW area of the LMA coverage for the particular day/episode. This area is included as a configuration parameter.
- Determination of the altitude percentiles. For a giving time, the percentiles 90, 75, 50 and 25 will be determined by means of the LMA source altitude distribution. To do that, periods centered at the corresponding time with duration of at least of 30 minutes will be evaluated if the number of LMA flashes is higher than 10.
- For each LMA flash ID occurring at the considered area, start  $t_{LMA\_start}$  and end  $t_{LMA\_end}$  times are obtained from the first and last source of the corresponding LMA flash ID.
- The start time and end time of a flash:  $t_{start} = t_{LMA\_start} - T$  and  $t_{end} = t_{LMA\_end} + T$ .
- LI events occurring within  $t_{start}$  and  $t_{end}$  will be obtained.

- LI events in which their flash centroid is located at a distance  $> D$  to the LMA flash centroid for the corresponding LMA ID flash will be removed.
- If there are LI events within  $t_{start}$  and  $t_{end}$  and LMA-LI flash centroid distances of  $< D$  this will be accounted as detected. The counter of the number of detected flashes will be increased. For these LI events their corresponding LI flashes will be identified. All the LI events of these identified flashes will be marked with the ID of the LMA flash. LMA flashes detected by LI will be marked as detected.
- Once all the LMA flashes within the analyzed area have been identified, FDE will be computed:
  - FDE is calculated as the total number of LMA flashes detected by LI divided by the total number of LMA flashes.
  - FDE (90,75,50,25) are calculated as the total number of LMA flashes that their maximum sources are below the percentiles 90,75,50,25 and have been detected by LI divided by the total number of LMA flashes that their maximum sources are below the percentiles 90,75,50,25, respectively.
- Generation of output data:
  - LI FDE data with identification of LI flashes that has been associated to LMA flashes.
  - LMA FDE with identification of LMA flashes that have been associated to LI flashes.

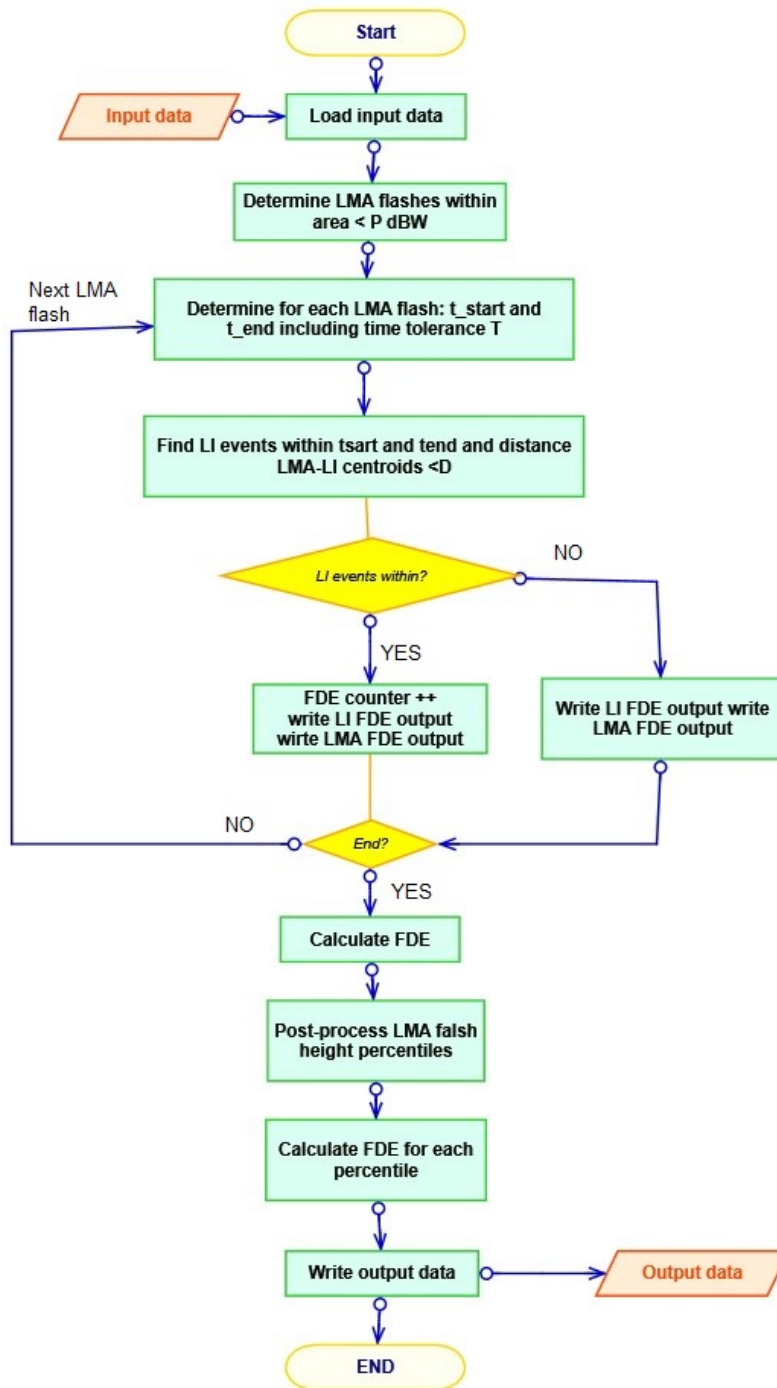


Figure 6.2.4 Flow chart for the evaluation of the FDE.

## Analysis of applicability and risk

<b>Assumptions</b>	<ul style="list-style-type: none"> <li>• LMA is the reference network (<math>DE_f \text{ LMA} = 100 \%</math>).</li> <li>• LMA flashes are taken as reference. It can happen that one LMA flash has assigned several LI flashes.</li> <li>• Constant performance of the LI during the studied period and over the domain of interest.</li> <li>• Constant performance of LMA for a giving period. This is provided as the area of <math>&lt;P</math> dBW for a giving period (typical one day).</li> </ul>
<b>Limitations</b>	<ul style="list-style-type: none"> <li>• Small areas due to the limited range of the LMA.</li> <li>• Episodes with high flash rates difficult the identification of individual flashes. E.g. some storms present almost continue flash activity. A more complex flash identification would be necessary for these cases.</li> <li>• LMA data needs to be transferred. Full data (science data) cannot be transferred and processed in real time. For continuous analysis periodicity should be defined.</li> </ul>
<b>Key configuration parameters</b>	<ul style="list-style-type: none"> <li>• LMA flash definition. In special for high lightning flash rates where identification of individual flashes can be difficult.</li> <li>• Area of analysis. Areas where LMA has low power detection capability (high sensitivity) are convenient in order to keep flash properties (e.g. size and duration). But this limits the evaluation range. Larger areas can be used for only FDE computation.</li> </ul>
<b>Confidence of success</b>	<ul style="list-style-type: none"> <li>• High.</li> </ul>
<b>Applicability</b>	<ul style="list-style-type: none"> <li>• High in terms of implementation of the method and conduction of the analysis.</li> <li>• For continuous evaluation a periodicity shall be defined according to the LMA data availability.</li> </ul>

## 6.2.2 Flash False Alarm (FFAR)

### Summary (FFAR)

Flash False Alarm (FFAR) corresponds to the identification of false LI flash detections. In this case, LI flashes not matched with LMA flashes are identified as candidates to False Alarm (FFA). For these candidates, LMA source data (LMA level-1 data) will be used to confirm false detections.

### Input data (FFA)

- LI level-2 data.
- LI level-2 FDE output that identifies LI matches with LMA-flashes.
- LMA level-1 data. This data corresponds to all the sources located by LMA.

LMA level-1 data format:

Date (YYYYMMDD) - Time UTC (s) – LAT – LON – Height (m) – Power (dBW) – Source ID

### Configuration parameters (FFA)

- Time tolerance (T) corresponding to the increase of time at the start and end of a LI flash. This is important to avoid cases of candidates to LI FFA that happen very close in time (e.g. less than 1 s) to LMA flashes.
- Distance tolerance (D) corresponding to the distance between LMA sources and the closest LI event for a corresponding LI flash.
- Area of concern. This area corresponds to the area where the LMA can detect sources with  $<P$  dBW for that particular day. This area will be provided in the same grid as the LI.

### Output data (FFAR)

- Number of LI FFA, number of total LMA flashes in the area of concern.

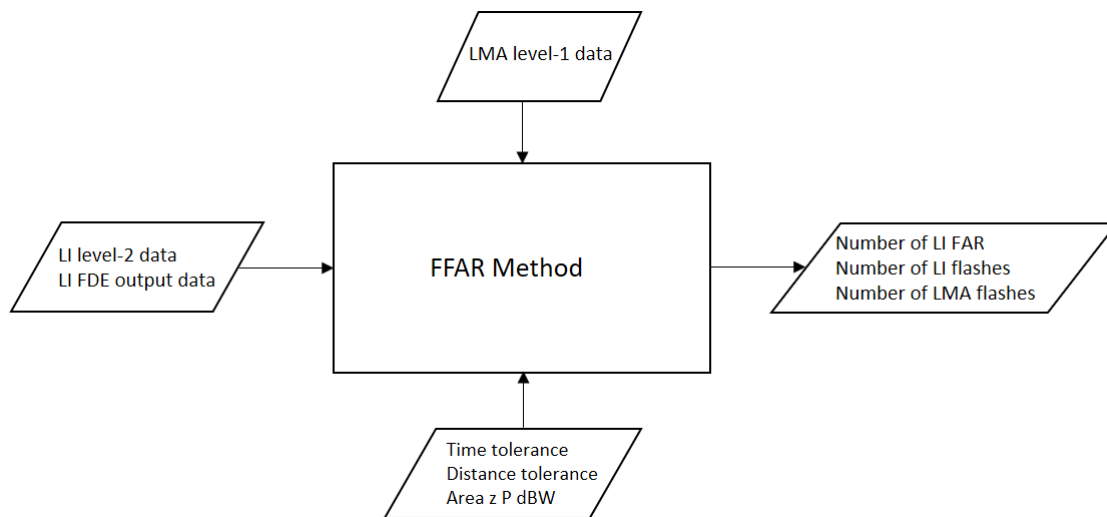


Figure 6.2.5 Summary of the input/output for the evaluation of the FFAR.

## Method (FFAR)

- Load output data of LI level-2 FDE.
- Load LMA level-1 data.
- Load grid data of <P dBW area.
- Identification of LI flashes that their flash ID has not been associated to any LMA flash.
- If LI flashes that has not been associated with LMA occur within the LMA coverage area of <P dBW, these will be identified as LI FFA candidates (flash false alarm).
- For each LI FFA candidate, start time and end time will be determined  $t_{start} = t_{LI\_start} - T$  and  $t_{end} = t_{LI\_end} + T$ .
- A LI FFA candidate will be considered as LI FFA if there are not LMA sources (LMA data level-1) occurring between  $t_{start}$  and  $t_{end}$  and within a distance D of the source location and the closest LI event for that particular LI flash.
- Generate output:
  - Number of FFA LI flashes.
  - Number of LMA flashes within the coverage area <P dBW.
  - Number of LI flashes within the LMA coverage area <P dBW.
  - Number of FFA LI flashes occurring during a 'fair weather day' (day or period without any lightning activity detected by the LMA). It will be considered 'fair weather' day or episode if within a period of  $\pm 3$  h from the time of the LI candidate there is not any LMA flash in the long range.
  - Number of FFA LI flashes occurring during active thunderstorms.

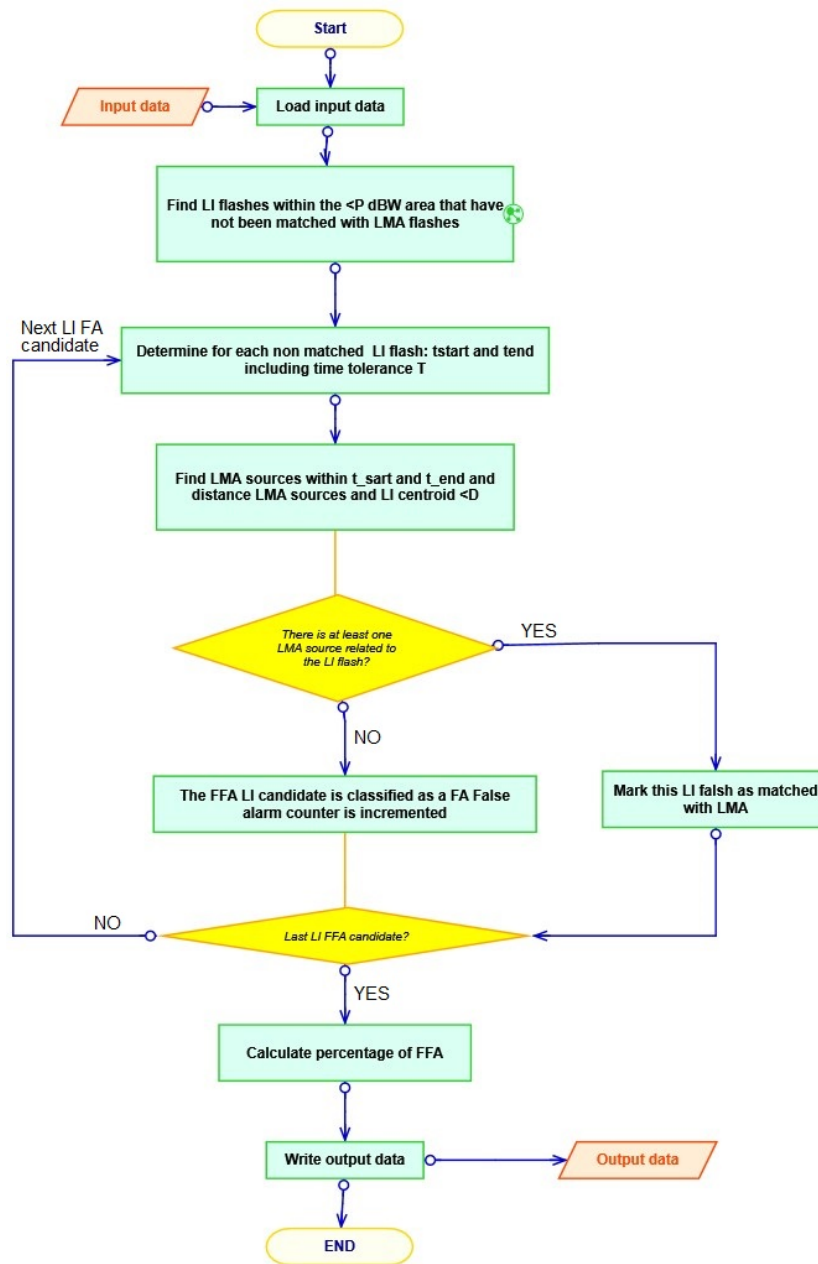


Figure 6.2.6 Flowchart for the analysis of the FFAR.

<b>Assumptions</b>	<ul style="list-style-type: none"> <li>• LMA is the reference network (<math>DE_f \text{ LMA} = 100 \%</math>).</li> <li>• LMA sources are taken as reference.</li> <li>• High performance of the LMA within the <math>&lt;P</math> dBW area.</li> </ul>
<b>Limitations</b>	<ul style="list-style-type: none"> <li>• Small areas due to the limited range of LMA.</li> <li>• LMA data needs to be transferred. Full data (science data) cannot be transferred and processed in real time. For continuous analysis periodicity should be defined.</li> </ul>
<b>Key configuration parameters</b>	<ul style="list-style-type: none"> <li>• Area of analysis. Area of high sensitivity where LMA has low power detection capability (<math>&lt; P</math> dBW) must be considered. This area shall correspond to the analysed day or episode.</li> <li>• Time tolerance (T) This is important in order to avoid cases of LI FFA candidates that happen very close in time (e.g. less than 1 s) to LMA flashes.</li> </ul>
<b>Confidence of success</b>	<ul style="list-style-type: none"> <li>• Moderate. Even there is low probability that using LMA level-1 data it will not be any source of a flash within the high sensitivity data. For those resulting FFA LI flashes, LMA level-0 data should be inspected to finally confirm a FA flash.</li> </ul>
<b>Applicability</b>	<ul style="list-style-type: none"> <li>• High, in terms of implementation of the method and conduction of the analysis for LMA level-1 data.</li> <li>• For the use of LMA level-0, this is recommended to be carried out by the LMA network operator.</li> <li>• For continuous evaluation periodicity needs to be defined according to the LMA data availability.</li> </ul>

### 6.2.3 Absolute Sample Position Knowledge Error (ASPKE) – Location Accuracy-

#### Summary (ASPKE)

Location accuracy (ASPKE) is proposed to be conducted using a gridded approach in which cells containing LMA sources of flashes are compared to the cells containing LI events.

#### Input data (ASPKE)

- LI level-2 data.
- LMA level-2 data.
- LI FDE output data

#### Configuration parameters (ASPKE)

- LI grid.
- Time tolerance (T), distance tolerance (D) and LMA sensitivity area of < P dBW are not needed if LI FDE output data is used.

#### Output data (ASPKE)

- Statistics of offset: latitude offset, longitude offset and absolute offset.
- Statistics of spatial overlap.
- Statistics of area (size) of LI and LMA flashes.

#### Method (ASPKE)

- For each LMA flash that has been matched with LI events in the FDE process the corresponding LMA level-2 sources are assigned the corresponding sources to the LI grid.
- From the LI FDE output data, assign the corresponding LI flash/es to the LMA flash to analyse.
- Determine offset per flash: offsets in latitude, longitude and absolute. LMA centroid is calculated from the LMA gridded data. LI centroids are obtained from LI level-2 data.
- Determine contingency table for overlapping:
  - A cell is classified as *hit* both LMA and LI located this cell. Count the *hit* grid cells.
  - A cell is classified as *false* if a cell is located by LI and not by LMA. Count the *false* grid cells.

- A cell is classified as a *miss* if it is located by LMA and not by LI. Count *miss* grid cells.
- A grid cell where there was not detection from any system is counted as *correct negative*. These cells are not used here.

L M A	LI	
	YES	NO
YES	Hit	Miss
NO	False	Correct negative

- Calculate statistics:

$$\text{Fraction of LMA grid cells correctly mapped by LI} = \frac{\text{hits}}{\text{hits} + \text{misses}}$$

$$\text{Fraction of LI grid cells not corresponditn to LMA} = \frac{\text{false}}{\text{hits} + \text{false}}$$

- Calculate area of LI and LMA flashes and their statistics.

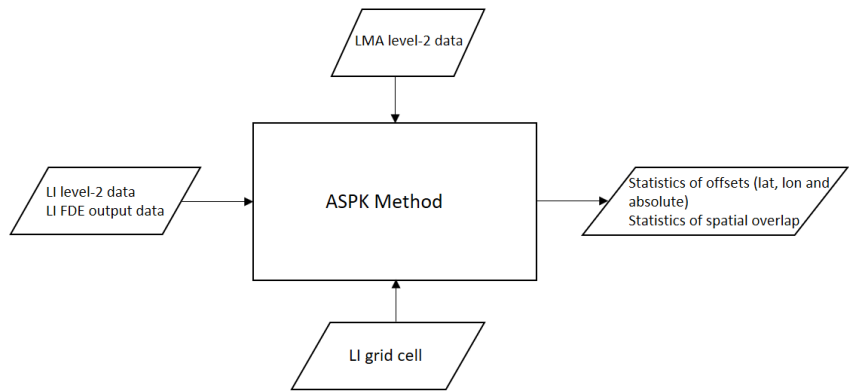


Figure 6.2.7 Summary of the input/output for the evaluation of the ASPK.

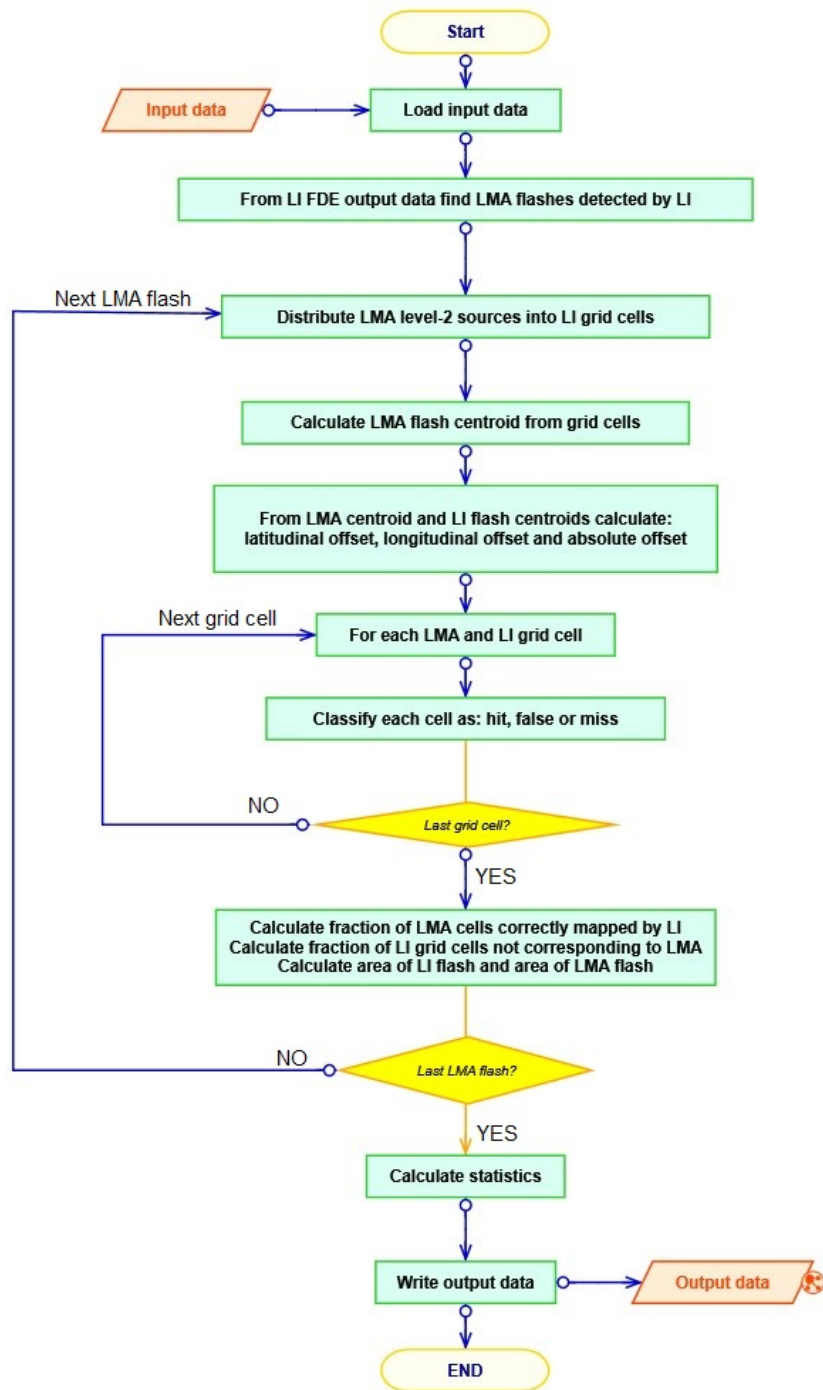


Figure 6.2.8 Flowchart for the evaluation of the ASPK.

<b>Assumptions</b>	<ul style="list-style-type: none"> <li>• LMA is the reference network (assumed no location error).</li> <li>• High performance of the LMA within the &lt;P dBW area.</li> </ul>
<b>Limitations</b>	<ul style="list-style-type: none"> <li>• Small areas due to the limited range of LMA.</li> <li>• LMA data needs to be transferred. Full data cannot be transferred and processed in real time. For continuous analysis periodicity should be defined.</li> </ul>
<b>Key configuration parameters</b>	<ul style="list-style-type: none"> <li>• Area of analysis. Area of high sensitivity where LMA has low power detection capability (&lt; P dBW) must be considered. This area shall correspond to the analysed day or episode.</li> <li>• LI grid.</li> </ul>
<b>Confidence of success</b>	<ul style="list-style-type: none"> <li>• High</li> </ul>
<b>Applicability</b>	<ul style="list-style-type: none"> <li>• High</li> </ul>

#### 6.2.4 Time Accuracy (TA)

##### Summary (TA)

Time accuracy at flash level is computed as the difference between the time of the initiation of a LMA flash (first source) and the time of the first event detected by LI.

##### Input data (TA)

- LI FDE output data that includes information of the LMA-LI matched flashes.
- LI level-2 data
- LMA level-2 data.

##### Configuration parameters (TA)

- None.

##### Output data (TA)

- Statistics on the time difference between flash initiations.

##### Method (TA)

- Check LI flashes that have been matched with LMA flashes. If several LI flashes are assigned to the same LMA flash, select the first LI flash that corresponds to the initiation.

- For the LI flashes obtained in the previous step, compute the time difference from their corresponding LMA flashes. Time difference corresponds to the time between the first source of the LMA in a flash and the first event of the LI flash.
- At the end, compute statistics between the time difference.

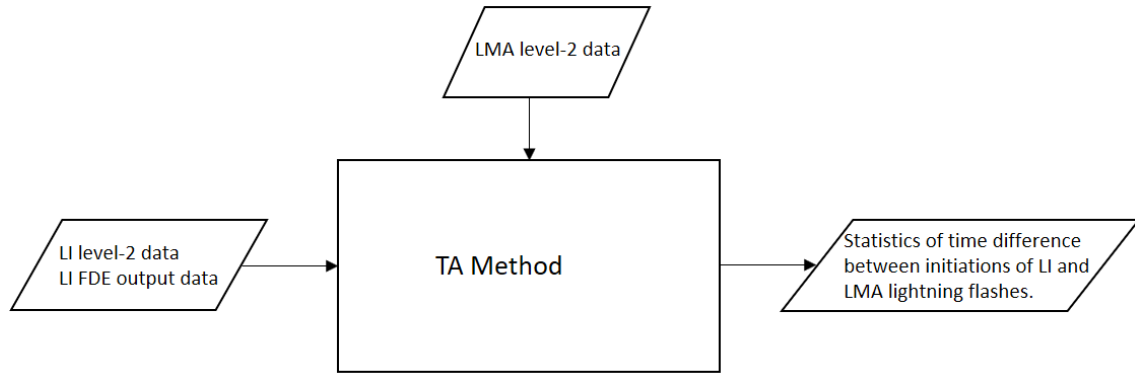


Figure 6.2.9 Summary of the input/output for the evaluation of the TA.

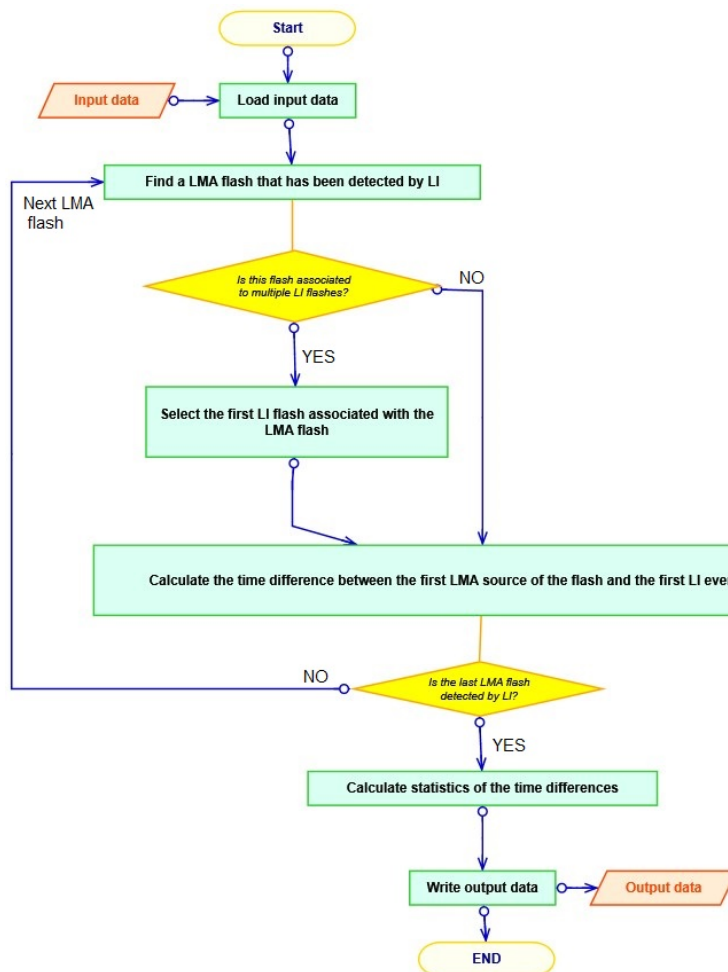


Figure 6.2.10 Flowchart for the evaluation of the TA.

<b>Assumptions</b>	<ul style="list-style-type: none"> <li>• LMA is the reference network (<math>DE_f \text{ LMA} = 100 \%</math>).</li> <li>• LMA detects the whole flash.</li> <li>• LMA sources are taken as reference.</li> <li>• High performance of the LMA within the <math>&lt;P \text{ dBW}</math> area.</li> </ul>
<b>Limitations</b>	<ul style="list-style-type: none"> <li>• The evaluation is limited to areas due to the limited range of LMA.</li> <li>• LMA data needs to be transferred. Full data cannot be transferred and processed in real time. For continuous analysis periodicity should be defined.</li> </ul>
<b>Key configuration parameters</b>	<ul style="list-style-type: none"> <li>• Area of analysis. Area of high sensitivity where LMA has low power detection capability (<math>&lt; P \text{ dBW}</math>) must be considered. This area shall correspond to the analyzed day or episode.</li> </ul>
<b>Confidence of success</b>	<ul style="list-style-type: none"> <li>• High.</li> </ul>
<b>Applicability</b>	<ul style="list-style-type: none"> <li>• Easy.</li> </ul>

### 6.2.5 LI L1b L2 Pulse detection efficiency (PDE)

In this study we have shown that there is not a straight relation between the detected lightning leaders by the LMA and the optical pulses detected by ISS-LIS. For example, the next figure shows a LMA flash, ISS-LIS events and LMA level-0 (raw) data.

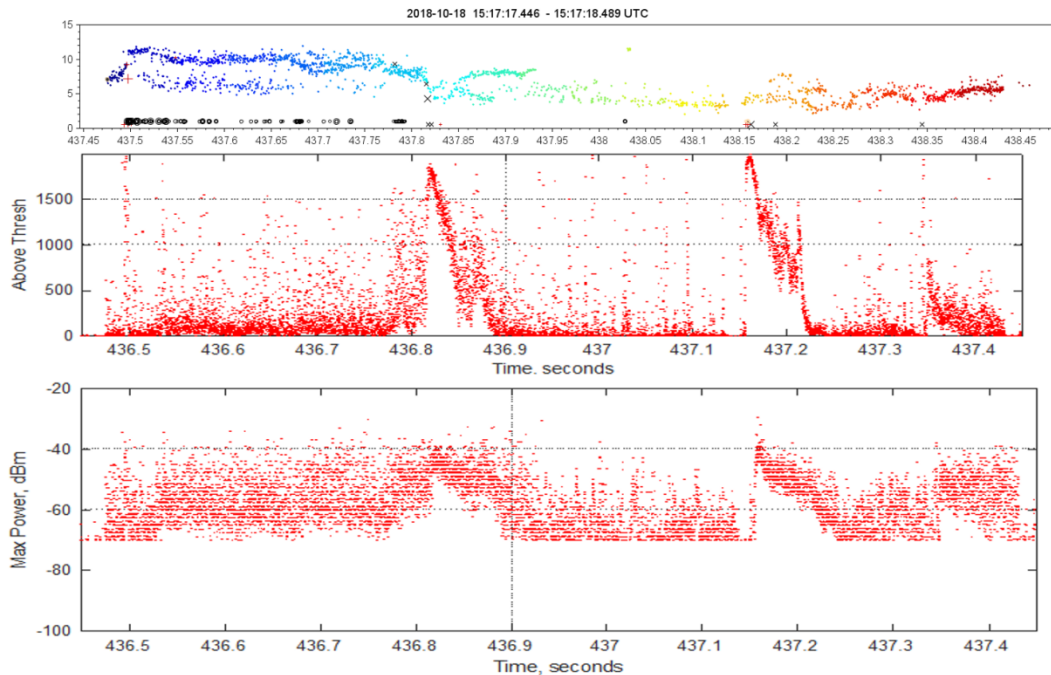
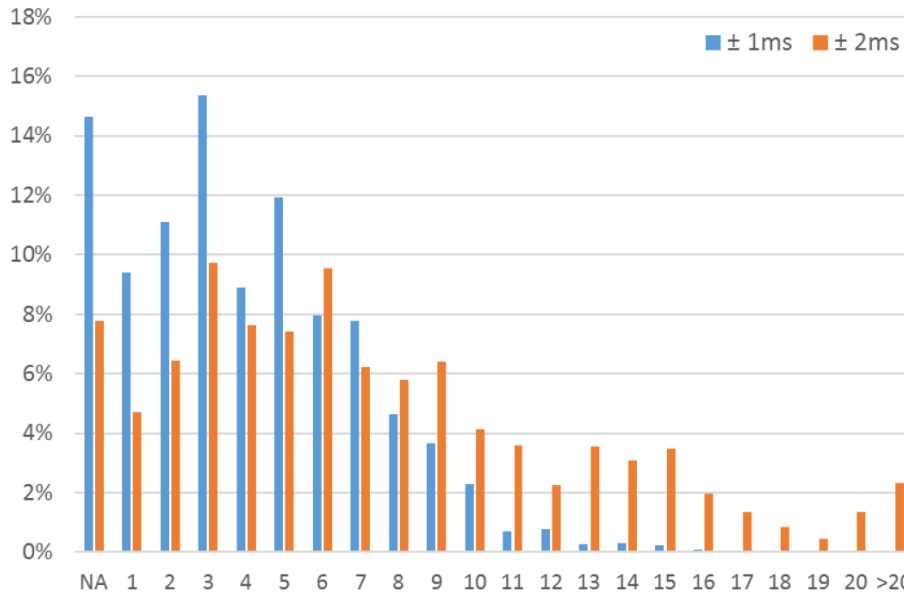


Figure 6.2.11 Example of LMA lightning flash and LMA raw data. *Top*: Altitude (km) of LMA sources vs. time (s), circles are ISS-LIS events, (+) and (x) are lightning strokes detected by an LLS. *Middle*: Number of VHF detections by the LMA. *Bottom*: Maximum power per detection. Note that one second needs to be added to the time in the middle and bottom plots.

As conclusion here, pulse detection efficiency (PDE) cannot be accurately evaluated by means of the LMA data. At pulse level, LMA can provide just the existence of LMA sources (LMA level-1) and VHF emissions (LMA level-0) during the period of a LI pulse. From the experience in this work, it can happen that few sources occur during the frame time (2 ms). In addition, it might happen that the luminosity related to a cloud-to-ground return stroke is not accompanied with LMA sources for a period of the frame time (2 ms).

A preliminary analysis shows the number of LMA sources per ISS-LIS event with a within a window of  $\pm 1$  ms and  $\pm 2$  ms.



**Figure 6.2.12** Number of LMA sources associated to ISS-LIS event considering a time window of  $\pm 1$  ms and  $\pm 2$  ms around the time of the ISS-LIS event.

The graph in figure 6.2.12 for a time window of  $\pm 2$  ms shows that about 8 % of the ISS-LIS events do not have any associated LMA source. So 92 % of the ISS-LIS events have at least one LMA source. The 8 % of events without LMA sources a might correspond to candidates to pulse false alarm (PFA) cases.

### Input data (PDE)

- LI FDE output data that includes the information of the LMA-LI matching.
- LI level-2 data.
- LI level 1b data.
- LMA level-1 data.

### Configuration parameters (PDE)

- Time uncertainty to extent the frame integration time. This corresponds to the absolute time accuracy of LI frames.

### Output data (PDE)

- Percentage of LI pulses related to LMA lightning leader activity.

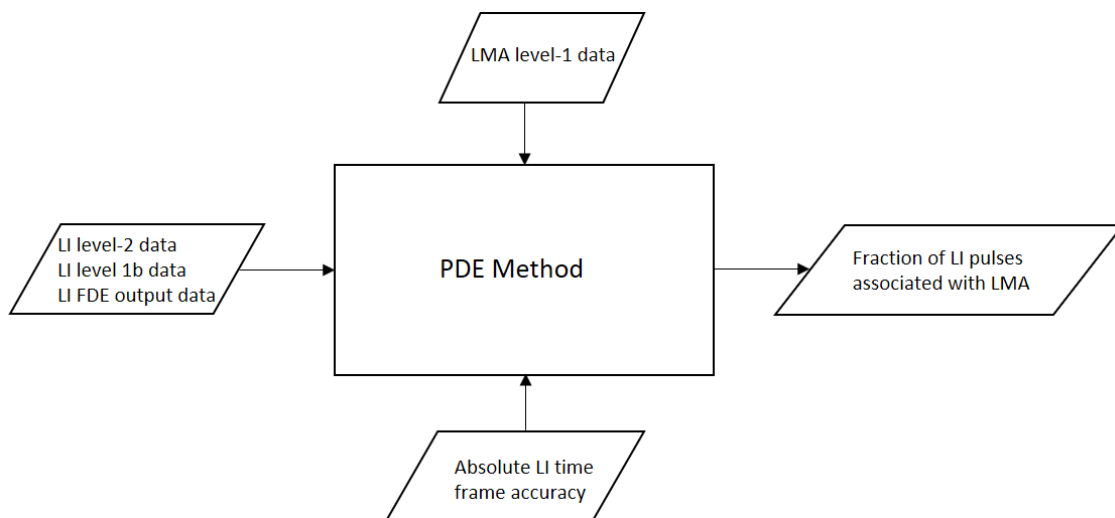


Figure 6.2.13 Summary of the input/output for the evaluation of the PDE.

### Method (PDE)

- Load input data.
- From LI FDE output, select flashes detected by both LI and LMA.
- For each LMA flash determine the start and end of each LI frame related to this flash. That means, divide the time of the LMA flash in periods of LI frames. This time shall include the time uncertainty.
- For each frame check if there are any LMA sources. In case there is at least one LMA source increase the counter of PDE.
- Once all the frames (pulses) are evaluated calculate the fraction of LI pulses with LMA sources versus the total number of frames.
- Repeat for all the selected flashes.
- Write statistics of the fraction of LI pulses associated with LMA sources.

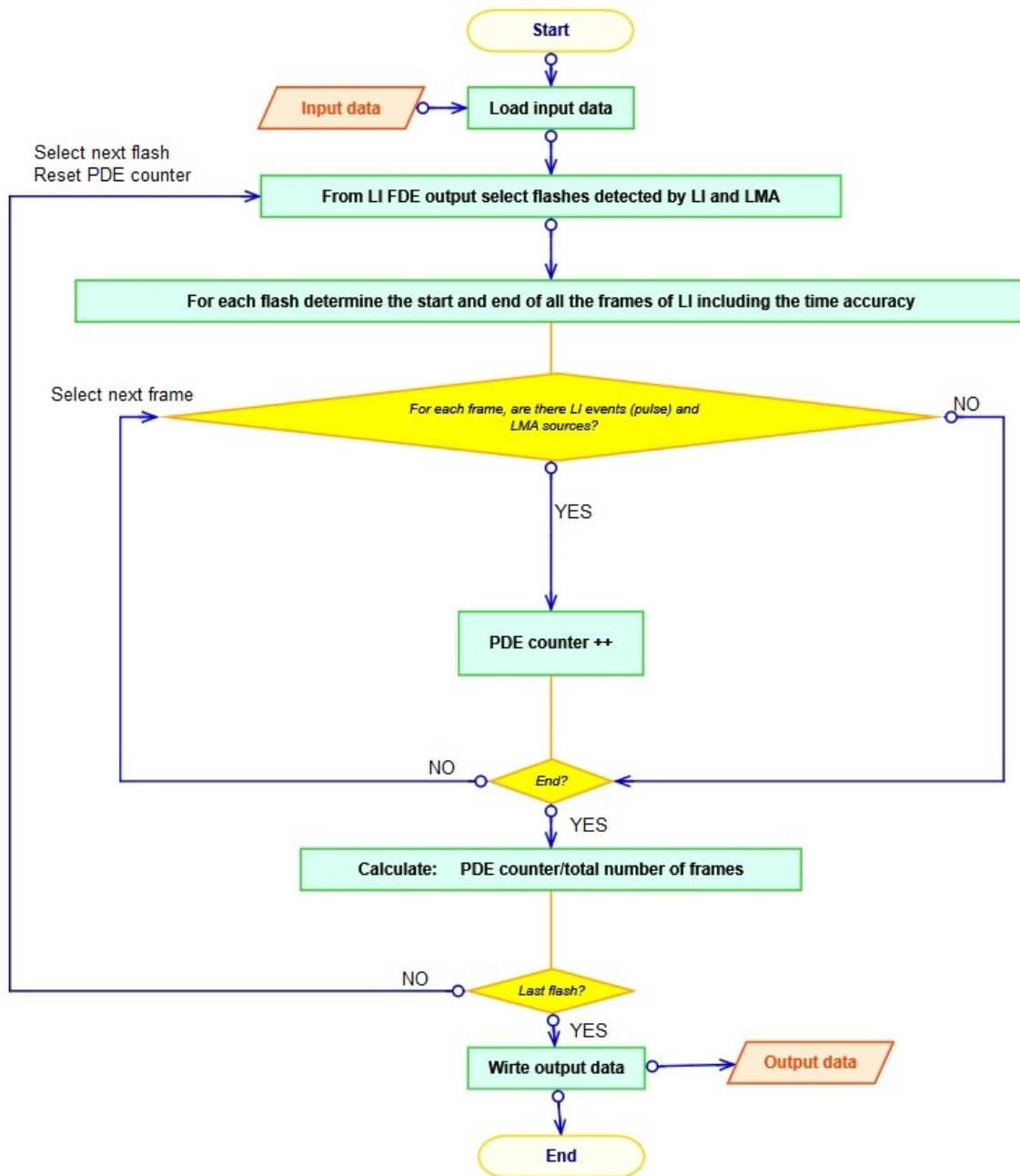


Figure 6.2.14 Flowchart for the evaluation of the PDE.

<b>Assumptions</b>	<ul style="list-style-type: none"> <li>• LMA is the reference network (<math>DE_f \text{ LMA} = 100 \%</math>).</li> <li>• <b>LMA sources are related to optical events. This affirmation has not been proved yet.</b></li> <li>• High performance of the LMA within the <math>&lt;P</math> dBW area.</li> </ul>
<b>Limitations</b>	<ul style="list-style-type: none"> <li>• The evaluation is limited to areas due to the limited range of LMA.</li> <li>• LMA data needs to be transferred. Full data cannot be transferred and processed in real time. For continuous analysis periodicity should be defined.</li> <li>• <b>Since it is not proved the relation between LMA sources and optical pulses, the results might be not representative.</b></li> <li>• The analysis is restricted to those flashes detected by LI and LMA.</li> </ul>
<b>Key configuration parameters</b>	<ul style="list-style-type: none"> <li>• Area of analysis. Area of high sensitivity where LMA has low power detection capability (<math>&lt; P</math> dBW) must be considered. This area shall correspond to the analysed day or episode.</li> <li>• Time uncertainty to include at the LI frame time period.</li> </ul>
<b>Confidence of success</b>	<ul style="list-style-type: none"> <li>• Low.</li> </ul>
<b>Applicability</b>	<ul style="list-style-type: none"> <li>• Easy.</li> </ul>

### 6.2.6 LI L1b L2 Pulse false alarm (PFAR)

This is similar as the previous L1b/L2 pulse detection efficiency. We have seen that LMA maps lightning leaders but LMA data is not directly related to optical pulses. In this case, similar than the PDE, LMA can provide evidence if there is an active lightning flash at the pulse level.

As example, in the preliminary analysis in figure 6.2.12, a 8 % of the events would be candidates of FA events considering time window of  $\pm 2$  ms centred on the event time.

#### Input data (PFAR)

- LI FDE output data that includes the information of the LMA-LI matching.
- LI level-2 data.
- LI level 1b.
- LMA level-1 data.

### Configuration parameters (PFAR)

- Time uncertainty to extent the frame integration time.

### Output data (PFAR)

- Percentage of LI pulses not related to LMA lightning leader activity.

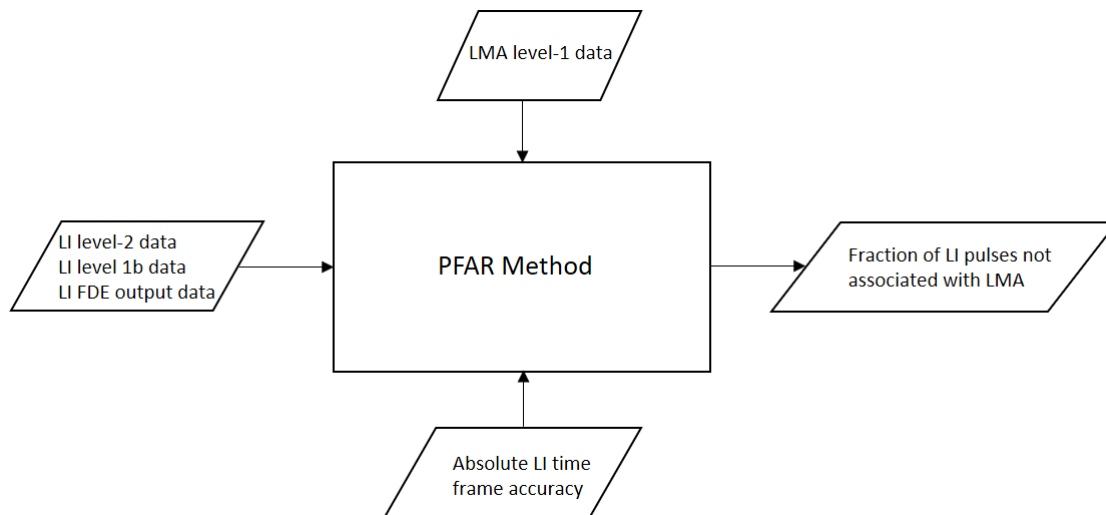


Figure 6.2.15 Summary of the input/output for the evaluation of the PFAR.

### Method (PFAR)

- Load input data.
- From LI FDE output, select flashes detected by LI and LMA.
- For each LMA flash determine the start and end of each LI frame related to this flash. That means, divide the time of the LMA flash in periods of LI frames. This time shall include the time uncertainty.
- For each frame check if there is any LMA source. In case that there is not any LMA source increase the counter of PFA.
- Once all the frames (pulses) are evaluated calculate the fraction of LI pulses without LMA sources versus the total number of frames.
- Repeat for all the selected flashes.
- Write statistics of the fraction of LI pulses not associated with LMA sources.

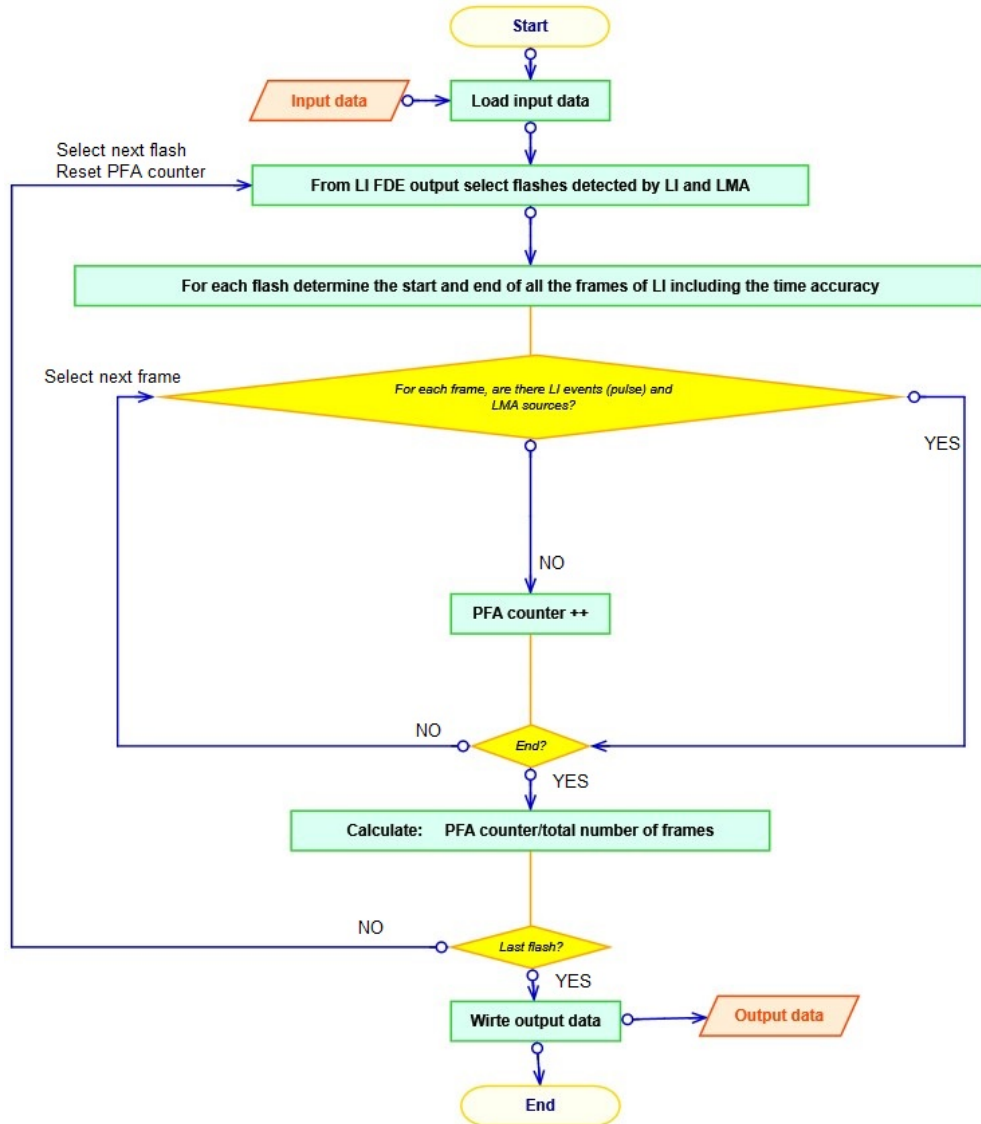


Figure 6.2.16 Flowchart for the evaluation of the PFAR.

<b>Assumptions</b>	<ul style="list-style-type: none"> <li>• LMA is the reference network (<math>DE_f \text{ LMA} = 100 \%</math>).</li> <li>• <b>LMA sources are related to optical events. This affirmation has not been proved yet.</b></li> <li>• High performance of the LMA within the <math>&lt;P</math> dBW area.</li> </ul>
<b>Limitations</b>	<ul style="list-style-type: none"> <li>• The evaluation is limited to areas due to the limited range of LMA.</li> <li>• LMA data needs to be transferred. Full data cannot be transferred and processed in real time. For continuous analysis periodicity should be defined.</li> <li>• <b>Since the relation between LMA sources and optical pulses is not well known, the results might be not representative.</b></li> <li>• The analysis is restricted to those flashes detected by LI and LMA.</li> </ul>
<b>Key configuration parameters</b>	<ul style="list-style-type: none"> <li>• Area of analysis. Area of high sensitivity where LMA has low power detection capability (<math>&lt; P</math> dBW) must be considered. This area shall correspond to the analysed day or episode.</li> <li>• Time uncertainty to include at the LI frame time period.</li> </ul>
<b>Confidence of success</b>	<ul style="list-style-type: none"> <li>• Low.</li> </ul>
<b>Applicability</b>	<ul style="list-style-type: none"> <li>• Easy.</li> </ul>

### 6.2.7 Conclusions

In the previous sections the methods for evaluating the performance of the LI compared to LMA have been described.

Although, FDE and FFAR have been proposed to analyze using LMA locations of sources/flashes, a gridded analysis similar to the ASPKE might be convenient. So, LMA shall be gridded using the same LI grid.

We have not found a straight relation between the ISS-LIS events (luminosity) and the LMA VHF sources. This limit the analysis of the pulse level (PDE and PFAR) as well the time accuracy (TA).

### 6.3 Strategy

In the previous section we have described the parameters and methods for evaluation. Now we discuss the strategy of the validation and evaluation of the LI using LMA networks.

#### 6.3.1 Locations of LMAs and experience in campaigns

In Europe, the Spanish Ebro-LMA (south of Catalonia) and the French SAETTA LMA (Corsica, e.g. *Coquillat et al.* 2019) are the only two LMA networks currently available. Both networks are located at the Mediterranean Basin. These networks have been in operation for more than 8 years.

LMA systems can easily deployed, so campaigns at other locations in the LI field of view can be organized. As example, in 2015 we installed a LMA network in Santa Marta (Colombia) and later, in 2018 we moved it to Barrancabermeja (Colombia) in 2018 (*López et al.* 2019). In addition, in 2017 we conducted a campaign in Switzerland (Santís tower) for three months (*Figuera-Ventura et al.* 2019). Typically, we are able to install six LMA sensors (minimal network) in less than a week.

#### 6.3.2 Annual number of thunderstorms

The Ebro-LMA has ~90 days (e.g. case 2016) with thunderstorms per year (figure 6.3.1) including summer and winter thunderstorms.

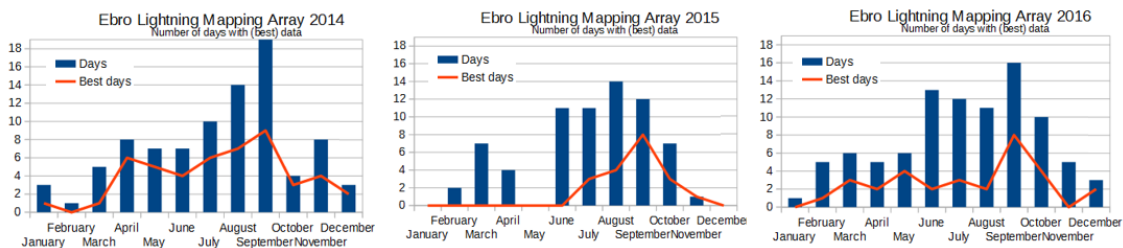


Figure 6.3.1 Number of thunderstorm days in the range of the Ebro-LMA.

In terms of lightning flashes, in a thunderstorm day the LMA can report more than ten thousand flashes, so several hundred thousand to one million of lightning flashes can be detected per year. Of course this is for the complete range of the network. For the high performance range of the Ebro-LMA several tens of thousands flashes can be available per year.

We do not have information about thunderstorm days data for the SAETTA LMA in Corsica.

### **6.3.3 Recommendations for validation and operation**

#### **Early observation phase**

LMA can be useful during the early observation phase in order to provide some total lightning reference data to compare with the initial LI data. We estimate that LMA can offer reliable data for investigate those LI flashes composed by single events.

For the Ebro-LMA science data for a single episode can be available in less than 24 h.

#### **Commissioning phase**

The metrics described in the section 6.2 can be evaluated for validation of the LI detections. In addition, identification of limitations can be performed in this phase. These limitations, among others, can be summarized as follows:

- Cloud depth occurrence of a lightning flash in order to be detected.
- Duration of a lightning flash in order to be detected.
- Minimum size of a lightning flash in order to be detected.
- Capability of LI to classify/separate lightning flashes.

LMA data (science data) can be delivered weekly.

#### **Operation phase**

For regular operation, LMA can be used to:

- Monitor MTG LI performance periodically (e.g. every month, every three months, etc).
- Evaluation of MTG LI performance for special cases such as severe thunderstorms, supercells, very high lightning flash rate thunderstorms, etc. Performance of MTG LI can be compared to the total lightning reported by the LMA. These cases might need the support or the analysis of the LMA network operator.
- Evaluation of MTG LI products: Products related to lightning can be evaluated using LMA as reference.
- Campaigns: The group of the UPC has experience in LMA campaigns. In Europe campaigns can easily be scheduled and conducted. In Africa campaigns are also possible but local support would be necessary.

## Summary

Figure 6.3.2 summarizes the proposed strategy for the evaluation of MTG-LI at different stages. In the Early observation phase LMA can offer reference episodes for early evaluation of the MTG-LI. Science data can be delivered in less than 24 h.

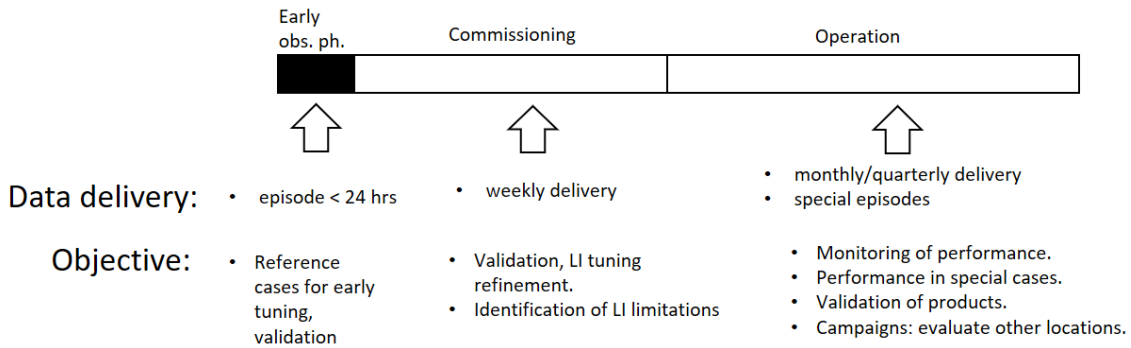


**Figure 6.3.2 Summary of the use of LMA data for LI evaluation.**

During the Commissioning phase, data can be delivered periodically and used for validation of the MTG-LI. In this phase limitations of MTG-LI can be identified or evaluated. During operation, monitoring of performance of the MTG-LI based on the LMA can routinely performed with attention to those special cases. At this stage also validation of products derived from the LI can be conducted using LMA data as reference. Finally, campaigns can be programmed to evaluate MTG-LI performance in locations of interest.

## 7. Conclusions

Lightning Mapping Arrays (LMAs) provide the most comprehensive picture of lightning flashes. These networks have been widely used in research to investigate lightning physics, thundercloud electrification and characterization of thunderstorms. Besides the scientific use, LMA allows to real-time decimated data for operational purposes.

In Europe, the first permanent LMA network was installed in 2011 in Spain (Ebro-LMA) and the second LMA network was installed few years later in Corsica (France). These networks will provide the best reference lightning data for evaluation of the MTG-LI.

The benefits of the LMA are summarized:

- Full 3D-time picture of lightning leaders. So the total size, altitude and duration is very well described compared to cloud-to-ground and/or intra-cloud VLF/LF detections by LLS.
- Typically, hundreds to thousands of sources per lightning flash.
- Discrimination of lightning leader polarity.
- Identification of thundercloud charge regions.
- Easy to setup for campaigns.

But the LMA presents the following cons:

- Range is limited, typically in the range of 100 km.
- Large amount of data to be processed in real-time. Data needs to be transferred and/or collected.
- Decimated data is used for the real-time. But this data does not have all the properties of the flashes.
- Lightning return stroke processes are not detected by the LMA.
- LMAs are commonly operated by research institutes and universities where funding is limited.

Performance of the LMA depends on many factors. The number of sensors and network geometry are important to define the coverage range and artifacts in the solutions of the sources. In addition, the noise level limits the theoretical range because the reduced capability to discriminate lightning emissions. Orographic effects can also limit the coverage in certain regions (e.g. blocking by mountains). So the performance of the LMA can vary from day to day due to several factors such as variations of the local noise at each station and availability of the stations.

In the second section of this report we have investigated the performance of the LMA from a theoretical and an experimental approach. We proposed several parameters to investigate that allowed to display coverage maps for each parameter. We have found that the sensitivity (power) and the number of sources are the most indicative parameters to define the best regions of performance. Sensitivity maps can be created by analyzing the minimum VHF source power detected in a particular location. A gridded method using the same LI grid will be more convenient in order to define the region of analysis. Moreover, sensitivity maps can be created per day or even for the evaluated event. These sensitivity maps will be provided by the LMA operators as input data for the LI evaluation. Further work is necessary to define a method to select the sensitivity power threshold for different LMA networks. Since LMA sensors are not calibrated, different networks can provide different power levels. We have proposed a method where statistics of power of sources related to positive breakdown are used to define the minimum sensitivity level. Positive leader sources are known to produce lower power levels and the detection of positive breakdown in lightning flashes is necessary in order to have a complete picture of a lightning flash.

For the future LI evaluation, LMA data and processing need to be defined and standardized. In agreement with the LMA SAETTA group we have defined the following levels of data:

- LMA level-0 data: that corresponds to the raw data for each individual station. In the regular LMA operation, the RF power (dBm) is provided for each detection every 80  $\mu$ s.

- LMA level-1 data: from level-0 data, the LMA processor obtains the sources. Sources are locations (x,y,z) and power (dBW).
- LMA level-2 data: sources from level-1 data are grouped to form lightning flashes. This grouping is conducted by post processing according to the experience of each LMA operator.

At this time, it is important to define the source grouping criteria to define a lightning flash. Further work is needed between the European LMA operators in collaboration with the US operators involved in the LI-MAG to create codes for obtaining LMA level-2 data.

In sections three and four we have presented the evaluation of ISS-LIS against the E-LMA. Average flash detection efficiency resulted to be >75 %. For some episodes, the efficiency is very high >90 % but for some particular episodes the efficiency has dropped to <50 %. We suspect some technical problems such as the known solar panel masking of the ISS-LIS to explain this dramatic drop. We have seen that the efficiency is sensitivity to the selected range and restrictions to the LMA data. That is mostly due to the short observation periods of the ISS-LIS that significantly limits the amount of data to evaluate. In addition to the detection efficiency we have found that in 40 % of the LMA flashes ISS-LIS has two or more flashes. That means that the grouping criteria used by ISS-LIS worked for 60 % of the cases.

Opposite to detection efficiency, in the flash false alarm we have investigated ISS-LIS flashes without a corresponding LMA flash. First, we looked for ISS-LIS false alarm candidates using LMA flash data (LMA level-2 data). All of the false alarm except one have been discarded when these have been compared to LMA source data (LMA level-1 data). These cases occurred far >100 km from the network. The remaining case that occurred around 50 km from the network we found that in this particular day one LMA station was no available limiting the detection range to the area where this flash occurred. That confirmed the necessity to use LMA sensitivity maps for each day or storm episode.

Regarding the duration of the flashes, the durations of ISS-LIS are about 30 % shorter than the LMA. To investigate the occurrence of the ISS-LIS events within lightning flashes, we normalized the duration of each flash. We found that in most of the ISS-LIS cases (>75 %), the first event is detected before the 20 % of the normalized flash duration. The last ISS-LIS event occurs generally around the 85 % of the normalized flash duration. ISS-LIS events are rather regular distributed in the first 60 % of the flash. Around the time corresponding to the 70 %, ISS-LIS events accumulate by a 20 %. Radiance of the events is rather constant along the flash.

We have seen that for those LIS – LMA matches, LMA presents sources at higher altitudes than for those LMA cases without a corresponding ISS-LIS detection. That suggests that optical emissions from lightning reaching higher altitude is less attenuated by the cloud. He have shown that detection efficiency drops to a ~20% when lightning

flashes occur below the 75 % altitude for a giving episode. Contrary, we have not found any relation between the power level of VHF LMA sources and the detected events. We also have seen that LMA flashes with high number of sources are better detected by ISS-LIS. Summing up, we have shown that lightning at higher altitude provides better conditions for ISS-LIS detection but we have not fund a straight relation between the LMA sources or leader processes with the optical emissions. That will limit the LI pulse level analysis.

Another parameter evaluated has been the location accuracy. For this metric, we employed a grid. LMA flash data has been gridded in 6 x 6 km cells (average ISS-LIS cell size). Computing flash centroids of the LMA and comparing to the ISS-LIS centroids, the mean absolute offset between ISS-LIS and LMA flash are 4.8 km. In longitude, the mean bias is -1.7 km whereas in latitude -1.3 km. This means that the overall calibration of ISS-LIS is really correct. Comparing LMA and ISS-LIS pixel overlap, on average 47 % of the LMA flash extension is covered by ISS-LIS. Finally, ISS-LIS flashes are apparently large than LMA flashes when the areas are computed.

In section five of this report we have provided some statistical data and plots useful for generating stochastic lightning. Duration, size, relation between duration and size, time between flashes and flash altitudes can be employed to generate lightning flashes. In addition, we have compiled part of the results of this work regarding the number of ISS-LIS events per flash and how these are distributed within a flash.

Section six has presented the strategy for the future validation and monitoring of the MTG-LI. Based on the experience in this work and the activity of the LI-MAG group we have described the method for different parameters: Flash Detection Efficiency, Flash False Alarm, Absolute Sample Position Knowledge Error, Time Accuracy, Pulse Detection Efficiency and Pulse False Alarm. Additionally, these methods allow to verify other parameters such as the MTG-LI flash grouping criteria. For all the parameters we exposed the assumptions, limitations, key configuration parameters, confidence of success and applicability. The main conclusions of the considered parameters are:

- The grade of success is high in most of the parameters except the pulse level parameters. We have not found any consistent relation between LMA VHF signals or sources and the luminosity pulses generated by lightning. This will limit the pulse level analysis.
- Evaluation region need to be restricted according to the sensitivity of the network for each particular day or episode.
- LMA data delivery is not immediate. Although LMA can produce decimated data for real time, evaluation will need science data level-1 and level-2 that require the transfer of large amounts of data and data processing.

Regarding the strategy on the evaluation, in Europe two LMA are operating in Spain and France (Corsica). We have divided the evaluations in three phases:

- Early observation phase: In this phase science LMA data can be provided for particular storm episodes within 24 h. These episodes can be used for initial evaluation and validations of the MTG-LI.
- Commissioning phase (after the early observation phase): LMA science data can be provided weakly. This can be used to evaluate and validate MTG-LI. In addition, identification of limitations can be conducted in this phase (e.g. minimum flash size to be detected, minimum flash duration, etc). Also the MTG-LI flash grouping can be refined in this phase using LMA data.
- Operation phase: during operation, monitoring of performance of the MTG-LI based on the LMA can routinely performed with attention to those special cases. At this stage also validation of products derived from the LI can be conducted using LMA data as reference. Finally, campaigns can be programmed to evaluate MTG-LI performance in locations of interest.

We have indicated the possibility to conduct campaigns in other locations within MTG-LI field of view. Our group has experience in campaigns with LMA in Europe and South America.

## References

Beirle, S., Koshak, W., Blakeslee, R., and Wagner, T.: Global patterns of lightning properties derived by OTD and LIS, *Nat. Hazards Earth Syst. Sci.*, 14, 2715-2726, <https://doi.org/10.5194/nhess-14-2715-2014>, 2014.

Blakeslee, R.J., H. Christian et al. Lightning Imaging Sensor (LIS) for the International Space Station (ISS): Mission Description and Science Goals. XV International Conference on Atmospheric Electricity, 15-20 June 2014, Norman, Oklahoma, U.S.A.

Bruning, E.C. and D.R. MacGorman, 2013: Theory and Observations of Controls on Lightning Flash Size Spectra. *J. Atmos. Sci.*, 70, 4012–4029, <https://doi.org/10.1175/JAS-D-12-0289.1>

Christian, H. J., Richard J. Blakeslee, and Steven J. Goodman. Lightning Imaging Sensor (US) for the Earth Observing System. NASA, February 1992.

Coquillat, S., Eric Defer, Pierre de Guibert, Dominique Lambert, Jean-Pierre Pinty, Véronique Pont, Serge Prieur, Ronald J. Thomas, Paul R. Krehbiel, and William Rison, 2019. SAETTA: high resolution 3D mapping of the total lightning activity in the Mediterranean basin over Corsica, with a focus on a MCS event. *Atmos. Meas. Tech. Discuss.*, <https://doi.org/10.5194/amt-2019-192>, 2019

Figueras i Ventura, Jordi, Nicolau Pineda, Nikola Besic, Jacopo Grazioli, Alessandro Hering, Oscar A. van der Velde, David Romero, Antonio Sunjerga, Amirhossein Mostajabi, Mohammad Azadifar, Marcos Rubinstein, Joan Montanyà, Urs Germann, and Farhad Rachidi, 2019. Polarimetric radar characteristics of lightning initiation and propagating channels, *Atmos. Meas. Tech.*, 12, 2881-2911, <https://doi.org/10.5194/amt-12-2881-2019>, 2019

Goodman, S., D. Mach, W. Koshak, R. Blakeslee. Algorithm Theoretical Basis Document. Center for Satellites Applications and Research. September 24, 2010.

Lopez, J.A, Pineda N., Montanya J., van der Velde, O.A., Fabro, F., Romero. D, 2017. Spatio-temporal dimension of lightning flashes based on three-dimensional Lightning Mapping Array Atmospheric Research 197: 255-264

López, J. A., Montanyà, J., van der Velde, O. A., Pineda, N., Salvador, A., Romero, D., et al. (2019). Charge structure of two tropical thunderstorms in Colombia. *Journal of Geophysical Research: Atmospheres*, 124. <https://doi.org/10.1029/2018JD029188>

Koshak, W. J., Solakiewicz, R. J., Phanord, D. D., and Blakeslee, R. J.: Diffusion model for lightning radiative transfer, *J. Geophys. Res.*, 99, 14361–14371, 1994.

Mazur, V. (2002), Physical processes during development of lightning flashes, *Comptes Rendus Phys.*, 3, 1393–1409.

Montanyà, J., van der Velde, O., Romero, D., March, V., Solà, G., Pineda, N., Arrayas, M., Trueba, J. L., Reglero, V., Soula, S. (2010), High-speed intensified video recordings of sprites and elves over the western Mediterranean Sea during winter thunderstorms. *Journal of Geophysical Research*, 115, A00E18, doi:10.1029/2009JA014508.

Montanyà J, van der Velde O, Solà G, Fabró F, Romero D, Pineda N, Argemí O. Lightning flash properties derived from lightning mapping array data. In: International Conference on Lightning Protection (ICLP), Shanghai. 2014a.p. 974–8. doi:doi:10.1109/ICLP.2014.6973264; EEEE.

Rison W., R.J. Thomas, P.R. Krehbiel, T. Hamlin, and J. Harlin, A GPS-based three-dimensional lightning mapping system: Initial observations in central New Mexico, *J. Geophys. Res.*, 26, 3573-3576 1999.

Soula, S., O. van der Velde, J. Palmieri, J. Montanya, O. Chanrion, T. Neubert, F. Gangneron, Y. Meyerfeld, F. Lefeuvre, and G. Lointier (2010), Characteristics and conditions of production of transient luminous events observed over a maritime storm, *J. Geophys. Res.*, 115, D16118, doi:10.1029/2009JD012066.

Thomas. R.J.. P. R. Krehbiel W. Rison T. Hamlin. D.J. Boccippio S.J. Goodman. H.J. Christian. 2000. Comparison of ground-based 3-dimensional lightning mapping observations with satellite-based LIS observations in Oklahoma. *Geophys. Res. Lett.*(27): 1703-1706 <https://doi.org/10.1029/1999GL010845>

Thomas, R. J., P. R. Krehbiel, W. Rison, T. Hamlin, J. Harlin, and D. Shown (2001), VHF source powers radiated by lightning, *Geophys. Res. Lett.*, 28, 143-146.

Thomas, R. J., P. R. Krehbiel, W. Rison, S. J. Hunyady, W. P. Winn, T. Hamlin, and J. Harlin (2004), Accuracy of the lightning mapping array, *J. Geophys. Res.*, 109, D14207, doi:10.1029/2004JD004549

Thomason, L.W. and Krider, E. P.: The effects of clouds on the light produced by lightning, *J. Atmos. Sci.*, 39, 2051–2065, 1982

Ushio. T., S. Heckman. K. Driscoll. D. Boccippio. H. Christian. and Z. I. Kawasaki (2002). Cross-sensor comparison of the Lightning Imaging Sensor (LIS). *Int. J. Remote Sens.*. 23. 2703–2712. doi:10.1080/01431160110107789.

van der Velde, O. A., and J. Montanyà (2013), Asymmetries in bidirectional leader development of lightning flashes, *J. Geophys. Res. Atmos.*, 118, doi:10.1002/2013JD020257.

## Annex A Weather radar

The Meteorological Service of Catalonia (SMC) operates a network of C-band weather radars. The network is composed by four radars, which are meant to cover the region of Catalonia ([www.meteo.cat](http://www.meteo.cat)). Polar volumes are acquired every 6 minutes. Further technical details of the SMC weather radars and network characteristics can be found in *Bech et al. (2004)* and *Argemí et al. (2014)*.

In particular, the radar echo top product (TOP) corresponds to the maximum height reached by the 12 dBZ reflectivity echoes. Therefore, the TOP-12 is a proxy for the maximum height reached by the thunderstorm (see Fig C.1). This product, in combination with the LMA data, can be used to estimate how close are the lightning channels of the cloud top (see Fig C2). This information can be useful to analyse the event radiance recorded by the ISS-LIS (see Fig C3)

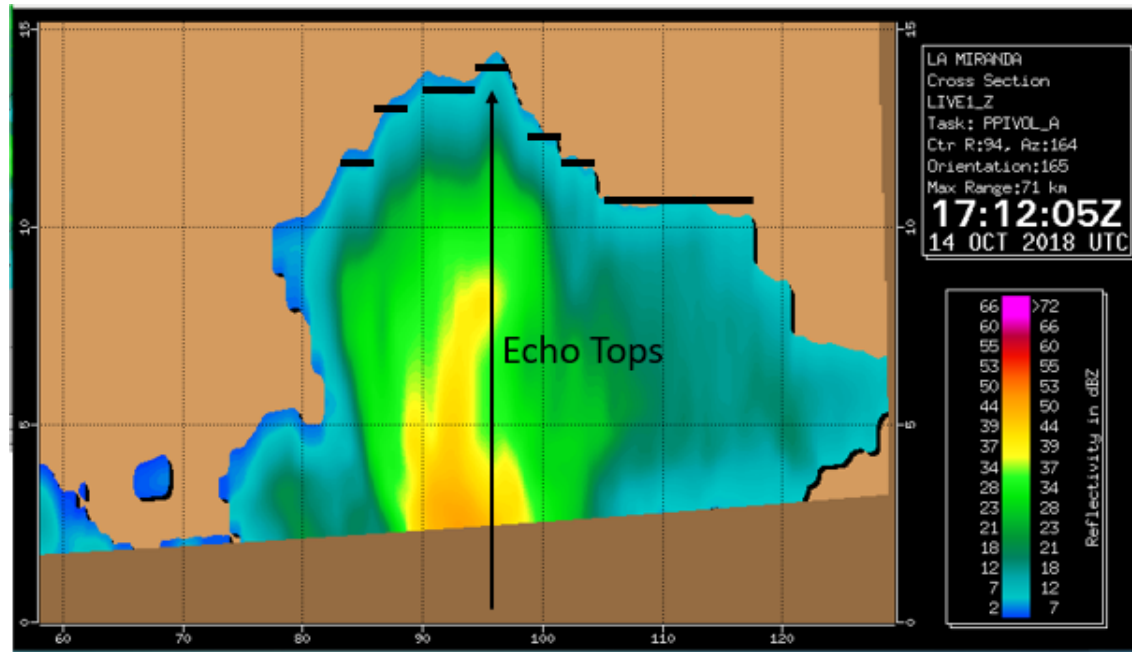


Figure C1. Schematic representation of the Echo-tops heights on a radar cross section

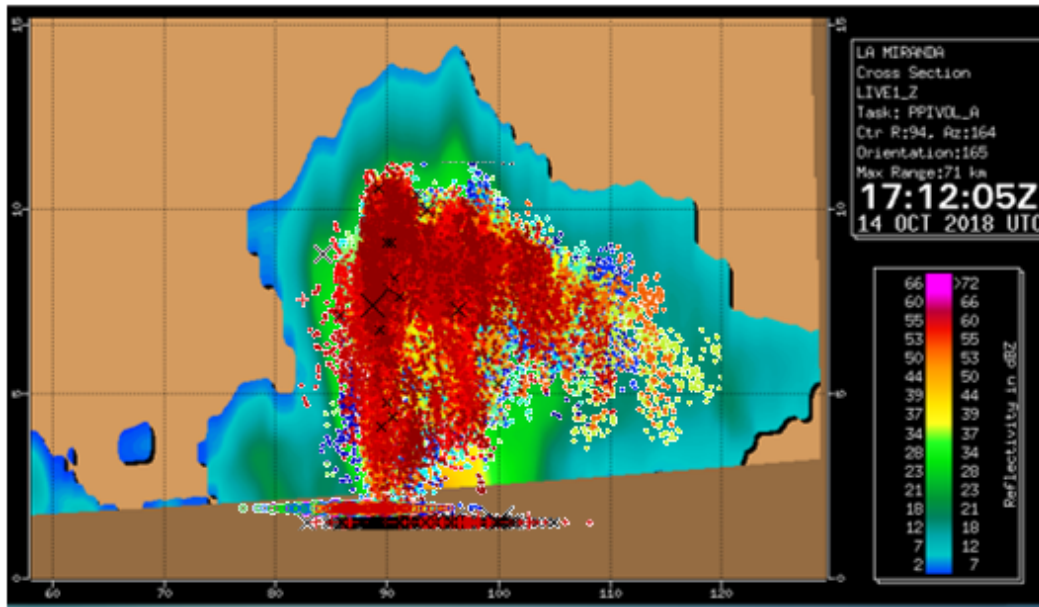


Figure C2. Schematic representation of a LMA cross section overlaid to a radar cross section.

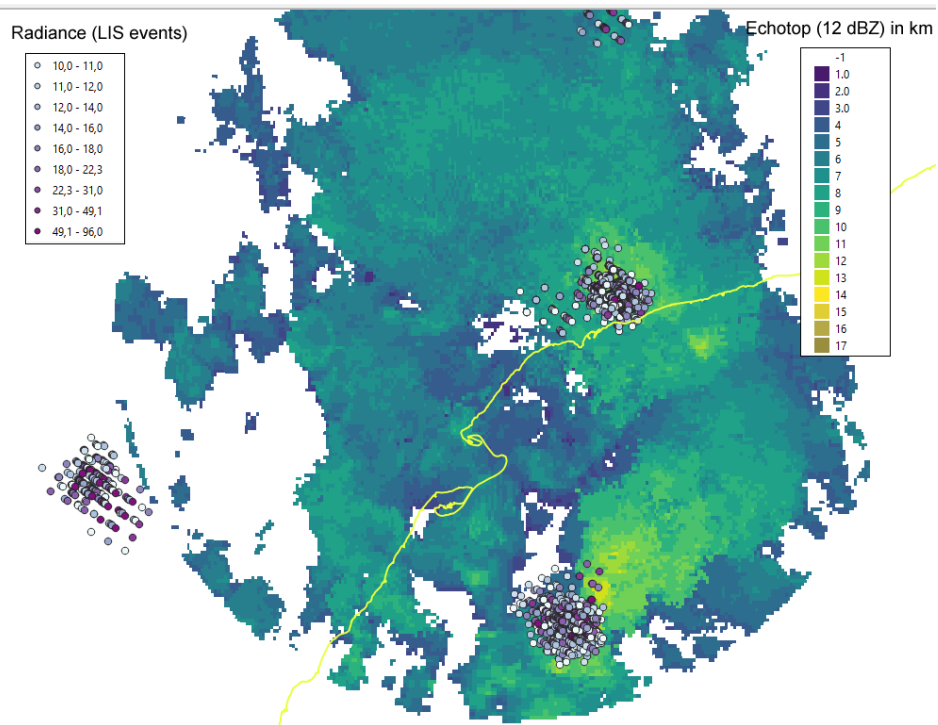


Figure C3. Plain view of the radar echo tops product (2018/10/14 17:06 UTC) from "La Miranda" radar (N 41° 05' 30.24" E 0° 51' 48.58"; 950 m above MSL), with the LIS events overlaid

## **Annex B Regional VHF interferometer total lightning location system**

Besides the radar network, the SMC operates a lightning location system (LLS) covering Catalonia with four Vaisala LS-8000 total lightning detectors. Total lightning is understood hereafter as the sum of intra-cloud (IC) and cloud-to-ground (CG) flashes. IC and CG flashes are detected and processed separately.

On one hand, IC flashes are detected in the very high frequency (VHF, 110 to 118 MHz) and located using interferometry (*Lojou and Cummins, 2006*). The combination of the four different concurrent observations provides two-dimensional location of the VHF sources, as the baseline (135 to 150 km) of the LS-8000 does not allow three-dimensional location. The LLS is able to locate a maximum of 100 detections per second in windows of 100- $\mu$ s time resolution.

On the other hand, CG return strokes are detected by a low frequency (LF) sensor and located using a combination of the TOA/MDF (Time-of-Arrival/Magnetic Direction Finding) technique (*Cummins et al., 1998*).

Throughout the years of operation, the LLS performance has been experimentally evaluated by means of electromagnetic field measurements and video recordings of natural lightning in successive campaigns (*Montanyà et al., 2006; Pineda and Montanyà, 2009; Montanyà et al., 2012*). Additionally, since 2011 data from a Lightning Mapping Array (*van der Velde and Montanyà, 2013*) operating in the area of coverage of the LLS has been used to establish the intra-cloud detection efficiency (DE) of the LLS. The analysis of the 2013-campaign establishes a CG flash DE for the LLS around 80-85% and an IC flash DE around 70-75%. Regarding the location accuracy, the estimated median location accuracy of the LLS for the CG strokes is around 1 km.

Although the SMC-LSS does not detect in 3D, it detects a large amount of VHF sources per flash, allowing to determine the detailed footprint of the lightning flash, compared to Lightning Location Systems that only detect cloud-to-ground strokes (see example in Fig C4)

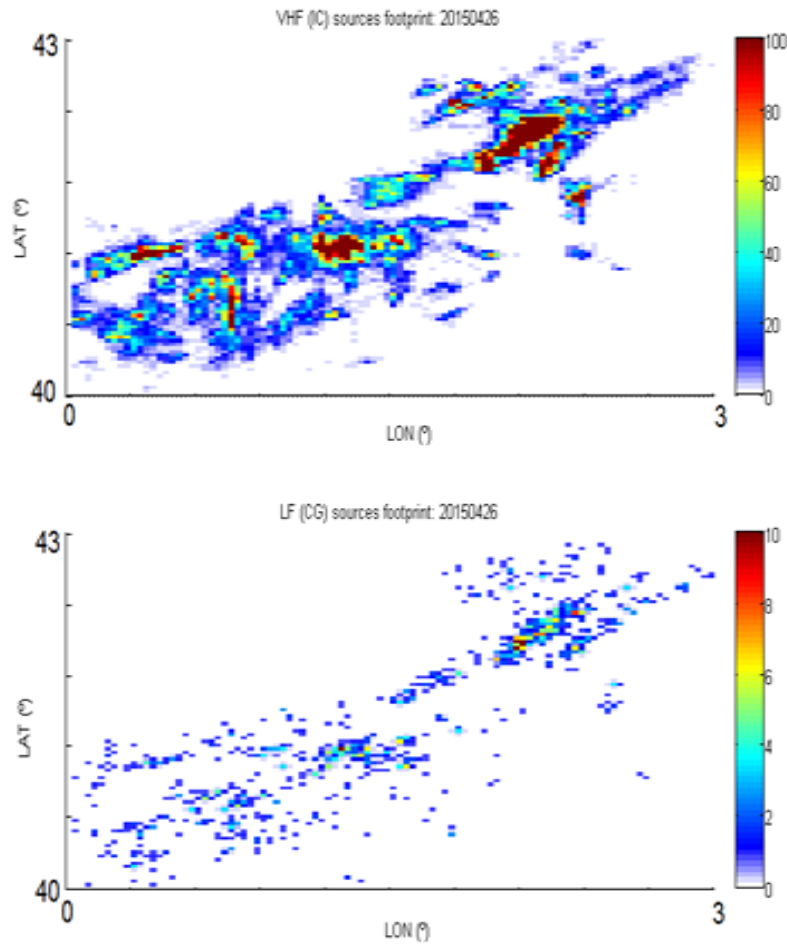


**Figure C4. Example of the footprint of a storm obtained from Total lightning (intracloud+cloud-to-ground) (top) and only cloud-to-ground (bottom).**

Figure C5 shows all ISS-LIS events occurred between March 2017 and October 2018 in the domain covered by the SMC radar and lightning networks. Figure C6 shows a comparison of the SMC-LLS Total Lightning and the ISS-LIS detections on the 15 June 2017 between 18:29 and 18:32 UTC. As commented, whereas the SMC-LLS cannot give information on the height of the IC channels, it can be useful to compare intra-cloud activity from ISS-LSS vs. a ground network on a larger area, compared to the LMA

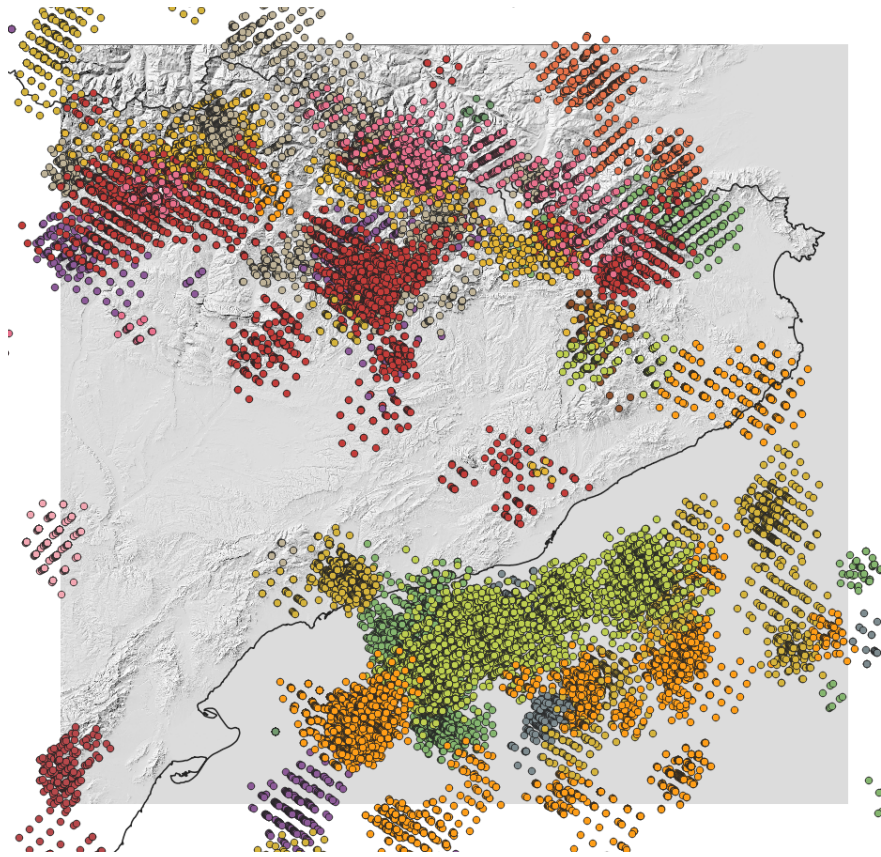


Figure C5. ISS-LIS events detected above Catalonia between 24 March 2017 and 31 October 2018.

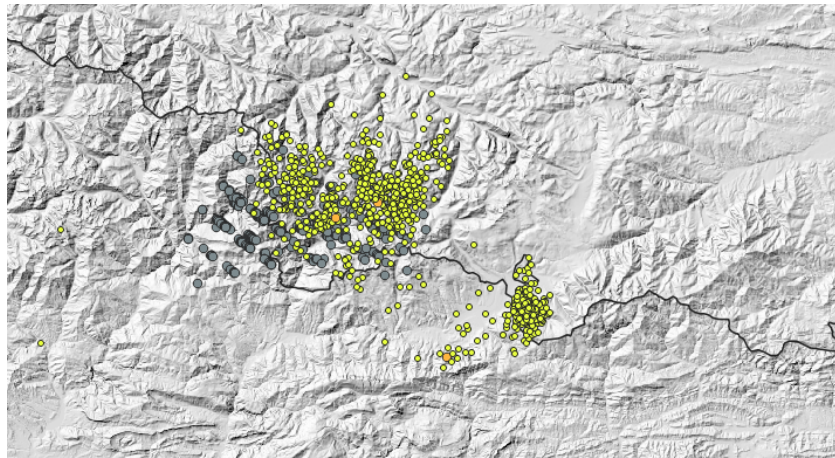


Figure C6. SMC-LLS Total Lightning (yellow dots for IC, orange for CG) and the ISS-LIS detections (grey dots) on the 15 June 2017 between 18:29 and 18:32 UTC.

## References of Annex A and B

- Argemí, O.; Altube, P.; Rigo, T.; Ortiga, X.; Pineda, N. and Bech, J. (2014). Towards the improvement of monitoring and data quality assessment in the weather radar network of the Meteorological Service of Catalonia, 8th European Conference on Radar in Meteorology and Hydrology (ERAD), Garmisch-Partenkirchen, Germany, Sept. 2014
- Bech, J.; Vilaclara, E.; Pineda, N.; Rigo, T.; López, J.; O'Hora, F.; Lorente, J.; Sempere, D. and Fàbregas, F.X. (2004). The weather radar network of the Catalan Meteorological Service: description and applications. Proceedings of the 3rd European Conference on Radar (ERAD 2004), Copernicus GmbH.
- Cummins, K. L., M. J. Murphy, E. A. Bardo, W. L. Hiscox, R. B. Pyle, and A. E. Pifer, 1998: A Combined TOA/MDF Technology Upgrade of the U.S. National Lightning Detection Network, *J. Geophys. Res.*, 103, 9035–9044.
- Lojou, J.Y., and K. L. Cummins, 2006: Total lightning mapping using both VHF interferometry and time-of-arrival techniques. In *International Conference on Lightning Protection*, Kanazawa, Japan, 391-396.
- Montanyà, J., N. Pineda, V. March, A. Illa, D. Romero, and G. Solà, 2006: Experimental evaluation of the Catalan Lightning Detection Network. In *19th International Lightning Detection Conference*, Tucson Vaisala, 7 pp.
- Montanyà, J., O. van der Velde, V. March, D. Romero, G. Solà, and N. Pineda, 2012: High-speed video of lightning and x-ray pulses during the 2009–2010 observation campaigns in northeastern Spain. *Atmos. Res.*, 117, 91-98
- Pineda, N. and J. Montanya, 2009: Lightning detection in Spain: the particular case of Catalonia. *Lightning: Principles, Instruments and Applications*. Betz, H.-D., Schumann, U., Laroche, P. (Eds.), Springer, Netherlands: 161-185.
- Van der Velde, O. A., and J. Montanyà, 2013: Asymmetries in bidirectional leader development of lightning flashes, *J. Geophys. Res. Atmos.*, 118, 13504–13519.